Operational Optimization of Hybrid Power System

Ph.D. ELECTRICAL ENGINEERING
RANA MUHAMMAD MUSHARRAF SAEED

PHEE-SP-19-001

Session:2019-

DEPARTEMENT OF ELECTRICAL ENGINEERING

SUPERIOR UNIVERSITY

Lahore, Pakistan

Operational Optimization of Hybrid Power System

Submitted to Superior University ,Lahore in

Partial fulfillent of the requirements

for the award of the degree

Ph.D. ELECTRICAL ENGINEERING

RANA MUHAMMAD MUSHARRAF SAEED

PHEE-SP-19-001

Session:2019-

Supervisor:

DR. Mustafa Shakir

DEPARTEMENT OF ELECTRICAL ENGINEERING

SUPERIOR UNIVERSITY

Lahore, Pakistan

Dedication

I dedicate this Dissertation to all people who don't give up on me to finish my Ph.D degree. Especially to my beloved parents, my family, my supervisor Dr. Mustafa shakir, and my co-supervisor Dr. Naveed Ahmad Khan.

I, Rana Muhammad Musharraf Saeed hereby state that my PhD thesis titled "Operational Optimization of Hybrid Power System" is my own work and has not been submitted previously by me for taking any degree from Superior University, Lahore or anywhere else in the country/abroad.

At any time if my statement is found to be incorrect even after my graduation, the University has the right to withdraw my PhD Degree.

(Rana Muhammad Musharraf Saeed) Registration No: PHEE-SP19-001

Author's Declaration

I, **Rana Muhammad Musharraf Saeed** Roll No. **PHEE-SP19-001** student of Departement of Electrical Engineering, The Superior University, Lahore in the subject of **Ph.D. Electrical Engineering**, hereby declare that the matter printed in this dissertation as **Operational Optimization of Hybrid Power System** is my own research work. The text and results mentioned in this dissertation have not been printed, published, or submitted in any form at any national or international organization. I hereby certify that this research doesn't involve any plagiarized material or results that have been published by another person. My colleagues and friends assisted me while carrying on this research ; I identified their contributions as well . If it contains any plagiarized information, I bear full responsibility.

Signature

Dated:

Rana Muhammad Musharraf Saeed

Registration No: PHEE-SP19-001

Plagiarism undertaking

I **Rana Muhammad Musharraf Saeed** , solemnly state that the research work illustrated in this dissertation titled **Operational Optimization of Hybrid Power System** is my own developed and proposed work without any remarkable contribution of any oher person. I also recogize the HEC and The Superior University, Lahore zero-tolerance policy towards plagiarism . Therefire, I as an author of the above-titled dissertation declare that this research doesnot involve any plagiarized material or result that have published by another person, and literature with reference i properly cited in the bibliography section. I bear full responsibility that if i am found guilty of any kind of plagiarism in the above titled dissertation even after the award of my degree, the University reserves the right to revoke my degree at any stage. Furthermore, HEC and University has the right to declare blacklisted any forum.

Signature

Dated:

Rana Muhammad Musharraf Saeed

Registration No: PHEE-SP19-001

List of publications

It is certified that the following publication(s) have been made of the research work that has been carried out for this thesis:

Journal Articles

1. Saeed, Rana Muhammad Musharraf, et al. "Maximizing Solar Share in Robust System Spinning Reserve-Constrained Economic Operation of Hybrid Power Systems." Energies 17.11 (2024): 2794

Acknowledgement

I humbly praise and grateful to ALMIGHTY ALLAH, Who permits me to live and accomplish tasks, including the research work presented in this thesis.

Dr. Mustafa Shakir, my Supervisor and the chairman of Electrical Engineering department of Superior University, is the person who is always there to help me during my entire PhD program. I would have been no where without him. I feel very proud while working under his kind supervision. I offer my sincerest thanks to him for his many years of patience, guidance, illustrious advices, useful suggestions, kind and dynamic supervision throughout the research work. His personal interest, valuable suggestions, constructive, thoughtful and affectionate behavior resulted in the completion of this thesis.

I would like to thank administration of Superior University for providing me with an excellent environment perfect for conducting research and a scholarship for PhD studies. I am also thankful to Dean, Faculty of Engineering, for their cooperation, help and valuable suggestions.

I also wish to express my feelings of gratitude to my father, mother , wife, brothers, sisters and other relatives, who prayed for my health and brilliant future. I would not have achieved these goals without their sincere co-operation and love. I am also using this opportunity to thank all my friends who prayed for me and encouraged me through their love and sincerity.

May ALLAH bless them all.

Rana Muhammad Musharraf Saeed

Dated:

ABSTRACT

The integration of renewable energy is rapidly leading the existing grid systems toward modern hybrid power systems (HPS's). These hybrid power systems are more complex due to the random and intermittent nature of RE and involve numerous operational challenges. The Integration of renewable energy sources in conventional electrical grid with energy storage system (ESS) at generation side have considerable affects on unit commitment, economical dispatch and allocation of system spinning reserve. The scheme for application of ESS in a HPS depends on the random and intermittent nature of renewable energy sources and formulation of system spinning reserve (SSR) for thermal units contingency events. This research presents the operational model and optimization problem for solar integrated power systems in presence and absence of ESS, to address the issues of economical operation, reliable solar power share with respect to SSR, energy deficit in case of contingency events, and the allocation of SSR. The results of optimization of HPS without storage system is compared with the simulation results of HPS with storage system. We proposed a novel scheme for application of ESS in order to maximize the solar share and minimize the thermal units fuel cost. A mixed-integer optimization is formulated to minimize the overall cost of the system operation and to maximize the solar share within the limits of robust system spinning reserve as well as under various practical constraints. A Pareto-optimal solution for the maximization of the number of solar power plants and minimization of the solar cost is also presented for reliable solar share. Further, a decomposition framework is proposed to split the original problem into sub-problems. The solution of joint optimization is obtained by exploiting a Lagrange relaxation method, a binary search Lambda iteration method, SSR analysis, contingency based system reserve (CBSR) analysis, and binary integer programming. MATLAB software is used to produce the simulation results for proposed model. The proposed model was implemented on an IEEE-RTS 26 units system and 40 solar plants.

Keywords: Hybrid power system; Reserve constraint unit commitment; Lagrange relaxation, Economic dispatch; Lambda iteration; System spinning reserve; Solar share; Storage application scheme; system spinning reserve analysis

TABLE OF CONTENTS

LIST OF TABLES

LIST OF FIGURES

LIST OF ABBREVIATIONS

BIP	Binary Integer Programming
BPSO	Binary PSO
CBSR	Contingency-Based System Reserve
DG	Distributed Generations
ED	Economic Dispatch
GW	Giga Watt
HPS	Hybrid Power System
LR	Lagrange Relaxation
MIOP	Mixed Integer Optimization Problem
MOPSO	Multi-Objective Particle Swarm Optimization
MW	Mega Watt
PSO	Particle Swarm Optimization
PV	Photo Voltaic
RTP	Real Time Pricing
RE	Renewable Energy
SG	Smart Grid
SSR	System Spinning Reserve
UC	Unit Commitment
VPE	Valve Point Effects

LIST OF SYMBOLS

a_i, b_i, c_i	Fuel cost coefficients of thermal generation unit;
b_i^t	Binary variable used to represent whether loss of load occurs when an outage of the i-th unit occurs in period t;
$b_{i,j}^t$	Binary variable used to represent whether loss of load occurs when a simultaneous outage of units i and j occurs during period t;
$EENS^t$	Expected energy not served during time t;
$KWh/m^2/d$	Kilo Watt Hour per Meter square per Day;
KWh	Kilo Watt Hour;
MWh	Mega Watt Hour;
SP	Total capacity of ESS;
SP_Γ	Reserve power from ESS for solar power outage;
SP_{th}	Reserve power from ESS for thermal contingency event;
NS	Total Number of hours in which solar power is not penetrated;
P_i^t	Power generated by the i-th thermal unit in time t;
$P_{i,min}$	The minimum power of the i-th unit;
$P_{i,max}$	The maximum power of the i-th unit;
Ps^t	Penetrated solar power in time t;
Pgs_j	Power generated by the j-thsolar plant;
Us_j	Binary variable used to represent the ON and OFF status of a solar plant;
P_d^t	Power demand in interval t;
p_i^t	Outage probability of the i-th unit at time t;
p_{ij}^t	Probability of the simultaneous outage of the i-th and j-th unit at time t;

$R^t_{i,up}$	Up-reserve power of the i-th unit in time t;
$R^t_{i,down}$	Down-reserve power of the i-thunit in time t;
$R^{\uparrow}_i$	Ramp-up rate of the i-th unit;
$R^{\downarrow}_i$	Ramp-down rate of the i-th unit;
S^t_j	Solar radiation at any given time t;
SSR^t	System spinning reserve available at time t;
SSR^t_{al}	Allocated SSR in time interval t;
$SSR^t_{opt(1,2)}$	Optimal SSR for first- and second-order thermal contingency event;
SSR^t_{ult}	The ultimate SSR in time interval t;
T	Time duration of each optimization interval;
T^t_a	Ambient temperature;
$T^t_{i,on}$	Consecutive cumulative ON time of the i-th unit until time t;
$T^t_{i,off}$	Consecutive cumulative OFF time of the i-th unit until time t;
$T_{i,up}$	The minimum uptime of the thermal generator;
$T_{i,down}$	The minimum downtime of the thermal generator;
U^t_i	Binary variable for the ON and OFF status of the i-th thermal unit at time t;
T^t_r	Reference cell temperature;
$VOLL$	Value of lost load;
u_i	Outage replacement rate of unit i;
α_j	Temperature coefficient;
ρ^t_j	Rated power of the j-th solar plant;
τ	The maximum allowable time for a thermal unit to ramp up or down;
ζ_j	Per unit cost of the j-th solar plant;
\$	Dollar

δ	Step size for solar share increment;
Γ_s	The maximum limit of the solar share within a robust range of the SSR;
Γ_c	The maximum solar share for the range in which a power deficit is experienced by the power system;
Γ^t	Solar share based on the SSR during time t;
Γ^t_{max}	The maximum limit of the solar share during time t;
Ω_1	The binary variable represents the occurrence of a solar outage ;
Ω_2	The binary variable indicate the thermal contingency event;
χ	Binary time-activation variable;
Υ_j	Per unit cost of j-th solar plant;
ζ_{ch}	Binary indicator of charging ;
ζ_{dis}	Binary indicator of discharging;
$\mathcal{R}^t_{tot}$	The total system reserve in any hour;
$\mathcal{R}^t$	The available system reserve at time t;
$\mathcal{R}^t_{\Gamma}$	Available system reserve in solar power penetration hours;
$\mathcal{R}_{req}$	The reserve power required by the system;

Chapter 1

Introduction

1.1 Background

Thermal power generation is a conventional way of producing electric power and is considered as a main source of electric power generation. Since decades, the power dispatch from thermal energy sources at minimum operational cost has been a significant part of research [1]. In thermal power generation, the relationship between the input (fuel consumption) and the output (power generated) of a thermal unit is typically characterized by a polynomial function . This polynomial represents how much fuel is required to produce a certain amount of electrical power. It is often referred to as the input-output curve or the fuel cost function [2]. The constrained operational optimization in a conventional power system involves two separate problems namely unit commitment (UC) and economic dispatch (ED), to minimize the overall cost of operation for a given set of load demand over a specified time period [3].

1.1.1 Unit commitment

UC problem aims to find the optimal combination of thermal units from available set of thermal units to meet the load demand and minimize the scheduling cost [3]. The objective function of UC is subjected to some constraints such as system spinning reserve (SSR) constraint, must run units, minimum up time of thermal units, and minimum down time of thermal units. Unit commitment problem is solved by many conventional methods, among them the most talked about include, Priority list scheme, dynamic programming, Lagrange Relaxation method, and mixed integer linear programming [3].

The operational constraints of unit commitment (UC) refer to the technical and practical limitations that must be considered when determining the ON/OFF scheduling of power generation units in a power system [4]. Unit commitment aims to determine which generators should be turned ON or OFF, and when, to meet the demand at the lowest possible cost while satisfying these constraints. The objective function of UC is formulated by using constraints and decision variables as shown in fig 1.1. The final out put of UC after execution of optimizer is UC schedule for complete time horizon. Some key operational constraints in

unit commitment include, power balance constraint, generation capacity limits, minimum up/ down time, start up and shut down cost, ramp rate limits, and SSR requirements

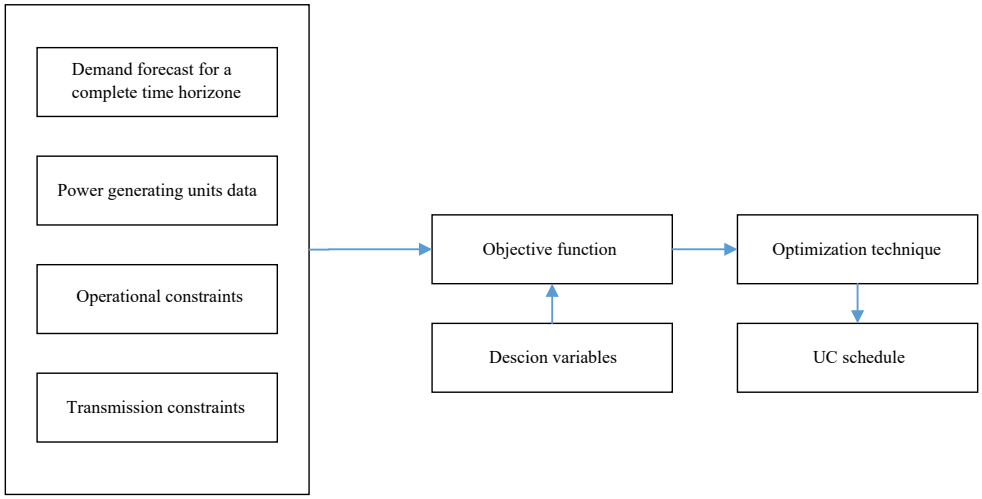

Figure 1.1: Block diagram of unit commitment (UC)

1.1.2 Economical dispatch

The economical power generation from each thermal unit is allocated by solving ED problem. Various types of optimization techniques are reported in literature to solve Ed problems. In the literature, many conventional and artificial intelligence (AI) optimization schemes have been proposed to address ED optimization. Conventional ED optimization schemes involve gradient search, lambda iteration, Newton's method, etc., whereas AI techniques involve algorithms such as the genetic algorithm [5], particle swarm optimization (PSO) [6], neural networks [7], tabu search [8], and evolutionary programming. The simplified block diagrame of ED is represented in figure 1.2. The operational constraints of economic dispatch are the limitations or requirements that power generation systems must meet while optimizing the cost of power production. Economic dispatch aims to minimize the total cost of generating electricity while meeting the system's load demand, but various technical and practical factors impose constraints. Key operational constraints include, power balance constraint, Generation capacity limits, Ramp rate limits, Minimum up/ down time, transmission lines limits, losses in transmission,

and operating reserve requirement constraint.

1.1.3 System constraints

Power system constraints are the technical, operational, and regulatory limitations that govern the operation of an electrical power system to ensure that it functions reliably, safely, and efficiently. These constraints must be respected in the processes of power generation, transmission, and distribution.

In a power system, these constraints ensure the system operates and are critical factors that must be considered during the operational optimization. When performing tasks like economic dispatch, unit commitment and reserve requirements, the major constraints like power balance constraint, generation capacity limits, ramp rate constraint, transmission line limits (Thermal limits), spinning reserve constraint,voltage constraints, frequency constraints, reactive power constraints, minimum up and down time, RE and energy storage constraints are typically encountered [9].

1.1.4 Hybrid power system

A conventional power system refers to the traditional method of generating, transmitting, and distributing electrical power using well-established technologies, primarily based on non-renewable energy sources. These systems have been the backbone of the electricity supply for many decades and typically involve large, centralized thermal power plants generating electricity from fossil fuels and nuclear energy. Conventional power systems are facing many challenges like, environmental Impact, resource depletion, operational inflexibility [10], and cost of maintenance and fuel.

In recent years, there has been a shift away from conventional power systems towards modern power systems. The modern power systems are undergoing major transformation from conventional power generation to hybrid power system (HPS) in which RE sources and energy storage systems (ESS) are being integrated with conventional power generation system in order to save depleting conventional energy sources (fossil oil, coal and natural gas) and to reduce the carbon di-oxide and other gases emissions [2, 11]. In [12], structure of regional integrated energy

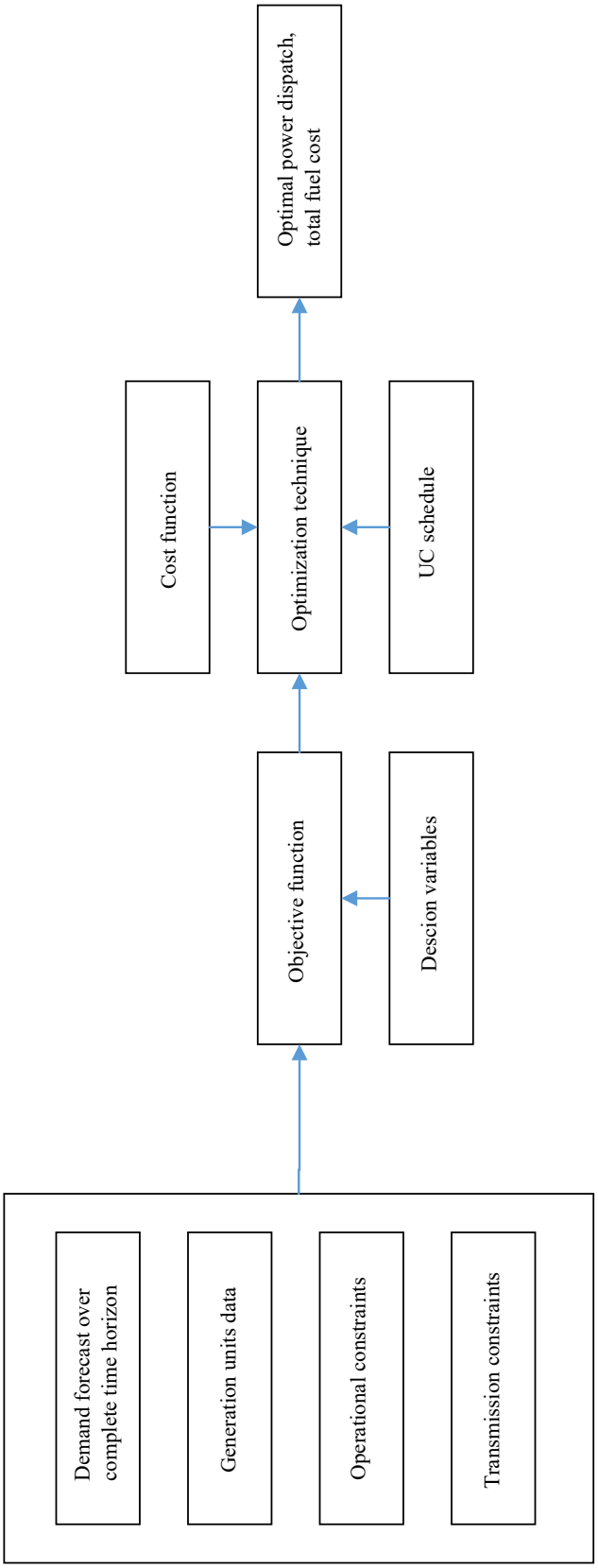

Figure 1.2: Block diagram of economical dispatch (ED)

system is discussed for operation optimization of multi energy stations as shown in figure 1.3. The most widely used renewable energy technologies are solar pho-

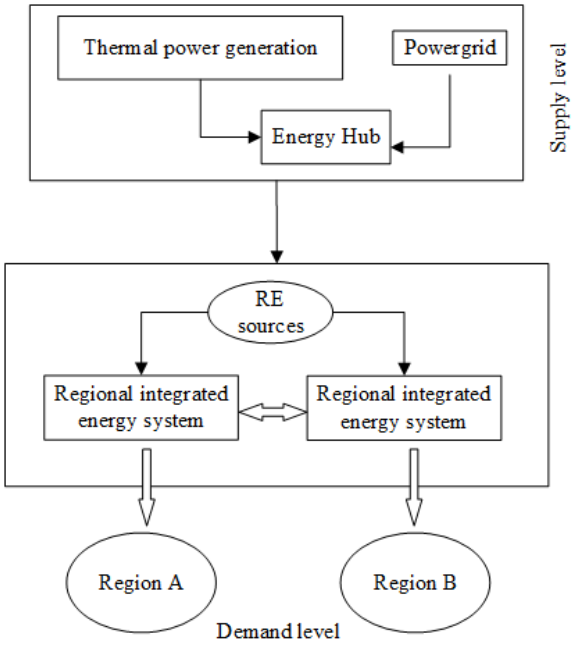

Figure 1.3: Regional integrated energy system structure [12]

tovoltaic (PV) systems and wind turbines. These sources have no operating cost and generate clean, environmentally friendly energy, which is their primary advantage; however, they also have a significant impact on system reliability and power quality [13, 14]. The energy generated from these sources created new technical and operational challenges for power system operators like, intermittency, transmission Constraints, and Energy Storage devices [15].

Renewable energy (RE) sources facilitate establishing a sustainable electricity supply; nevertheless, they significantly impact reliability and power quality as they are stochastic, uncontrollable, variable, and mostly unpredictable. In addition, most of the commonly preferred RE technologies do not provide inertia support, which makes the grid vulnerable in the event of fault conditions. Overcoming these challenges requires additional auxiliary support systems and, more importantly, a monitoring and communication network.

To obtain aforementioned benefits of R.E sources in a hybrid power system, it is necessary to optimize over all operation of this power system.

1.1.5 Operational optimization in HPS

Operational optimization in HPS is subjected to various thermal units and system constraints such as, power generation bounds, ramping limits, power balance, system spinning reserve limits, etc [2, 4, 16]. Reliability in a power system is an important issue to deal, therefore, the factor of intermittent nature of RE sources is considered as a challenge during operational optimization. A reliable integrated power system must remains functional and meet load power demand in case of outages of RE sources or thermal contingencies events.

1.2 System spinning reserve

Spinning reserve of a committed power generating unit refers to extra power which can be delivered, above its power being dispatched in a certain time interval [2]. The cumulative spinning reserve power of all committed units is referred to as the system spinning reserve (SSR), which serves as a rapid response mechanism to sudden load increases or unexpected outages of thermal units. It is necessary to provide sufficient amount of SSR to a power system for the continuity of electrical power to connected loads. In conventional economic operation, adequate SSR is desired to guarantee secure system operation in case of any thermal contingency event. The increasing tendency of penetration of intermittent and price responsive RE has posed new challenges to the allocation and formulation of SSR. In such power systems, deficiency of spinning reserve may result in curtailment of RE as well as load shedding. Thus, an adequate amount of SSR must be allocated to ensure reliable system operation in case of RE outage as well.

Scheduling sufficient SSR can reduce the probability and severity of loss of load [17]. Thus it can mitigate considerable social and economical costs of occasional supply interruption caused by outage of power system components. However providing SSR has a substantial cost because additional units may need to be committed and some other units may operate less than their optimal output. When the SSR requirement increases, the total operation or scheduling cost of power systems increases while the social and economical cost caused by unexpected loss of load decreases [17]. Conversely, when the SSR requirement decreases, the to-

tal operation or scheduling cost of power systems decreases while the social and economical cost increases. So the SSR requirement needs to be assigned appropriately.

1.2.1 SSR estimation in power system

The allocated SSR has been formulated using deterministic, stochastic, and robust models [18]. The deterministic formulation of the SSR allocates a predetermined reserve power that is equal to a specified fraction of the peak load demand or the capacity of the largest committed generating unit. In a probabilistic formulation approach, the SSR is allocated based on the probability of failure of the thermal units as well as the intermittent behaviour of RE generation. Thus, the optimal probabilistic reserve depends on the penetration level of the RE sources and their uncertainty models [19]. The robust SSR formulation allocates an 100%–upward SSR for the worst case scenario of the outage of RE sources while less conservative alternatives recommend lower margins according to their origin, scale, and dispersion [20, 21].

1.2.1.1 Optimize SSR by successive iteration of Unit Commitment

in [22,23] SR is optimized within the UC problem. This approach postprocesses the UC schedule to compute the system reliability level in each optimization period. If the reliability level is greater than the specified target, SSR is adjusted and the UC optimization process runs again. This approach is computation intensive since several UC computations have to be performed before the specified risk target is realized.

1.2.1.2 Optimizing SR by cost/benefit analysis

in [24], the SR requirement is determined by the cost/benefit analysis. The objective is minimizing the scheduling cost (SC) and the expected interruption cost (EIC). The benefit is represented by the reduction of EIC. Compared with the conventional UC problem, an additional term (EIC) is added in the objective function. When SSR increases, the SC increases while the EIC decreases. When SSR decreases, the SC decreases while the EIC increases. This approach can

automatically determine the optimal SSR by a tradeoff between reliability and economics. The relationship between SC, EIC, and total cost is illustrated in figure. 1.4.

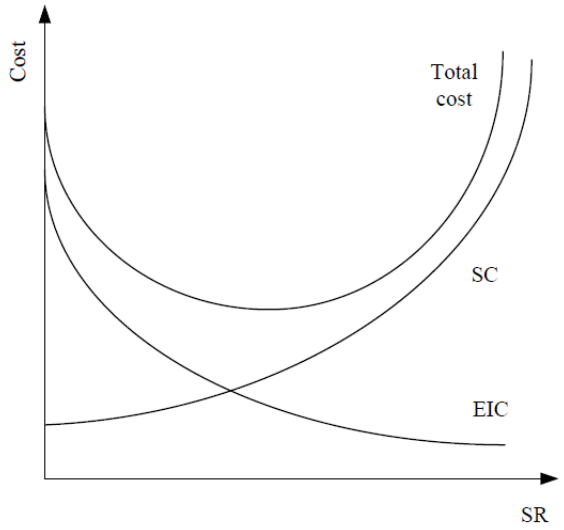

Figure 1.4: Cost benefit analysis [24]

1.3 Motivation and objectives of proposed work

The economic operation of modern RE integrated power systems has become more complex and challenging optimization problem as compare to conventional power systems due to the uncertain and intermittent nature of RE sources [13–15]. This uncertain behaviour of power generation from RE sources in a HPS effects the optimization of thermal power generating sources also. SSR formulation and its allocation, storage system capacity, and power penetration from RE sources depend on each other. Network topological changes is another factor which increase complexity of a HPS. The intermittency of RE sources draw our attention to the issue in HPS that, a HPS must be in functional in worst case scenarios. One of the worst case which is dealt in our research is that, the complete outage of RE sources and thermal contingency event occur at same time.

We aim to find out the limits of power penetration from RE sources , when multiple RE sources are integrated with thermal units under the consideration of worst case scenario. It involves optimization of fuel cost, cost of RE, penetration

level of RE, and an optimal selection of RE sources subject to various constraints such as power balance, power bounds on thermal powers, RE penetration limits, reserve power limits, ramp rate limits, etc. To fulfil this aim , the following research objectives have been established:

- The first objective of this thesis is to maximize the RE share and minimize the thermal generation fuel cost, such that the HPS remains robust for worst case scenario.
- The second objective of this research is to maximize the number of renewable energy RE sources contributing power, thereby enhancing system dependability while minimizing the cost of renewable power penetration in presence and absence of storage system.

The storage scheme will be implanted in such a way that it will be allowed to charge by RE sources only and this ESS will be responsible to provide the reserve power in case of solar power outage or thermal units contingency event. The HPS will be then optimized in order to reduce the operational cost and maximize the RE share. We will emphasize to analyse the problems for possible simplifications and to seek efficient solutions by implementing appropriate optimization techniques. We also aim to extend the work further to the operation of more challenging problem with dispatchable load.

1.4 Research gaps and problem statement

A power system has always a limited amount of spinning reserve power due to system constraints, which leads to a limited amount of power penetration from RE sources into the power system. The SSR of a power system, in literature is allocated by using deterministic, probabilistic/ chance based senarios and robust criterion [18].

In [17], [25–28] for a RE integrated power system, the probability of outage of power from RE sources and the probability of occurrence of contingency event in thermal power generating unit is used to calculate probabilistic SSR and then the amount of power penetration from RE sources is made equal to the reserve capacity of of power system . The chance based scenarios are considered in [18] in order to

make an efficient allocation of SSR. In probabilistic or chance based allocation of SSR, the partial or complete power outage from RE sources is successfully coped by the reserve power allocated to thermal units and ESS. However the simultaneous outage of power from RE sources and thermal contingency event leads to power deficit. According to our best knowledge, the following limitations are found in literature,

- The simultaneous occurrence of outage of RE and thermal contingency event in presence or abscess of ESS is not dealt for a robust system.
- The affect on penetration level of power from RE sources has not been analysed in literature, if system is made robust against thermal contingency event or complete outage of power from RE sources (which event occurs first will be dealt first).

The first novelty of presented research is that, the limits of RE share in a HPS are calculated so that the system maintain its robustness with in these limits. As, most of the RE sources are weather dependent and their outage probability is high, therefore, the limits of RE penetration are calculated under the worst case scenario in which thermal contingency event and RE outage takes place simultaneously. The second novelty of this research is the determination of renewable energy share limits in hybrid power systems, ensuring system robustness under thermal contingencies and renewable outages when these events do not occur simultaneously. Furthermore, if an ESS is available, then a scheme of implementation of ESS is presented.

1.5 Major Contributions of this thesis

This research presents an RE integrated power system operation and identifies research laps in the existing literature. Based on these research gaps, this research develops an optimization framework. Following are the main contributions of this work:

- The solar share is maximized within the boundaries of a robust SSR such that the power deficit does not exist.

- The range of a robust SSR is determined that can accommodate an additional RE share provided that compromise on the power deficit is possible in case of thermal contingency event.
- This study minimizes the operational cost and maximizes the number of solar plants with an ON status in order to enhance the solar power availability.
- The proposed model was implemented and simulated on an IEEE-RTS 26-unit system.
- The optimal reserve constraint UC (ORCUC) was carried out using Lagrange relaxation (LR), and ED was executed through a Lambda iteration binary search method [3]. Furthermore, a set of Pareto-optimal solutions was found for the selection of solar plants.
- A novel application scheme of storage system in HPS is introduced in order to lift the burden of reserve power from thermal units for thermal contingencies.
- Solar power share is maximized by using ESS.

The above mentioned contributions of our research will make existing HPS more robust for the worst case scenario. The worst case scenario occur when thermal units contingency event and solar share outage occur simultaneously. Th applied ESS will decrease the fuel cost of thermal units by excluding cost of optimal reserve and increase the solar share without any compromise on robustness of the system.

Distributed solar PV plants at generation side are the only RE sources which are considered in this thesis, however, any solar PV plant can be replaced with other RE source like wind turbine or bio-fuel power plant. This replacement of RE sources will not effect the proposed methodology.

1.6 Scope of the thesis

Economical dispatch, unit commitment, solar share optimization of a solar PV and ESS integrated power system consisting of thermal power units, fall in the scope of this thesis. The process of determining the reliable RE share in a HPS belongs to the scope of this research also. The calculation of environmental benefits

by integration of RE sources with power system is out of the scope of this thesis. Energy storage solutions from RE sources, power electronics devices attached with RE sources, climate resilience, policy and regulatory of power systems, forecasting and planning of RE sources, energy security and independence, and cybersecurity is also out of the scope of this thesis.

1.7 Research Methodology

The research adopts an optimization-based framework to analyze unit commitment, spinning reserve allocation, renewable energy integration, and the role of energy storage systems in HPS. The methodology is carried out in two projects.

In the first project, a mixed-integer optimization problem is formulated to achieve the objectives of minimizing system operating costs while maintaining reserve adequacy and maximizing the RE share. The problem is decomposed into subproblems for computational tractability, after which unit commitment with reserve constraints is performed for a 24-hour horizon using the Lagrangian Relaxation method. Economic Dispatch is then executed by applying the Lambda Iteration method to meet the hourly load demand at minimum cost. Based on the committed generation units, the system spinning reserve is calculated for each hour. Renewable energy penetration is then gradually introduced into the system in increments of 20 MW. For each incremental penetration level, Economic Dispatch is repeated and the SSR is recalculated. This process continues until the available spinning reserve becomes less than the renewable penetration, which defines the maximum allowable renewable share. At this stage, various results are recorded, including economic dispatch outcomes, hourly spinning reserve, thermal generation and its associated fuel cost, and the limits of renewable energy penetration under contingency and outage scenarios. To further ensure a balanced integration, binary integer programming is employed to obtain Pareto-optimal solutions that maximize the number of solar plants while minimizing solar integration costs, thereby identifying a reliable solar penetration share.

In the second project, the methodology is extended by incorporating an ESS. In this case, unit commitment is performed without reserve constraints, both UC and ED is executed for each incremental level of renewable penetration. Results are

obtained in this project include ED results, spinning reserve, thermal generation, and renewable share limits. The results of both projects are then compared to determine the performance improvements and reliability benefits achieved through the application of ESS.

This structured methodology enables the research to systematically address spinning reserve requirements, quantify renewable penetration limits, and evaluate the advantages of energy storage in enhancing both system reliability and cost-effectiveness.

1.8 Key decision variables of research frame wok

A detailed mathematical formulation will be provided in Chapte 3; however, main decision variables considered in this research are summarized in Table 1.1. In this study, our focus was on SSR allocation and its analysis in hybrid power systems by considering the constraints of thermal units, solar power generation and penetration limits, SSR constraints, ramping limits, minimum up/down times, storage system constraints, and power balance. Variables such as network constraints, demand-side participation, or other renewable energy sources were not included in order to keep the scope of the research clearly aligned with the stated objectives. Including these aspects would significantly expand the problem complexity and deviate from the primary focus of this thesis

Table 1.1: Key Decision Variables of the Study

Variable	**Description**
P_i^t	Power generated by i-th thermal unit at time t
U_i^t	Binary variable for the ON and OFF status of the i-th thermal unit at time t
Ps^t	Penetrated solar power during time t
Us_j^t	Binary variable used at time t to represent the ON and OFF status of a solar plant
Γ^t	Solar share based on the SSR during time t

1.9 Thesis organization

This thesis is organized as follows

- Chapter 2 consist of related work and detailed literature review of our research work.

- Chapter 3, presents modelling of solar PV integrated power systems. The model is investigated for the range of robust SSR and penetration of solar power within this range. The amount of power deficit and robust SSR is calculated if penetrated solar power is greater then the robust SSSR. The limits of solar power are also calculated when optimal allocated SSR is not allowed to dispatch in case of complete or partial solar power outage.

- In Chapter 4 , the optimization model is enhanced by including additional feature of ESS and adopting a novel decomposition framework.

- Finally, Chapter 5 provides conclusions and the future directions of this work.

1.10 Summary

This Introduction chapter of thesis serves to provide a foundational understanding and an overview of proposed research work, its significance, and the overall research objectives. In this chapter, the problem statement and objectives to be achieved are clearly stated and the context of dealt problem is presented with its background and related topic like UC, ED, SSR estimation, optimization techniques, and system constraints. The objectives, that are achieved in this dissertation and major contributions of proposed research work are listed.

Chapter 2

Literature review

2.1 Related works and limitations

UC and ED has been one of the most frequently investigated problems in conventional thermal power systems [29, 30]. It was the time of 1954, when the the computational efficiency started to increase by means of digital computers [31]. Developments in computer aided computations continued and provided ways to find the efficient solution of ED and UC in power system. In recent years, there has been extensive research around the concept of optimal Unit Commitment (UC) in power systems, particularly exploring the efficiency of deterministic and stochastic programming approaches [32]. UC problem is solved by conventional Lagrange relaxation method in [32–37]. During the time period of 1977-1988, many variants of ED optimization were developed such as optimal power flow, dynamic dispatch, and ED dealing with automatic generation control [38]. The economical dispatch point of a power system consisting of thermal units is determined by using fuel cost function of a each thermal unit. [16].

Traditionally, smooth convex cost function is used for solving ED problem and many efficient solution have been proposed [39, 40]. However, fuel cost function remains no more smooth convex and becomes non-convex when complex characteristics of commonly used generation facilities are involved [41]. For instance, ripples like effects in the cost function of a thermal uni equipped with multi-valve steam turbine are originated due to oppening and closing of valves which make cost function essentially a non-convex [42]. Other aspects in addition to valve point effect such as multi fuel options and prohibited zones are also the causes of non-smoothness of cost function in ED optimization [43,44]. Non-convex transmission-constrained ED problem is approximated by the convex problem obtained by linearising the constraints around some base-case state [45]. In literature, complex ED problem is addressed by various artificial intelligence based optimization techniques e.g., neural network [7, 46], genetic algorithm [5, 47, 48], evolutionary programming [49]– [50] particle swarm optimization (PSO) [6,51–53], and tabu search [8]. In [54], improved butterfly optimization algorithm is used for stand-alone system and Numerous methods have been proposed in literature to allocate optimal SSR to the committed thermal units. The available SSR models

have been formulated as deterministic, stochastic, and robust model [18].

Deterministic formulation for allocation of SSR provides a predetermined amount of reserve equal to a specified fraction of peak load of power demand (P_d) or the capacity of the largest committed generating unit. In probabilistic formulation approach, SSR is allocated based on probability of failure of thermal units as well as intermittent behaviour of RE generations. Thus, the optimal probabilistic reserve depends on the penetration level of RE sources and their uncertainty models [19]. The robust SSR formulation allocates 100 % upward SSR for outage of RE sources while less conservative alternatives recommend lower margins according to their origin, scale, and dispersion [20, 21].

In [9, 55–57], deterministic SSR of $0.3P_d$ was allocated to RE integrated power systems. However, the contingencies events of thermal units were ignored and thus, the optimal reserve allocations to individual units were missing. The authors in [58] proposed deterministic SSR allocation by Lagrange relaxation (LR) while taking into account the thermal contingencies and adaptive semi-infinite program was used in [59] to allocated SSR based on uncertainty sets. Furthermore, the authors in [60] proposed $N-1$ criterion for allocation of deterministic SSR and solved the optimization by mixed integer linear programming. However, deterministic approach intrinsically ignores the actual reserve requirements as well as uncertain behavior of RE sources [61].

In [62], the authors developed a day-ahead scheduling model for power systems with high RE integration. The model incorporates RE uncertainty into the UC framework to optimize both generation scheduling and reserve allocation. Case studies showed that the approach enhances economic efficiency while maintaining system reliability. However, the study did not include an ESS model, ignored thermal unit outages, and applied a deterministic reserve allocation based on a fixed percentage of system load. As a result, the allocated reserve could only compensate for a fraction of RE outages and may be insufficient under large-scale contingencies. Thus, the probabilistic approach has been adopted in literature to reduce the reserve cost by considering probability of occurrence of contingency. The works in [17] and [25] proposed a multi-step method in which EENS function was approximated as linear function to find out the probabilistic optimal SSR for

conventional as well as RE integrated power systems. In [63], probabilistic SSR model was adopted and the optimal SSR was calculated for conventional power systems considering first order as well as second order thermal unit contingencies. In this work, the cost of dispatched power as well as the cost of EENS were modelled as a function of SSR and the composite optimization of dispatched power cost and EENS cost was solved for optimal SSR using cost benefit analysis technique. Further, the work [64] developed a new constraint known as umbrella contingency constraint and carried out umbrella contingency constrained UC optimization to find out probabilistic optimal SSR for conventional power systems. Security constrained day ahead economic operation of solar PV aided micro grid was carried out in [65] to calculate the optimal probabilistic operating reserve. The PV uncertainty was assigned according to different scenarios and their probabilities of occurrence at each half hour. The authors in [66] proposed simultaneous optimization of load shedding, RE curtailment and optimal SSR by priority list schemes as well as genetic algorithm. In [67], stochastic programming was exploited to obtain stochastic scenario-based SSR for wind aided power systems. This work was further extended by [68] in which the authors achieved scenario based SSR for hydro and wind integrated power system by weighted improved PSO.

In [69], an EENS ratio-based approach was introduced to quantify spinning reserve requirements in high wind penetration systems, explicitly incorporating unit outages, load variations, and wind forecast errors. Building on this quantification, the authors developed a coordinated generation and reserve dispatch model that minimizes system operating costs while satisfying reliability constraints. However, the probabilistic reserve was allocated only among thermal units, and the ESS was not considered.

The work in [70] developed an operating reserve optimization model for high-renewable power systems, integrating the contribution of ESS as reserve providers to enhance system flexibility. Case studies demonstrated that the method improves reliability and reduces operating costs. However, the analysis was limited to a relatively small test system, excluded unit commitment decisions, and was restricted to a purely probabilistic framework. In addition, simultaneous outages of renewable and thermal generation units were not explicitly investigated.

Probabilistic allocation of SSR does not ensure continuity of system operation in case of RE outages. Thus, most of the recent works have proposed robust models of SSR for RE integrated power systems e.g., hybrid PSO in [71] and Gaussian based bayesian optimization in [72] for both the PV and wind connected power system provided the robust SSR formulation. In [27], cluster based robust SSR model was developed for the economic operation of RE integrated power system consisting of thermal generation units, solar PV, wind, biomass, and storage devices. The value of allocated SSR is chosen between maximum value of available RE power and value of power generated from largest capacity thermal unit. This work was focused to investigate the impact of ESS on cost of UC optimization with robust allocation of SSR. The study in [73] introduced a robust day-ahead reserve scheduling strategy that coordinates the passive thermal storage of buildings with conventional generators to manage spinning reserves under uncertainties from RE and potential generator failures. However, the work primarily focused on addressing load rebound issues, and did not incorporate UC or ESS models. The SSR calculated in this way will be no more robust in case of simultaneous outage of RE power and thermal contingency and loss of load will occur.

The work in [74] presented operation model for autonomous RE integrated power systems under additional frequency constraints and frequency based allocation of the spinning reserve. The applications of ESS in power grids with RE sources is discussed in [75]. In [76], the study examined a hybrid energy system for residential buildings that integrates ESS's with RE in which multi-objective optimization approach is employed to simultaneously address energy, economic, and environmental objectives. The work [77] developed a model for grid connected RE sources of an institution to reduce the power system's NPV over its lifespan.

This work is limited to the demand side management with RE sources, which is a small portion of a HPs. The grid was supposed to be always available to deliver any reserve power in case of RE failure. However, the scenario becomes different when large scale RE sources are integrated with thermal power generating units and the combined power of RE sources and thermal units has to dispatched to meet the power demand of large area. Thus, these research could not address the challenges of actual RE integrated power systems at generation side.

in [78], A modified bacterial foraging algorithm is proposed to optimise wind power generation integrated power system with storage, in order to reduce wind power curtailment, reserve cost, and reduction of thermal generation cost. The study proposed in [79], a novel optimization operation framework for a pumped storage power station driven by the peak-shaving and valley-filling operation for boosting power grid absorbing ability to renewable energy inputs. Similarly, the assessment of performance of pumped hydro power ESS connected to hybrid system of solar PV and wind turbines was carried on in [80]. The work presented in [58]calculated optimal power rating and energy capacity of storage system, modelled and evaluated via a life-cycle cost analysis, to facilitate the RE integration to conventional power system. ESS is used to replace the SSR deficit. However the effect of RE penetration and storage system on reserve power of thermal units was missing. The advent of RE sources marks a pivotal transition towards sustainable and eco- friendly power generation. RE technologies like solar, wind, and hydro are gaining prominence, offering cleaner alternatives to traditional fossil fuels.

Table 2.1: Comparative list of optimization of existing power systems with respect to SSR formulation and UC objectives

Refs.	**UC method**	**Formulation of SSR**	**Contributions**	**Limitations**
[81]	Priority list	Deterministic	Use of fast converging technique used for large scale power system.	RE and ESS were not considered.
[67]	UC with Stochastic programming	Stochastic scenario based	Multi stages decomposition technique is applied to a wind integrated power system.	ESS was not integrated.

[82]	Improved MILP approach	Roust	Optimize HPS with thermal, hydro, wind, and pumped storage system.	Optimal selection of RE sources from available RE sources was not performed and the worst case scenario in HPS was not considered. Power penetration from RE sources is limited by SSR, i.e., 10% of load demand.
[58]	Lagrange Relaxation method	Deterministic	Time interval classification based solution with PV and batteries.	Worst case scenario and solar plants optimization in HPS was not considered.
[68]	Gravitational search algorithm	Robust	Multi objective optimization with hydro solar, and pumped storage. Trade-off between cost and utilization of RE	Worst case scenario and RE optimization is missing.
[83]	Weighted improved PSO	Scenario based	Efficient utilization of RE with Wind, hydro, emissions, and pumped storage.	Worst case scenario and RE optimization is missing.
[72]	Gaussian process-based Bayesian optimization	Robust	Uncertainty-aware machine learning model is used to enhanced RE integration and to reduce production cost.	ESS, RE sources selection optimization and worst case scenarios were not considered.
[71]	Hybrid PSO	Robust	PV and wind	ESSand worst case scenarios were not considered.
[84]	Sequential quadratic programming	Distributional robust	Efficient evaluation of maximum ramping capabilities with PV, wind and storage.	Worst case scenario in HPS is not considered.

[85]	Stochastic programming	scenario-based	Reliability and expected cost of system is reduced by considering pumped storage system.	RE is not integrated in system.
[59]	Adaptive semi-infinite program	Uncertainty sets .	Discussed the temporal and spatial correlations of wind and solar power under effect of ESS	Optimal selection of RE sources and worst case scenario were missing.
[86]	Mixed integer cone programming	Data-adaptive robust	flexible and higher range results with wind power for hybrid networks.	ESS and worst case scenario was not considered.
[87]	Stochastic programming	Forecast confidence level-based	An applicable function satisfy the forecast deviation in a wind a Pv integrated power system.	ESS, RE sources selection optimization, and worst case scenarios were not considered.
[60]	Mixed integer linear	N-1 criterion	Comparison of priority list method and MILP for a PV and wind integrated system.	Storage system and worst case scenarios were not discussed.

Proposed work	The proposed system consist of thermal units integrated with distributed solar PV plants and storage system. Optimal SSR is provided by reserve constrained UC through Lagrange relaxation optimization technique. Solar power share is penetrated with in the limits of robust SSR. The worst case scenario for a HPS is dealt. The optimization for selection of solar plants is performed by MILPand pareto optimal solutions are obtained.	The assessment of environmental benefits from integrating renewable energy (RE) sources into the power system is beyond the scope of this research. Likewise, topics such as energy storage, power electronic interfaces for RE systems, climate resilience, policy and regulatory issues, RE forecasting and planning, energy security, and cybersecurity are not addressed in this study.

From the above-cited literature, it can be deduced that the SSR is calculated by using either a deterministic, probabilistic, or robust approach, and the reserve-constrained UC (RCUC) is carried out based on that pre-calculated SSR. However, the worst case scenario in which simultaneous outage of RE sources and thermal contingency events occur, are not discussed in literature after allocation of SSR. Rather, whichever event occurs first is served by dispatching the allocated SSR. Thus, if the other event occurs at the same time, it may lead to either a partial loss of load or complete blackout, i.e., the failure of system operation. Furthermore, it may not be viable for the system operator to penetrate all the available RE due to system constraints. To the best of our knowledge based on the most recent and relevant literature, there has not yet been a comprehensive work that has dealt with such issues.

Unlike the existing literature, this study proposes a two-step model for the reserve-constrained economic operation of solar-integrated power systems. In the first step, the optimal SSR is calculated, and then, the optimal reserve-constrained

unit commitment (ORCUC) is executed. Next, the limits of the robust SSR are determined for the maximum penetration of the RE, and ED is carried out. Our proposed model is able to address the aforementioned problems of the existing literature by answering following research questions in presence and absence of an ESS:

(i) What are the limits of the robust SSR as well as of the corresponding RE share in RE integrated power system?

(ii) To what level can the RE share be increased such that the allocated SSR lies within the robust range and $SSR^{t}_{opt(1,2)}$ is dedicated for thermal contingencies only?

(iii) How much can the RE power share be supported by a set of committed thermal units under the robust SSR if $SSR^{t}_{opt(1,2)}$ is supposed to be dispatched for RE as well as thermal outages?

(iv) What is the value of the maximum SSR SSR^{t}_{ul} that can be achieved with a set of committed thermal units?

(v) How the addition of ESS affects the level of power penetration from RE sources?

(vi) What would be the application scheme of storage system that is to be added in HPS under the consideration of thermal contingency, RE outages, and storage power dispatching hours.?

2.2 Summary

This chapter has presented a variety of research work in the field of optimization of conventional and RE integrated power systems. HPS's with and without ESS are optimized in literauture by using different optimization techniques. We have analysed, compares, and evaluates various studies and critically reviewed many aspects of recent researches presented in section 2.1. It is found that there are areas within the existing body of research that have not been sufficiently addressed and further investigation is needed. We identified research gaps in the form of

questions in section 2.1. We proposed an optimization approach, contributing new insights and applications to fill these voids that will move the this research field forward.

Chapter 3

ED and SSR in Solar Integrated Power System

3.1 Introduction

Thermal units contingencies events and outage of RE from a solar PV integrated power system may occur,therefore a sufficient amount of SSR is required in order to avoid loss of load. Most of existing work in literture integrates RE sources on the basis of deterministic formulation of SSR. Moreover this SSR is dispatched without any discrimination whether the power outage occured from thermal units or from solar plants. This chapter presents a novel method of determining the limits of power penetration from RE sources within the limits of robust SSR. We also find the amount of power deficit in case of power penetration more than the limit of SSR and the limits of robust SSR and penetrated power from RE source, on the basis of $SSR_{opt(1,2)}$ is allowed or disallowed to dispatch for solar power outage.. We have solved the problem in MATLAB by using conventional optimization method i.e., Lagrangian relaxation and Lambda iteration binary search.

3.2 System model and problem formulation

3.2.1 System model

We consider a solar PV and thermal units HPS, consisting of n number of thermal units and m number of solar power generating plants, supplying power to satisfy the connected load power demand P_d as shown in Fig, 4.1. Let P_i is the economical power dispatched by i^{th} thermal generating unit, the fuel cost $F_i(P_i^t)$ of i^{th} thermal unit is determined by P_i and cost coefficients a_i, b_i, and c_i as:

$$F_i(P_i^t) = a_i P_i^2 + b_i P_i + c_i \tag{3.1}$$

where a_i, b_i, and c_i are the fuel cost coefficients of the i-th thermal unit. Any thermal generation unit may be desired to turn ON or OFF to fulfil the requirements of the system operation. A binary variable U_i^t is introduced to denote the ON and OFF status of the i-th generating unit at any given time t. The ON/OFF status of the i-th unit is give by

$$U_i^t = \begin{cases} 1, & \text{if } i\text{-th generation unit is ON,} \\ 0, & \text{otherwise.} \end{cases} \tag{3.2}$$

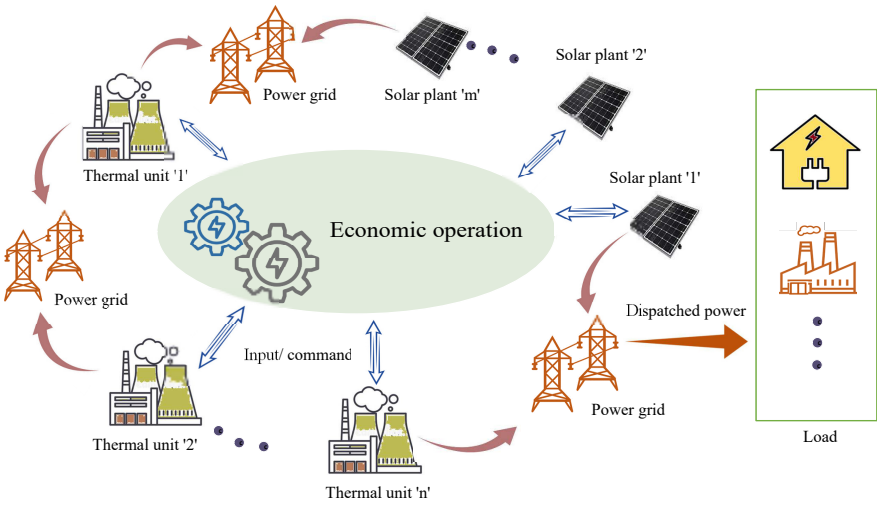

Figure 3.1: System model

Furthermore, P_i must not exceed its upper and lower bounds, i.e.,

$$P_{i,min} \leq P_i^t U_i^t \leq P_{i,max} \qquad \forall i = 1, 2, \ldots, n, \tag{3.3}$$

where $P_{i,min}$ and $P_{i,max}$ are the minimum power limit and maximum power limit of the i-th thermal generation unit, respectively.

A thermal generation unit cannot follow abrupt load variations to increase or decrease its power. Rather, the power P_i^t can only be varied with certain ramp up and ramp down rates. Thus, the available up-reserve and down -reserve at any given time are limited by such ramping rates as

$$R_{i,up}^t = min(P_{i,max} U_i^t - P_i^t U_i^t, \tau R_i^{\uparrow} U_i^t), \tag{3.4}$$

$$R_{i,down}^t = min(P_i^t U_i^t - P_{i,min} U_i^t, \tau R_i^{\downarrow} U_i^t), \tag{3.5}$$

where $R_i^{\uparrow}$, $R_i^{\downarrow}$, and τ are the ramp-up rate, ramp-down rate, and time allowed for ramping, respectively. The individual reserves of the on-bar thermal units sum up to produce the SSR to be allocated, i.e.,

$$SSR_{al}^t = \sum_{i=1}^{n} U_i^t R_{i,up}^t. \tag{3.6}$$

An adequate SSR must be allocated to guarantee continuous operation during contingency events. In case of thermal contingencies, the allocated SSR must satisfy

$$SSR_{al}^t \geq SSR_{opt(1,2)}^t, \tag{3.7}$$

$$SSR_{al}^{t} \leq \sum_{i=1}^{n} P_{i,max} U_i^t - P_d^t, \tag{3.8}$$

where $SSR_{opt(1,2)}^{t}$ is the predetermined optimal SSR for the first-order and second-order contingencies in time interval t. Equation (3.7) determines the lower limit of the allocated SSR and states that the SSR must not be allocated to be less than the pre-calculated optimal SSR for the first- and second-order contingencies. Similarly, Equation (3.8) determines the upper limit of the SSR allocation, which states that the allocated SSR must not exceed the maximum of the on-bar reserve power.

The thermal generation units can't be switched from one state of operation to another before the minimum time required by that state is elapsed. For instance, if a generation unit is turned ON at any given time, it cannot be turned OFF again until the minimum ON time is elapsed. Similarly, once a generation unit is turned OFF, it cannot be turned ON before the elapse of the minimum OFF time. Thus, for the transition of the i-th generation unit from one state to another, the following constraints must be satisfied:

$$(T_{i,on}^{t-1} - T_{i,up})(U_i^t - U_i^{t-1}) \leq 0, \tag{3.9}$$

$$(T_{i,off}^{t-1} - T_{i,down})(U_i^{t-1} - U_i^t) \leq 0, \tag{3.10}$$

where $T_{i,on}$, $T_{i,off}$, $T_{i,up}$, and $T_{i,down}$ are the cumulative ON time, cumulative OFF time, minimum uptime, and minimum downtime of the i-th generation unit, respectively.

Between any two consecutive time slots, the power share of the i-th generation unit must not vary beyond certain ramping rates provided that the generation unit remains ON for those time slots. If the power is increased, it should not exceed the ramp-up rate, and if it is decreased, it should not exceed the ramp-down rate, i.e.,

$$P_i^t - P_i^{t-1} \leq R_i^{\uparrow},\ if\ U_i^t = 1,\ U_i^{t-1} = 1, \tag{3.11}$$

$$P_i^{t-1} - P_i^t \leq R_i^{\downarrow},\ if\ U_i^t = 1,\ U_i^{t-1} = 1. \tag{3.12}$$

Let the power of the j-th solar plant be denoted by Pgs_j. The cost at which the plant owner sells energy to the system operator at any given time t is given by

$$G_j^t \left(Pgs_j^t\right) = \zeta_j Pgs_j^t, \tag{3.13}$$

where ζ_j is the per unit of the j-th solar plant. The solar power can be calculated using the watt model as follows [88]:

$$Pgs_j^t = \rho_j^t\{1 + \alpha_j \left(T_a^t - T_r^t\right)\}\frac{S_j^t}{1000}, \tag{3.14}$$

where ρ_j^t is the rated power of the j-th solar plant, α_j is the temperature coefficient, T_a^t is the ambient temperature, T_r^t is the reference cell temperature, and S_j^t is the solar radiation at any given time t.

3.3 Problem formulation

This work deals with the reserve-constrained economic operation of solar-integrated power systems. It aimed to minimize fuel costs, minimize solar costs, maximize solar shares, and maximize the number of solar plants under the provision of a robust SSR. At any time during operation, the robust approach ensures that the allocation of the 100%–upward SSR for any solar power outage. Thus, the system operation becomes more reliable, and the loss of load can be avoided. In contrast, the SSR evaluations from the probabilistic approach come out to be significantly less than the penetrated RE. As the solar energy exhibits an intermittent nature, there always exists a higher risk of loss of load in a probabilistic SSR, which may lead to the failure of the system operation. As the proposed model aims to maximize the solar share, the probabilistic allocation of SSR may increase this risk further in the case of total solar power outage. Furthermore, this work ignored the storage system for simplicity, which also makes the probabilistic approach less promising for the proposed model. Keeping in view such advantages, the authors adopted the robust approach to allocate the SSR.

Before formulating the problem, the questions posed in Section 2.1 must be answered as follows:

Answer (i): The answer to question (i) defines the overall structure of the model in terms of a robust SSR and RE share.

Answer (ii): This answer evaluates the RE share and range of a robust SSR for the scenario if the $SSR_{opt(1,2)}^t$ is dedicated for thermal contingencies. The evaluated RE share should be limited to make the system resilient to any RE outages.

Answer (iii): This answer evaluates the RE share and the limits of a robust SSR

for an undedicated scenario.

Answer (iv): This answer evaluates the overall SSR, whether robust or non-robust, and the corresponding RE share. The problem can be formulated as follows:

$$\min_{P_i^t, U_i^t, Ps^t, Us_j^t} \sum_{t=1}^{T} \left[\sum_{i=1}^{n} F_i \left(P_i^t \right) U_i^t - Ps^t - \sum_{j=1}^{m} Us_j^t + \sum_{j=1}^{m} G_j^t \left(Pgs_j^t \right) Us_j^t \right] \tag{3.15}$$

s.t.,

$$Ps^t + \sum_{i=1}^{n} P_i^t U_i^t - P_d^t = 0, \tag{3.16}$$

$$0 \leq \Gamma^t \leq \Gamma_{max}^t, \tag{3.17}$$

$$0 \leq Ps^t \leq min(\Gamma^t, \sum_{j=1}^{m} Pgs_j^t), \tag{3.18}$$

$$\sum_{j=1}^{m} Pgs_j^t Us_j^t \geq Ps^t, \tag{3.19}$$

and (3.3)-3.12). Where Ps^t denotes the penetrated solar power at any given time t, P_d^t is the load demand, Γ^t is the solar share based on the SSR, Γ_{max}^t is the maximum limit of the solar share based on the available SSR, and Us_j^t is a binary variable used to represent the ON or OFF status of the j-th solar plant. Depending on operation requirements, the j-th solar plant may be turned ON to participate in system operation or may remain OFF otherwise. Equation (3.16) presents a power balance constraint that states that adequate generation must be committed at any given time to satisfy the load demand. Constraint (3.17) presents the solar share based on the SSR and states that a limited amount of solar power can be penetrated into the system, which must not exceed the limits prescribed by the SSR. The variable Ps^t in problem (3.15) and constraint (3.18) correspond to answer (i). The maximum limits of the solar share based on the SSR are defined as follows:

$$\Gamma_{max}^t = \begin{cases} \Gamma_s^t, & \text{if } 0 \leq SSR^t \leq \Gamma^t, \\ \Gamma_c^t, & \text{if } \Gamma^t \leq SSR^t \leq SSR_{ult}^t, \end{cases} \tag{3.20}$$

where Γ_s^t is the maximum limit of the solar share within a robust range of the SSR, when $SSR_{opt(1,2)}^t$ is allowed to dispatch in case of solar power outage. Γ_c^t is the maximum solar share for maximum SSR that can be provided by a committed set of thermal units by RCUC. Power deficit is experienced by the power system, when solar share is selected within the range of Γ_s^t to Γ_c^t . Similarly if . $SSR_{opt(1,2)}^t$

is not allowed to dispatch in case of solar outage then the maximum solar share with in the range of robust SSR will be equal to Γ_d^t.

Furthermore, the solar share also depends on the aggregate available solar power. Thus, the actual solar share must be limited by the aggregate available solar power from the selected solar plants. Constraint (3.18) states that the actual solar share must not exceed the minimum of the solar share based on the SSR and the total available solar power. Finally, constraint (3.19) states that the solar plants must be selected such that there exists enough on-bar solar power to obtain the desired solar share.

Prior to solving problem (3.15), the optimal reserve for the first- and second-order thermal contingency events, i.e., $SSR^t_{opt(1,2)}$, must be evaluated first. To calculate the $SSR^t_{opt(1,2)}$, the following optimization is solved:

$$\underset{SSR}{min}\{f_t(SSR^t) = D(SSR^t) + E(SSR^t)\} \tag{3.21}$$

where $f_t(SSR^t)$, $D(SSR^t)$, and $E(SSR^t)$ are the total cost, running cost, and the EENS cost, respectively. The running cost for each load level must be minimized for a given SSR requirement. Thus,

$$D(SSR^t) = \underset{P_i^t, U_i^t}{min} \sum_{t=1}^{T} F_i\left(P_i^t\right) U_i^t \tag{3.22}$$

$$\text{s.t.,} \quad \sum_{i=1}^{n} P_i^t U_i^t - P_d^t = 0, \tag{3.23}$$

$$\sum_{i=1}^{n} U_i^t R_{i,up}^t \geq SSR^t, \tag{3.24}$$

(3.3)- (3.5) and (3.9) -(3.12).

The EENS cost is calculated as

$$E(SSR^t) = VOLL \times EENS^t, \tag{3.25}$$

and,

$$\begin{aligned} EENS^t \approx & \sum_{t=1}^{T}\sum_{i=1}^{n} p_i^t b_i^t \Big(P_i^t + R_{i,up}^t - SSR^t\Big) + \\ & \sum_{t=1}^{T}\sum_{i=1}^{n}\sum_{j>i}^{n} p_{i,j}^t b_{i,j}^t \Big(P_i^t + R_{i,up}^t + p_j^t + R_{j,up}^t - SSR^t\Big), \end{aligned} \tag{3.26}$$

where p_i^t and b_i^t denote the outage probability of a single unit, i.e., the i-th unit, and the loss of load due to this outage, respectively. Similarly, $p_{i,j}^t$ and $b_{i,j}^t$ denote

the probability of the simultaneous outage of the i-th and j-th units and the loss of load due to this simultaneous outage, respectively. $R^t_{i,up}$ is the available up-reserve from the i-th unit, and VoLL represents the value of the lost load, which is a survey-based fixed value. The EENS is calculated for first-order and second-order thermal outage events only. The higher-order contingency events are neglected, as such events rarely occur in power systems. The first-order outage probability p^t_i and second-order outage probability $p^t_{i,j}$ are calculated as follows [89]:

$$p^t_i = u_i U^t_i \prod_{j=1, j\neq i}^{n} (1 - u_j U^t_j) \quad \forall i, t, \tag{3.27}$$

$$p^t_{i,j} = u_i u_j U^t_i U^t_j \prod_{k=1, k\neq i,j}^{n} (1 - u_k U^t_k) \quad \forall i, j, t, i \neq j, \tag{3.28}$$

$$b^t_i = \begin{cases} 1, & \text{if } P^t_i + R^t_{i,up} > SSR^t \\ 0, & \text{otherwise} \end{cases} \tag{3.29}$$

$$b^t_{i,j} = \begin{cases} 1, & \text{if } P^t_i + R^t_{i,up} + P^t_j + R^t_{j,up} > SSR^t \\ 0, & \text{otherwise} \end{cases} \tag{3.30}$$

where $U_.$ and $u_.$ are the ON/OFF status and the outage replacement rate (ORR) of the .-th thermal generation unit, respectively. The ORR of the i-th generation unit is taken from [89], which is given by

$$u_i = \gamma_i T, \tag{3.31}$$

where γ_i is the failure rate of the i-th unit, and T is the time duration of each optimization interval. It is assumed that unit failures are exponentially distributed and the time to repair is so long that if a unit is failed during an optimization period, it will not be available for the subsequent periods. The resulting $SSR^t_{opt(1,2)}$ is dispatched in case of the occurrence of first- and second-order thermal contingency events [63].

3.4 Propose solution

To solve optimization (3.15), first, problem (3.21) is solved to determine $SSR^t_{opt(1,2)}$ by using the same method as detailed in [63]. Optimization (3.15) is a mixed-integer binary programming task that is hard to solve in its composite form because numerous objectives and constraints are involved. To simplify the solution,

the decomposition of the problem is proposed. By definition, if any part of a problem is independent of the coupling constraints, it can be solved as an independent sub-problem without loss of optimality. Problem (3.15) involves four objectives and one coupling constraint, i.e., constraint (3.16). In looking at the problem carefully, it can be found that the last two objectives are independent of coupling constraint (3.16), as the decision variable Us_j^t does not belong to the coupling constraint. Amongst the rest of the constraints, this variable, i.e., Us_j^t, appears in constraint (3.19). Thus, the last two objectives of problem (3.15) can be detached and solved as an independent sub-problem subject to constraint (3.19). The rest of this problem is sorted out as sub-problem I. Thus, the structure of the problem allows us to decompose it into two independent sub-problems without the loss of optimality. The following subsections describe the nature and solution of these sub-problems.

3.4.1 Sub-problem I

The first sub-problem aims to minimize the thermal cost (scheduling and dispatch costs) and to maximize the solar share. This sub-problem is given by

$$\underset{P_i^t, U_i^t, Ps^t}{min} \sum_{t=1}^{T} \Big[\sum_{i=1}^{n} F_i^t \left(P_i^t \right) U_i^t - Ps^t \Big] \tag{3.32}$$

$$\text{s.t., (3.3)-(3.12), and (3.16)-(3.18).}$$

The questions posed in the Introduction section is addressed by solving problem (3.32). The steps carried out to solve problem (3.32) are as follows:

(i) First of all, ORCUC is performed by using LR method without any solar share i.e., $Ps^t = 0$. to minimize the scheduling cost and to allocate the SSR. The Lagrangian function is formulated as

$$\begin{aligned} \mathcal{L}(U, P, \lambda, \mu) = & \sum_{i=1}^{n} \sum_{t=1}^{T} F_i(P_i^t) U_i^t + \sum_{t=1}^{T} \lambda^t (P_d^t - \sum_{i=1}^{n} P_i^t U_i^t) + \\ & \sum_{t=1}^{T} \mu^t (P_d^t + \sum_{i=1}^{n} R_{i,up}^t U_i^t - \sum_{i=1}^{n} P_{i,max} U_i^t), \end{aligned} \tag{3.33}$$

where λ and μ are assigned as non-negative Lagrangian multipliers to coupling constraints (3.8) and (3.16). Power loss is ignored for simplicity in the power balance constraint. The LR method temporarily relaxes the coupling

constraints, and then via dual optimization, the Lagrangian function $\mathcal{L}$ is maximized as a function of Lagrangian multiplier λ^t and μ^t while minimizing as a function of control variables P_i^t and U_i^t; that is,

$$q(\lambda^*, \mu^*) = \max_{\lambda,\mu} q(\lambda, \mu), \tag{3.34}$$

where

$$q(\lambda, \mu) = \min_{U,P} \mathcal{L}(U, P, \lambda, \mu). \tag{3.35}$$

The Lagrangian in Equation (3.33) can be rewritten as

$$\begin{aligned}\mathcal{L}(U, P, \lambda, \mu) = \sum_{i=1}^{n}\sum_{t=1}^{T}\Big[F_i(P_i^t) - \lambda^t P_i^t - \mu^t P_{i,max}\Big]U_i^t + \\ \sum_{t=1}^{T}[\lambda^t P_d^t + \mu^t(P_d^t + \sum_{i=1}^{n} R_{i,up}^t U_i^t)].\end{aligned} \tag{3.36}$$

The first term of Equation (3.36), i.e., $\sum_{i=1}^{n}\sum_{t=1}^{T}\Big[F_i(P_i^t) - \lambda^t P_i^t - \mu^t P_{i,max}\Big]U_i^t$, can be minimized separately for each thermal generation unit, whereas the second term of the equation is constant and can be dropped. Thus, the simplified problem is given by

$$\begin{aligned}min\,\mathcal{L}(U, P, \lambda, \mu) = &\sum_{i=1}^{n} min \sum_{t=1}^{T}\Big[F_i(P_i^t) - \lambda^t P_i^t - \mu^t P_{i,max}\Big]U_i^t \\ &\text{s.t., (3.3)-(3.5), (3.7), and (3.9)- (3.12).}\end{aligned} \tag{3.37}$$

(ii) Once the units are committed, ED optimization is carried out to calculate optimal output powers from committed generation units using the binary search lambda iteration algorithm [3]. In this algorithm, the optimal power output of each unit is found on the basis of an incremental cost rate (λ).

If $P_i^t < P_{i,min}$, then set $P_i^t = P_{i,min}$, and

if $P_i^t > P_{i,max}$, then set $P_i^t = P_{i,max}$.

Binary search proceeds as follows:

$$P_i^t = (\lambda^t - b_i)/2c_i, \tag{3.38}$$

$$\Delta\lambda = (\lambda_{max} - \lambda_{min})/2, \tag{3.39}$$

$$\lambda_i = \lambda_{min} + \Delta\lambda. \tag{3.40}$$

The following conditions are verified, and λ is updated as follows:
If $\sum_{i=1}^{n} P_i > P_d$, then
$\Delta\lambda = \Delta\lambda/2$ and $\lambda_{i+1} = \lambda_i - \Delta\lambda$.
If $\sum_{i=1}^{n} P_i < P_d$, then
$\Delta\lambda = \Delta\lambda/2$ and $\lambda_{i+1} = \lambda_i + \Delta\lambda$, and
If $\sum_{i=1}^{n} P_i - P_d \leq$ tolerance, the algorithm is terminated.
The value of ED from each thermal unit for zero solar share is shown in A.1

(iii) For a set of committed thermal units, problem (3.32) is solved to maximize the solar share within the range of a robust SSR. To solve this problem, the SSR ranges must be defined, and SSR^t as well as the solar share limit Γ^t must be evaluated for each range. Thus, to answer the questions posed in the Introduction section, the data sets $SSR_d^{'t}$, $SSR_s^{'t}$, and $SSR_c^{'t}$ are generated to define the SSR ranges for the answers (ii), (iii), and (iv), respectively. The solar share Γ^t is initialized with a value equal to zero and increased iteratively with step size δ. For each iteration, ED is carried out to evaluate P_i^t, Ps^t, and SSR^t. The resulting evaluations of SSR^t are allocated to either of the previously defined ranges based on the following criteria

$$SSR^t \in \begin{cases} SSR_d^{'t}, & \text{if } \Gamma^t \leq SSR^t - SSR_{opt(1,2)}^t, \\ SSR_s^{'t}, & \text{if } \Gamma^t \leq SSR^t, \\ SSR_c^{'t}, & \text{if } \Gamma^t \geq SSR^t. \end{cases} \tag{3.41}$$

The process is repeated until convergence. For any total number of iterations, say Y, the data sets are given by

$$\begin{aligned} SSR_d^{'t} &= \left\{SSR_{d1}^{'t}, SSR_{d2}^{'t}, \ldots, SSR_{di}^{'t}, \ldots, SSR_{dD}^{'t}\right\} \quad \forall i \in D \leq Y, \\ SSR_s^{'t} &= \left\{SSR_{s1}^{'t}, SSR_{s2}^{'t}, \ldots, SSR_{si}^{'t}, \ldots, SSR_{sS}^{'t}\right\} \quad \forall i \in S \leq Y, \\ SSR_c^{'t} &= \left\{SSR_{c1}^{'t}, SSR_{c2}^{'t}, \ldots, SSR_{ci}^{'t}, \ldots, SSR_{cC}^{'t}\right\} \quad \forall i \in C \leq Y, \end{aligned} \tag{3.42}$$

where D, S, and C are the maximum number of iterations for each range, respectively. The maximum limits of the robust SSR range and solar share are found when $SSR_{opt(1,2)}^t$ is dedicated to thermal contingencies only, i.e., the outcomes of answer (ii) are as follows:

$$SSR_d^t = max(SSR_d^{'t}), \tag{3.43}$$

$$\Gamma_d^t = \Gamma^t(ind_d), \tag{3.44}$$

where ind_d is the index of the maximum value in $SSR_d^{'t}$, i.e.,

$$ind_d = (\arg\max_x \ (SSR_d^{'t})). \tag{3.45}$$

Furthermore, the SSR for solar outage, i.e., SSR_{ded}^t, can be evaluated simply by subtracting the $SSR_{opt(1,2)}^t$ from SSR_d^t. Similarly, the evaluations corresponding to answers (iii) and (iv) are given by

$$SSR_s^t = max(SSR_s^{'t}), \tag{3.46}$$

$$\Gamma_s^t = \Gamma^t(ind_s), \tag{3.47}$$

$$SSR_c^t = max(SSR_c^{'t}) = SSR_{ul}^t, \tag{3.48}$$

$$\Gamma_c^t = \Gamma^t(ind_c), \tag{3.49}$$

where ind_s and ind_c are the indices of the maximum values in $SSR_s^{'t}$ and $SSR_c^{'t}$, respectively, i.e.,

$$ind_s = (\arg\max_x \ (SSR_s^{'t})), \tag{3.50}$$

$$ind_c = (\arg\max_x \ (SSR_c^{'t})). \tag{3.51}$$

In this way, the problem is solved to evaluate the robust SSR, and the procedure is called SSR analysis. The procedural flow of the solution of problem (3.32) is shown in Figure 3.2, in which the highlighted portion shows the SSR analysis. The alogrith for SSR analysis is presented in Algorim 1. For further clarifications, a graphical illustration of the SSR analysis will be discussed in detail in Section 3.5.

3.4.2 Sub-problem II

The objective of sub-problem II is to maximize the number of solar plants with ON status in order to increase reliability of solar power along with the minimization of solar cost. This problem has the following mathematical form for each hour:

$$\min_{Us_j^t} \sum_{t=1}^{T} \Big[w_1 \sum_{j=1}^{m} G_j^t \left(Pgs_j^t \right) Us_j^t - Kw_2 \sum_{j=1}^{m} Us_j^t \Big] \tag{3.52}$$

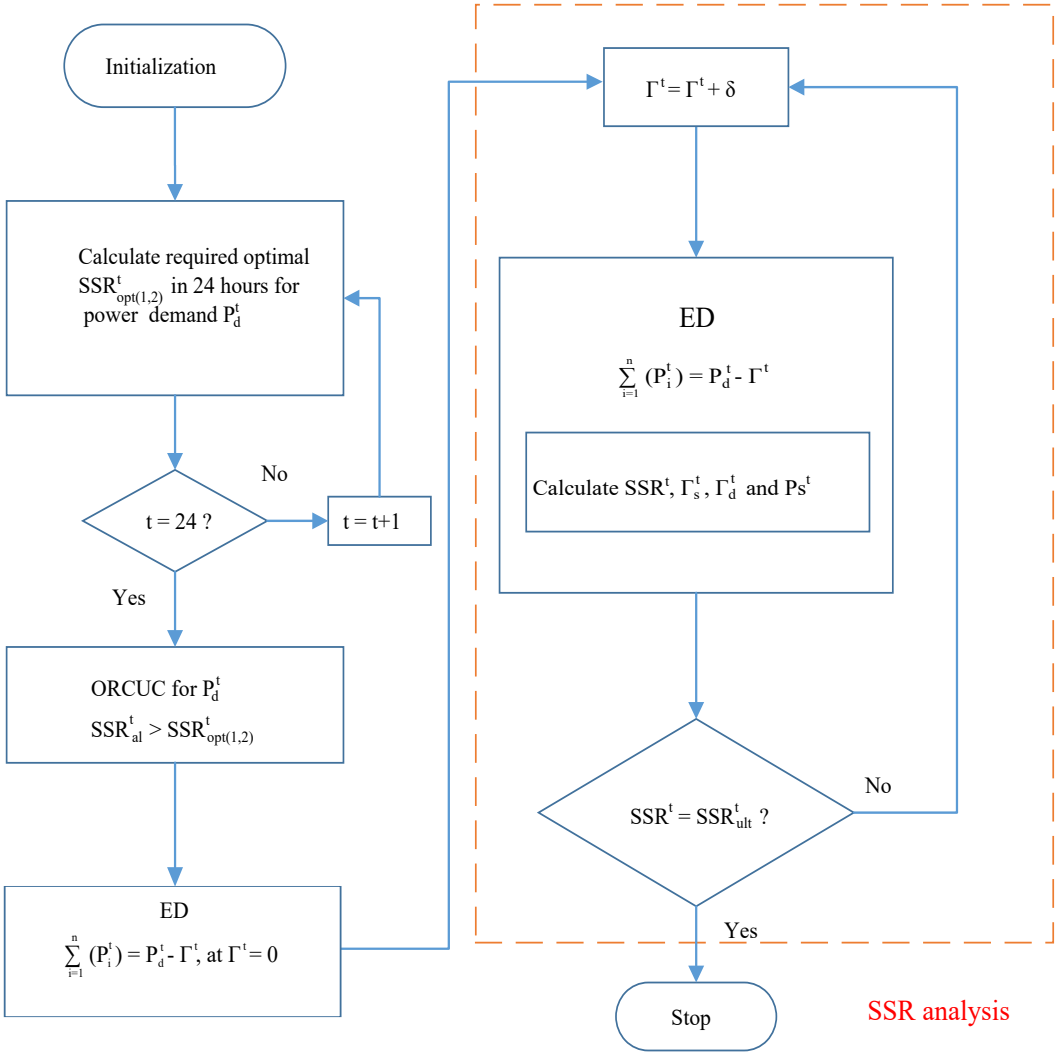

Figure 3.2: Proposed solution of sub-problem I

s.t., (3.19),

where w_1 and w_2 are the weights assigned to the solar cost and number of committed solar plants, respectively. K is the parameter used to determine the significance of the maximization of the number of solar plants compared to the solar cost minimization. For the readers' convenience, $\mathscr{F}_1^t$ and $\mathscr{F}_2^t$ are defined to denote the solar cost and the number of solar plants, respectively, and we rewrite problem (3.52) as follows:

$$\min_{Us_j^t} \sum_{t=1}^{T} \left[w_1 \mathscr{F}_1^t - K w_2 \mathscr{F}_2^t \right] \tag{3.53}$$

s.t., (3.19), with

$$\mathscr{F}_1^t = \sum_{j=1}^{m} G_j^t \left(Pgs_j^t \right) Us_j^t, \tag{3.54}$$

$$\mathscr{F}_2^t = \sum_{j=1}^{m} Us_j^t. \tag{3.55}$$

The value of K is empirically set to make the fitness evaluation of the second objective $\mathscr{F}_2^t$ compatible with that of the first objective $\mathscr{F}_1^t$. For more clarity, the relationship and the impact of the k-value on sub-problem II will be discussed in detail in Section 3.5. The simplified block diagram of proposed model and its solution is shown in fig. 3.3.

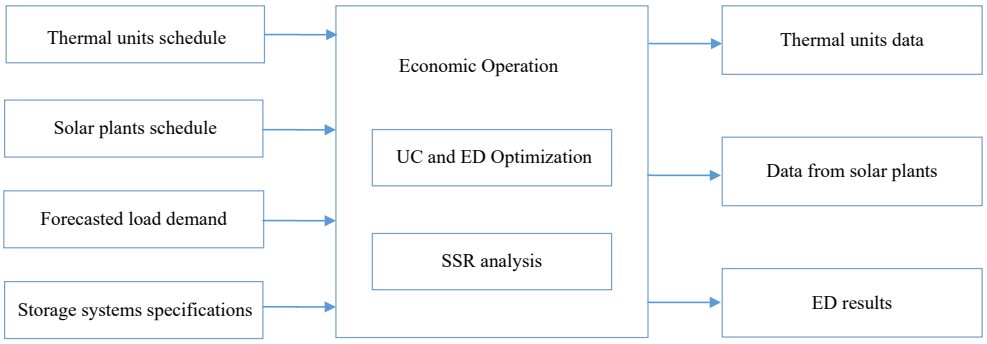

Figure 3.3: Simplified block diagram of proposed model and its solution

3.5 Test system and simulation results

The test system involves 26 thermal units and 40 solar plants. The data for capacity, coefficients, ramping limits of thermal units and load profile were obtained

Algorithm 1 Algorithm of SSR analysis after RCUC has been performed

procedure

Initiate factors: $P_{i,min}$, $P_{i,max}$, P_{load}, $R_i^{\uparrow}$, $R_i^{\downarrow}$, λ, $\Delta\lambda$, λ_{min}, λ_{max}, U_i a, b, c

for $\Gamma = 0, 20, 40, ...1400$ **do**

i = *1:26*

Calculate $P_{ed,i}$

if $P_{ed,i} > P_{i,max}$ **then** $P_{ed,i} = P_{i,max}$

end if

if $P_{ed,i} < P_{i,min}$ **then** $P_{ed,i} = P_{i,min}$

end if

$i \leftarrow$ *i+1*

Calculate $\sum_{i=1}^{26} P_i^t U_i^t$

Calculate ΔP= P_{load}- $\sum_{i=1}^{26} P_i^t U_i^t$

if ΔP $\leq$ *tolerance* **then** *goto step*

end if

if ΔP < 0 **then** $\Delta\lambda = \Delta\lambda/2$, $\lambda_{i+1} = \lambda_i - \Delta\lambda$,

goto *step 4*

end if

if ΔP > 0 **then** $\Delta\lambda = \Delta\lambda/2$, $\lambda_{i+1} = \lambda_i + \Delta\lambda$,

goto *step 4*

end if

Calculate SSR= $\sum_{i=1}^{26} (Ri, up)U_i$

$p_{load} = p_{load} - \Gamma$

end for

Plot SSR–Γ

Calculate and plot 's' and 'd' points

end procedure

from [90]. Step 1 of the optimization is solved by executing ORCUC to determine the optimal scheduling of the thermal units and SSR^t_{al}. The resulting optimal schedule of the thermal units is shown in Table 3.1. The load demand is given in Table 3.2, and evaluation results of the SSR^t_{al} are shown in Figure 3.4 as well as in Table 3.3.

A zero in Table 3.1 refers to the OFF status of a thermal generation unit, whereas a one means that the generation unit is ON. It is observed from Figure 3.4 that SSR^t_{al} comes out to always be higher or equal to $SSR^t_{opt(1,2)}$. This is due to the binary scheduling of the thermal generation units and their associated minimum power limits. Ideally, SSR^t_{al} must follow $SSR^t_{opt(1,2)}$, as can be observed during time slots 6, 7, 8, 9, and 24. However, it can be seen from the figure that SSR^t_{al} varies regardless of the $SSR^t_{opt(1,2)}$ for the rest of the time slots. Such behavior is due to variations in load demand as well as the UC schedule. The reserve of individual thermal unit is shown in Table A.2. For instance, the load demand decreases from 2590 MW at time slot t = 13:00 to 2550 MW at time slot t = 14:00, as given in Table 3.2. As a result, the SSR^t_{al} is increased from 210 MW to 249

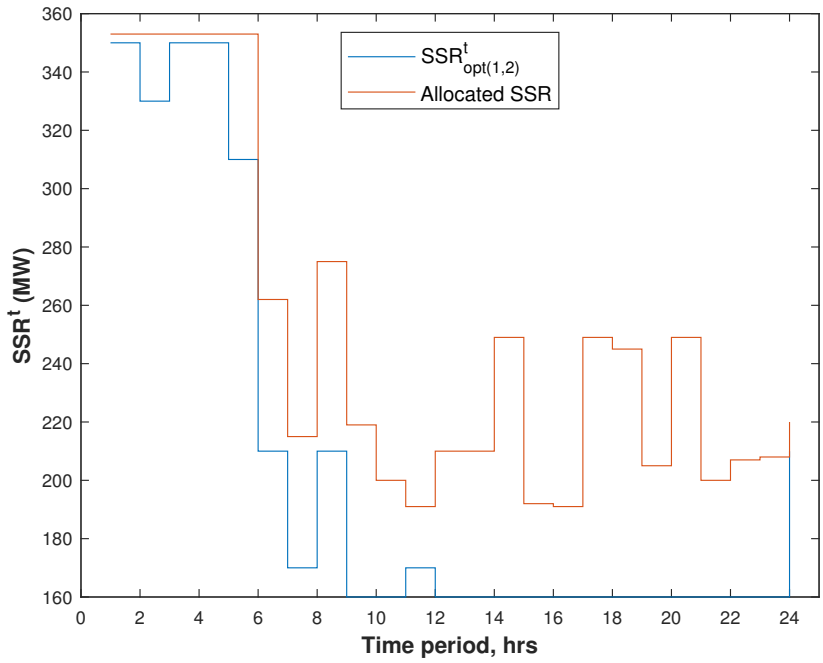

Figure 3.4: SSR scheduled by using ORCUC and $SSR_{opt(1,2)}$ with VOLL = 1000 \$/MWh for 24 h

Table 3.1: ORCUC schedule for $24hrs$

t (hr)	unit (1-26)																									
	U_1	U_2	U_3	U_4	U_5	U_6	U_7	U_8	U_9	U_{10}	U_{11}	U_{12}	U_{13}	U_{14}	U_{15}	U_{16}	U_{17}	U_{18}	U_{19}	U_{20}	U_{21}	U_{22}	U_{23}	U_{24}	U_{25}	U_{26}
1	0	0	0	0	0	0	0	0	0	1	1	1	1	1	1	1	1	1	1	1	1	1	0	1	1	1
2	0	0	0	0	0	0	0	0	0	1	1	1	1	1	1	1	1	1	1	1	1	1	0	1	1	1
3	0	0	0	0	0	0	0	0	0	1	1	1	1	1	1	1	1	1	1	1	1	1	0	1	1	1
4	0	0	0	0	0	0	0	0	0	1	1	1	1	1	1	1	1	1	1	1	1	1	0	1	1	1
5	0	0	0	0	0	0	0	0	0	1	1	1	1	1	1	1	1	1	1	1	1	1	0	1	1	1
6	0	0	0	0	0	0	0	0	0	1	1	1	1	1	1	0	1	1	1	1	0	0	0	1	1	1
7	1	1	1	1	1	0	0	0	0	1	1	1	1	1	1	1	1	1	1	1	0	0	0	1	1	1
8	1	1	1	1	1	0	0	0	0	1	1	1	1	1	1	1	1	1	1	1	1	1	1	1	1	1
9	1	1	1	1	1	1	0	0	0	1	1	1	1	1	1	1	1	1	1	1	1	1	1	1	1	1
10	1	1	1	1	1	1	1	1	1	1	1	1	1	1	1	1	1	1	1	1	1	1	1	1	1	1
11	1	1	1	1	1	1	1	1	1	1	1	1	1	1	1	1	1	1	1	1	1	1	1	1	1	1
12	1	1	1	1	1	1	1	1	1	1	1	1	1	1	1	1	1	1	1	1	1	1	1	1	1	1
13	1	1	1	1	1	1	1	1	1	1	1	1	1	1	1	1	1	1	1	1	1	1	1	1	1	1
14	1	1	1	1	1	1	1	1	1	1	1	1	1	1	1	1	1	1	1	1	1	1	1	1	1	1
15	1	1	1	1	1	1	1	1	1	1	1	1	1	1	1	1	1	1	1	1	1	1	1	1	1	1
16	1	1	1	1	1	1	1	1	1	1	1	1	1	1	1	1	1	1	1	1	1	1	1	1	1	1
17	1	1	1	1	1	1	1	1	1	1	1	1	1	1	1	1	1	1	1	1	1	1	1	1	1	1
18	1	1	1	1	1	1	1	1	0	1	1	1	1	1	1	1	1	1	1	1	1	1	1	1	1	1
19	1	1	1	1	1	0	0	0	0	1	1	1	1	1	1	1	1	1	1	1	1	1	1	1	1	1
20	1	1	1	1	1	1	1	1	1	1	1	1	1	1	1	1	1	1	1	1	1	1	1	1	1	1
21	1	1	1	1	1	1	1	1	1	1	1	1	1	1	1	1	1	1	1	1	1	1	1	1	1	1
22	1	1	1	1	1	0	0	0	0	1	1	1	1	1	1	1	1	1	1	1	1	1	1	1	1	1
23	0	0	0	0	0	0	0	0	0	1	1	1	1	1	1	1	1	1	1	1	1	1	0	1	1	1
24	0	0	0	0	0	0	0	0	0	1	1	1	1	1	1	1	1	1	1	1	0	0	0	1	1	1

Table 3.2: Results of proposed solution from $10^{th}hr$ to $20^{th}hr$ of a day

Time of the Day	**10:00**	**11:00**	**12:00**	**13:00**	**14:00**	**15:00**	**16:00**	**17:00**	**18:00**
Robust SSR^t_{ded} for solar share at point 'd' (MW)	108	21	118	118	110	106	31	110	92
Solar share at point 'd' = Γ^t_d (MW)	100	20	100	100	100	100	20	100	80
Robust SSR^t at point 's' = SSR^t_s (MW)	344	268	345	345	345	345	301	345	330
Solar share at point 's' = Γ^t_s (MW)	340	260	340	340	340	340	300	340	320
SSR^t at point 'c' = SSR^t_{ult} (MW)	540	540	540	540	540	540	540	540	525
P_{load} (MW)	2600	2670	2590	2590	2550	2620	2650	2550	2530
Thermal generation (MW) for Γ^t_s	2260	2410	2250	2250	2210	2280	2350	2210	2210
Thermal generation (MW) for Γ^t_d	2500	2660	2490	2490	2450	2520	2630	2450	2450
Thermal fuel cost (\$/MWh) with Γ^t_s	31,210	32,974	30,883	30,883	30,321	31,309	32,319	30,321	30,107
Thermal fuel cost (\$/MWh) with $\Gamma^t_s = 0$	36,889	38,496	36,696	36,696	35,930	37,324	38,025	35,930	35,354
E_{def}	0	0	0	0	0	0	0	0	0
Thermal fuel cost without ORCUC (\$/MWh)	36,150	37,796	35,763	35,928	34,955	36,619	37,324	34,955	34,572
Reserve cost (\$)	739	700	933	768	975	705	701	975	782

MW, as can be seen in Table 3.3. This increase in the SSR^t_{al} for a decreased load demand is due to the fact that the UC schedule has remained unchanged during respective time slots, as evident in Table 3.1. In contrast, SSR^t_{al} is decreased as the load demand has been decreased at t = 19 because thermal units 6, 7, and 8 have been turned OFF at t = 19, and they were previously ON.

Table 3.3: SSR^t under the ORCUC without solar share

Time of the Day	**1**	**2**	**3**	**4**	**5**	**6**	**7**	**8**	**9**	**10**	**11**	**12**
	13	**14**	**15**	**16**	**17**	**18**	**19**	**20**	**21**	**22**	**23**	**24**
SSR^t_{al} before inclusion of solar share	353	353	353	353	353	262	215	275	219	200	191	210
	210	249	192	191	249	245	205	249	200	207	208	220
$SSR^t_{opt(1,2)}$	350	330	350	350	310	210	170	210	160	160	170	160
	160	160	160	160	160	160	160	160	160	160	160	210

When the solar power penetrates into the system, the overall thermal share is reduced to satisfy the specified load demand, and the power outputs of individual thermal units are adjusted to new set points. As a result, the SSR^t is increased, and it cannot exceed SSR_{ult}. As our objective is to maximize the solar share, the algorithm keeps on adding the solar power until the SSR_{ult} is reached or other constraints limit the level of the penetration of solar share. The variations and convergence of SSR^t with changes in solar power share in the 10-th hour of a day are depicted in Figure 3.5. The SSR allocated with ORCUC in this hour, i.e., SSR^{10}_{al}, is 200 MW. When the solar share of Γ^{10} in the 10-th hour is included in the system with a step size of δ = 20 MW and when ED is executed for every step of the solar share inclusion, the SSR^{10} starts to increase from its initially allocated value. The SSR^{10} and Γ^{10} at points 'c', 'd', and 's' are denoted as SSR^{10}_c, Γ^{10}_c, SSR^{10}_d, Γ^{10}_d, SSR^{10}_s, and Γ^{10}_s. At point 'c' the SSR^{10}_c has been converged to the SSR^t_{ult}, and it does not increase further when the solar share is moved beyond the Γ^{10}_c point due to the ramping-up constraint. The 's' point is located where Γ^{10}_s becomes equal or nearly equal to SSR^{10}_s, and it is evident from Figure 3.5 that at point 's', the SSR^{10} = 345 MW is slightly greater than Γ^{10}_s = 340 MW. Beyond this point, toward point 'c', the SSR^{10} comes out to be less than Γ^{10}_s, which reveals that the robust SSR can be allocated until this point 's'. Thus, the range of the robust SSR for the 10-th hour comes out to be within 0

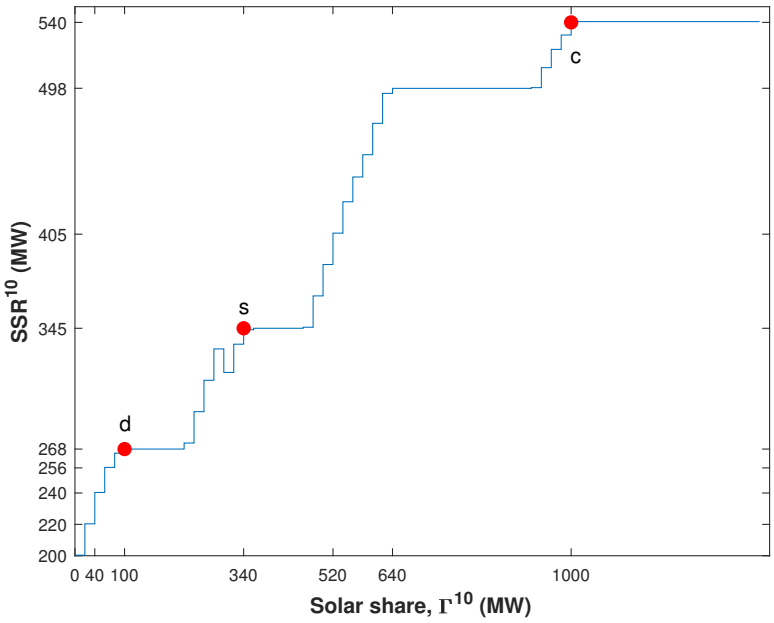

Figure 3.5: SSR variation with respect to solar share at 10-th hour
d: $\Gamma^{10} \leq SSR^{10}$ and $SSR^{10}_{opt(1,2)}$ is not allowed to be dispatched for solar outage
s: $\Gamma^{10} \leq SSR^{10}$ and $SSR^{10}_{opt(1,2)}$ is allowed to be dispatched for solar outage
c: ultimate SSR^{10}

MW$\leq SSR^t \leq$345 MW and the maximum solar share, i.e., ($\Gamma^{10}_{max} = \Gamma^{10}_{s}$) comes out to be 340 MW. Within this range of the robust SSR, the system has sufficient reserve power to compensate for the power deficit in case of the occurrence of either a thermal contingency event **or** complete/partial solar power outage, whichever event occurs first. However, the system will experience a power deficit if both events occur simultaneously. Similarly, the power deficit is experienced if Γ^{10} is adjusted more than Γ^{10}_{max}, i.e., the point of system operation is moved beyond point 's' toward 'c'. A scenario is considered in which the power system is being operated at point 'x' such that the solar share is $\Gamma^{10}_{x} = \mathcal{X}$ MW $> \Gamma^{10}_{max}$. Let the corresponding value of the SSR be $SSR^{10}_{x} = \mathcal{Y}$ MW and suppose that the complete outage of solar power occurs. For this outage of $\mathcal{X}$ MW, the system is able to serve only $\mathcal{Y}$ MW, and the rest of the solar outage, i.e., $\mathcal{X} - \mathcal{Y}$ MW, remains uncompensated. Thus, the power deficit is experienced by the system as given below:

$$P_{def} = \Gamma^{10}_{x} - SSR^{10}_{x}. \tag{3.56}$$

For instance, if 520 MW of solar share is intended to be added in the system, the corresponding SSR comes out to be 405 MW, as can be seen in Figure 3.5. Thus, the power deficit for this solar outage will be 115 MW. To cope with the power deficit in case of the simultaneous outages of solar and thermal powers, a dedicated SSR allocation to thermal, as well as solar contingencies, is proposed. The dedicated SSR allocated to the thermal contingency events is $SSR^{10}_{opt(1,2)}$ and that for solar power outage is given as follows:

$$SSR^{10}_{ded} = SSR^{10}_{d} - SSR^{10}_{opt(1,2)}, \tag{3.57}$$

where SSR^{10}_{d} is the SSR at point 'd' and calculated by executing ED repeatedly for every step increment of the solar share. For further illustration, Table 3.4 presents the values of SSR^{10} and SSR^{10}_{ded} as functions of Γ^{10}. It can be seen from the

Table 3.4: Variation in SSR^{10} and SSR^{10}_{ded} $w.r.t$ Γ^{10}

$\Gamma^{10}(MW)$	0	20	40	60	80	100	120	-	-
$SSR^{10}(MW)$	200	220	240	256	265	268	268	-	-
SSR^{10}_{ded}	40	60	80	96	105	108	108	-	-

Table that SSR^{10} as well as SSR^{10}_{ded} increase as the Γ^{10} increases. Furthermore, it is evident from the Table that, initially, the robust SSR^{10}_{ded} comes out to be greater than the Γ^{10} and becomes less than Γ^{10} when Γ^{10} increases beyond 100 MW. Thus, the upper limit of the robust SSR, which can handle simultaneous outages of thermal and solar powers, comes out to be 268 MW. In Figure 3.5, this value of the SSR is located at point 'd', i.e., SSR^{10}_{d}, and the value of Γ^{10} at this point is Γ^{10}_{d}. Therefore, the limits of the robust SSR for simultaneous outages of thermal and solar powers are 200 MW $\leq SSR^{t} \leq$ 268 MW, and the solar share limit within the range of this robust SSR^{t} appears to be 0 MW $\leq \Gamma^{10} \leq$ 100 MW. The variation in SSR^{t} with a change in Γ^{t} from the 11-th hour to the 19-th hour is presented in Figure 3.6. Table 3.2 presents the optimization results for the time window when solar power is available, i.e., from the 10-th hour to the 18-th hour. To elaborate on the results, the rows of the Table are distributed in four parts. The first three parts of the Table present the proposed ORCUC-based results,

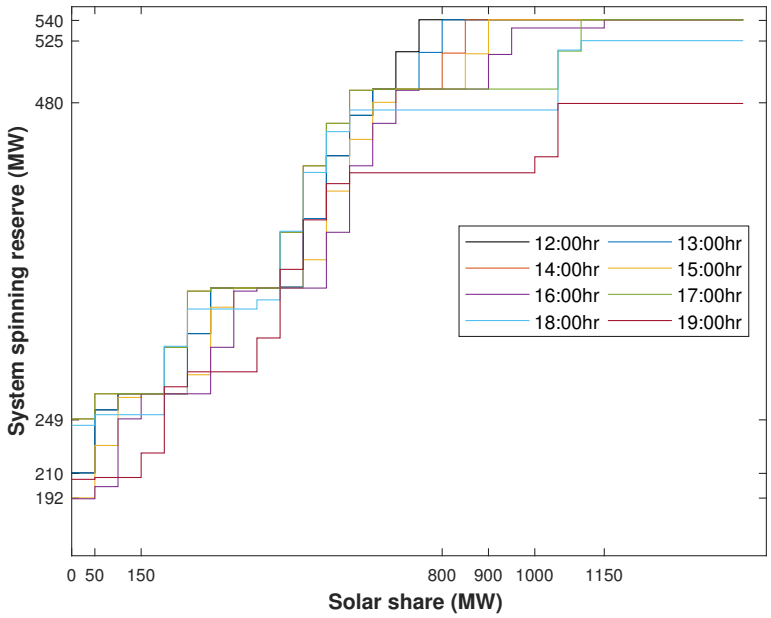

Figure 3.6: Variation in SSR with respect to solar share from $11^{th}hr$ to $19^{th}hr$ of a day

whereas the last part presents those without ORCUC. The first part of the Table presents the resulting SSR for various conditions and corresponding solar share penetrations. It can be observed from the results that the robust SSR at point 's', i.e., SSR^t_s, always come out to be greater than the robust SSR at point 'd', i.e., SSR^t_{ded}. For instance, SSR^t_s comes out to be 344 MW at the 10-th hour, where SSR^t_{ded} is 108 MW. This is due to fact that the SSR allocations in later condition are dedicated to respective outages, e.g., $SSR^t_{opt(1,2)}$ is not allowed to be dispatched if a solar outage occurs. As expected, similar relationships can be found in corresponding solar shares due to the same reason. The last row of this part presents the ultimate SSR, i.e., the maximum power outage supported by the system beyond which the failure of system operation occurs. The second part of the Table presents the thermal shares at points 'd' and 's'. The thermal share at any point depends on the load demand and solar share at that point. The thermal share increases with an increase in load demand and decreases as the solar share is increased and vice versa. For instance, the load demand increases from 2600 MW at t = 10:00 h to 2670 MW at t = 11:00 h, and the solar share Γ^t_s decreases from 340 MW to 260 MW. Thus, the thermal share is increased from 2260 MW to

2410 MW. The third portion of Table presents the impact of the total solar outage ($\Gamma_s^t = 0$) on the fuel cost at point 's'. In this case, the thermal power generation is supposed to meet the load demand without any energy deficit. Thus, for a given load demand, the fuel cost is increased in case of solar contingency. For simplicity, the similar results of point 'd' are not demonstrated. Finally, in the last part of the Table, the resulting cost for the case if the optimal reserve is neglected in UC are presented. It can be seen that the fuel cost increased in this case because an excessive reserve cost was emerged due to an unoptimized reserve. To demonstrate the results more completely, the UC schedules of the thermal units are presented in Table 3.1, and the corresponding optimized powers to be dispatched of the units are shown in Table 3.6. Up reserve of individual unit, after penetration of solar share at point $'s'$ and $'d'$ is shown in Table A.2 and Table A.3. respectively. The available SSR after solar share penetration at poit $'d'$ and $'s'$ are presented in Table 3.8 and in Table 3.9. The system has 40 solar plants of different power ratings that are assumed to be distributed across the power system and to take part in the system operation. The data for the solar plants are presented in Table 3.5.

In this study, the power ratings of the solar plants were chosen arbitrarily. However, these power ratings may have many interesting impacts on the results of sub-problem II. For instance, the second objective of sub-problem II is to maximize the number of participating solar plants. If the installed solar capacity involves the plants of lower power ratings, more plants will be selected to participate in the dispatch for a specified solar share. In this case, if the solar outage occurs, the impact of such an outage will be lesser due to the lower power rating of the solar plant under contingency. On the other hand, solar costs will be increased. Furthermore, the lower power ratings of the solar plants ensure a more accurate convergence in terms of constraint (19). There may exist numerous other similar impacts; however, the evaluation of such impacts is beyond the scope of this study. Weight w_1 is initially set to 1 and reduced successively with the iterations, while w_2 is increased accordingly, and the value of K is set to 10^4. Figure 3.7 depicts the impact of different values of K on the solution of sub-problem II for an arbitrarily chosen time slot t = 1000 h. In this figure, the horizontal axis represents the objective $\mathscr{F}_1$, and the vertical axis represents multiplicative inverse

Table 3.5: Power ratings and per unit costs of solar plants

Number of Plants	$\mathbf{P_{rated}}$ (MW)	Unit Rate ($/KWh)
3	10	0.19,2× 0.18
5	12	5×0.19
1	15	0.2
3	18	3 ×0.2
2	20	2×0.23
4	24	4×0.23
4	25	4×0.23
2	30	2×0.24
5	35	0.25,0.26,0.23,2 × 0.24
7	40	2x0.27,2x0.275,3× 0.28
2	50	2×0.18
1	60	0.21
1	80	0.22

of the objective $\mathscr{F}_2$. It can be seen from the figure that the highest number of Pareto-optimal solutions are obtained with the value of K set to 10^4 compared to the other values. As the algorithmic behavior is similar for all the time slots, the similar results for the rest of the time slots are not shown. Figure 3.9 shows the variations in $\mathscr{F}_1$ and $\mathscr{F}_2$ with respect to various settings of w_1 and w_2. In this figure, the horizontal axis represents the number of iterations, where for each iteration, distinct values are assigned to w_1 and w_2. The vertical axis on the left side shows the number of selected solar plants, and the vertical axis on the right side depicts the cost associated with the selected solar plants. It can be seen from the figure that, initially, less solar plants are selected for a specified solar share, and the number of plants is increased as further iterations are elapsed. Similarly, the solar cost is increased in the same manner with the passage of iterations. Such an increase in the number of solar plants as well as the solar cost are due to different values of w_2 and w_1, respectively. For instance, the lesser plants are selected for initial iterations because w_2 is initiated with a low value. As our objective is to

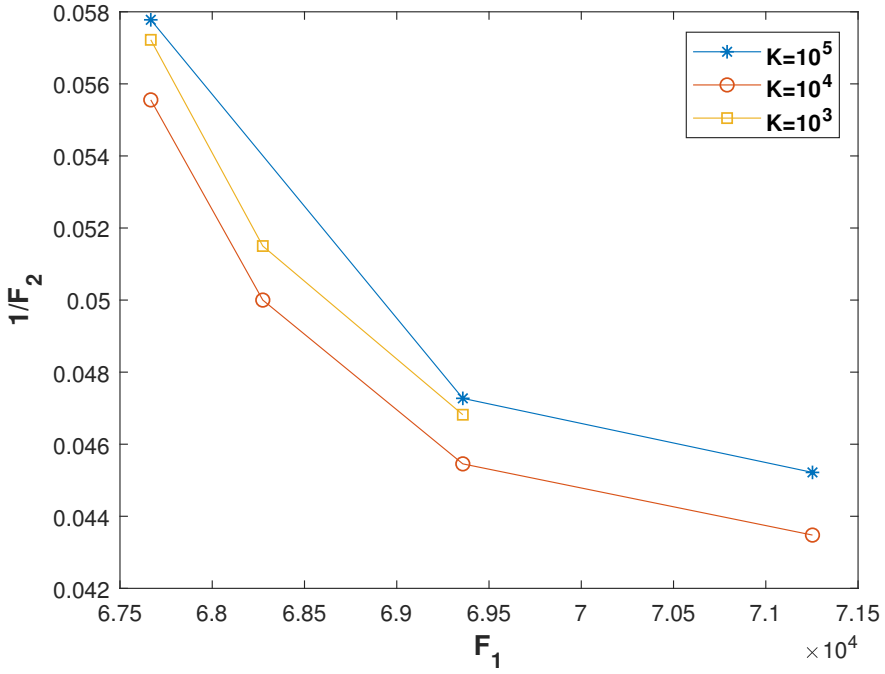

Figure 3.7: Effect of 'K' on sub-problem II

maximize the number of solar plants, higher values are assigned to w_2 with the passage of iterations, which increases the significance of the maximization of $\mathscr{F}_2$. As a result, more solar plants are selected for a higher number of iterations. On the other hand, the solar cost is increased as more iterations are elapsed because its associated weight w_1 is decreased successively. Since our objective is to minimize the solar cost, its significance is reduced with the passage of iterations, which results in an increase of the solar cost. Interestingly, the solar cost and the number of selected plants are discrete functions of the weights w_1 and w_2, respectively. For instance, it can be observed from the figure that 18 solar plants are selected during the first three iterations, and an increase in the value of w_2 from 0.0100 to 0.0300 has no effect on the maximization of solar plants. At iteration number 4, the number of selected plants is increased to 20 when w_2 is assigned the value of 0.0400 and remains unchanged until $w_2 = 0.0700$ at iteration number 7. Such discrete variations are due to binary optimization. Thus, it is essential to note that only a few Pareto optimal solutions can be obtained with this optimization. Therefore, appropriate step sizes of weights w_1 and w_2, as well as an appropriate number of iterations, must be chosen carefully in such an optimization. The step

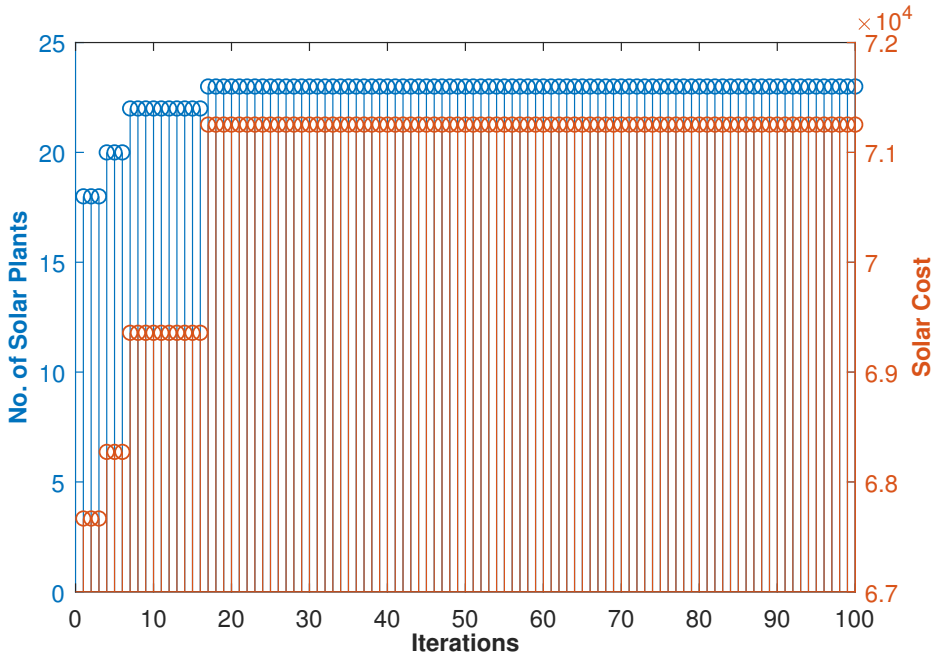

Figure 3.8: Results of sub-problem II: number of selected solar plants vs. solar cost over 100 iterations

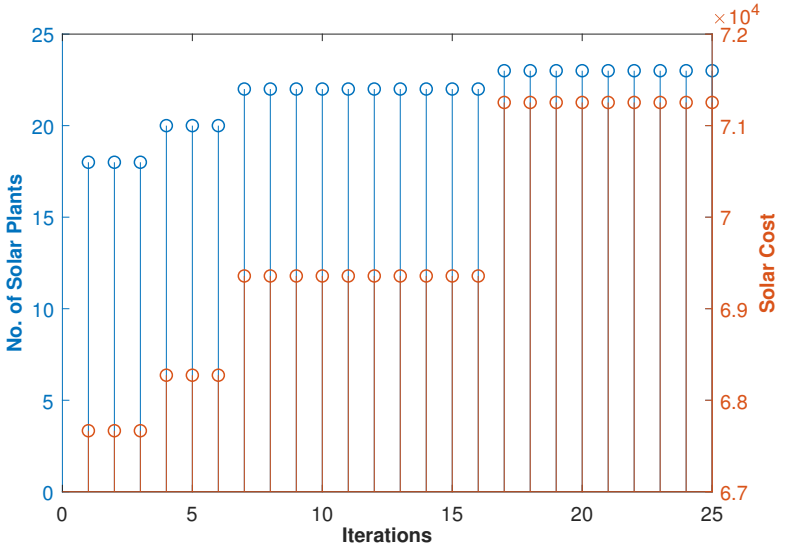

Figure 3.9: Results of sub-problem II: number of selected solar plants vs. solar cost over 25 iterations

sizes of the weights were set empirically to be 0.0100 for our case. Too small or too large a step size will result in a reduced number of solutions for a specified number of iterations. Similarly, too small a number of iterations results in a reduced number of solutions, whereas too large a number of iterations results in excessive computational effort without exploring any further solutions. It can be analyzed from Figure 3.9 that if the number of iterations is reduced, one may obtain less solutions. For instance, if the number of iterations is set to 10, the resulting number of solutions is reduced to 3, and so on.

Figure 3.8 depicts the results for 100 iterations. In this figure, 100 iterations are implemented to ensue that w_1 and w_2 cover the entire range of possible values, i.e., $0 \leq w_i \leq 1$. In comparison of Figures 3.8 and 3.9, it can be observed that further solutions cannot be achieved after 25 iterations. The aforementioned discussions reveal that the solar share maximization and the solar cost minimization are contradictory objectives. Furthermore, as only a few Pareto-optimal solutions are possible, the choice of the final solution depends on the priorities established by the system operator. For instance, the system operator may choose an appropriate solution based on the priorities of the objectives. Different system operators may have different priorities based on the local energy market and the energy policies of the territory. For instance, some system operators may assign higher ranks to the cost of operation, while reliable system operation may be more significant for the others.

We can summarize this chapter, that, ED and SSR are both the most important objectives which make ensure reliable and inexpensive provision of electricity from a solar integrated power system. There exist several ED models and optimization techniques for delivering cost effective power to customers. reliable and continuous provision of electricity is an issue which belongs to tje unit commitment problem in which reserve power is a constraint. Renewable energy is being included in the energy mix worldwide for several compelling rasons like, alternatives to traditional fossil fuel, to reduce greenhouse enissions, mitigate climate changes, decentralization power production, to reduce the vulneraability of centralized grid to disruptions, virtually inexhaustible and enhance energy security. Due to Rapid escalation of fuel prices, governments, organizations, and industries

are actively promoting their integration to reduce reliance on fossil fuel. This chapter presents a hybrid power system which involve integrating multiple solar PV plants with thermal power generation units. Our model of HPS is eassentially a MIOP, based on the nature of descion variables. Lagrange relaxation for UC and binary search Lambda iteration method for ED is used to solve the optimization problem for a scenario involving 26 thermal units and 40 solar PV plants. solar share limits within the range of robust SSR are determined by analysing the simulation results abtained from optimization for three different conditional cases. First case, the limits of robust SSR and the maximum limit f solar share within the range of robust SSR are determined, if $SSR_{OPT(1,2)}$ is allowed to dispatch for solar power outage. In second case, solar maximum limits of robustSSR and the solar share limits within the limits of this reserve are determined, if $SSR_{OPT(1,2)}$ is not allowed to dispatch ifor a solar power outage. The third case deals with calculations of robust SSR and power deficite values, if penetrated solar power exceeds the maximum limit of ROBUST SSR.

Table 3.6: ED results of thermal units when solar share= Γ_s^{10}

t (h)	ED results after solar share added at s point																								
	U1	**U2**	**U3**	**U4**	**U5**	**U6**	**U7**	**U8**	**U9**	**U10**	**U11**	**U12**	**U13**	**U14**	**U15**	**U16**	**U17**	**U18**	**U19**	**U20**	**U21**	**U22**	**U23**	**U24**	**U25**	**U26**
1	0.00	0.00	0.00	0.00	0.00	0.00	0.00	0.00	0.00	15.20	15.20	15.20	15.20	25.00	25.00	25.00	100.37	95.98	92.17	88.82	68.95	68.95	0.00	248.96	400.00	400.00
2	0.00	0.00	0.00	0.00	0.00	0.00	0.00	0.00	0.00	15.20	15.20	15.20	15.20	25.00	25.00	25.00	104.70	100.23	96.35	92.94	68.95	68.95	0.00	262.08	400.00	400.00
3	0.00	0.00	0.00	0.00	0.00	0.00	0.00	0.00	0.00	15.20	15.20	15.20	15.20	25.00	25.00	25.00	98.92	94.57	90.78	87.45	68.95	68.95	0.00	244.58	400.00	400.00
4	0.00	0.00	0.00	0.00	0.00	0.00	0.00	0.00	0.00	15.20	15.20	15.20	15.20	25.00	25.00	25.00	100.37	95.98	92.17	88.82	68.95	68.95	0.00	248.96	400.00	400.00
5	0.00	0.00	0.00	0.00	0.00	0.00	0.00	0.00	0.00	15.20	15.20	15.20	15.20	25.00	25.00	25.00	107.59	103.06	99.13	95.69	68.95	68.95	0.00	270.83	400.00	400.00
6	0.00	0.00	0.00	0.00	0.00	0.00	0.00	0.00	0.00	34.45	34.45	34.45	34.45	49.09	41.81	0.00	135.09	130.56	126.63	123.19	0.00	0.00	0.00	305.83	400.00	400.00
7	2.40	2.40	2.40	2.40	2.40	0.00	0.00	0.00	0.00	42.79	40.39	38.26	35.92	25.00	25.00	25.00	155.00	155.00	154.13	150.69	0.00	0.00	0.00	340.83	400.00	400.00
8	12.00	12.00	12.00	12.00	12.00	0.00	0.00	0.00	0.00	62.04	59.64	57.51	55.17	50.50	50.50	50.50	155.00	155.00	155.00	155.00	27.50	27.50	27.50	350.00	400.00	400.00
9	6.11	3.42	2.40	2.40	2.40	4.00	4.00	4.00	4.00	76.00	76.00	76.00	74.42	76.00	76.00	76.00	155.00	155.00	155.00	155.00	68.95	68.95	68.95	350.00	400.00	400.00
10	2.40	2.40	2.40	2.40	2.40	4.00	4.00	4.00	4.00	36.00	36.00	36.00	34.42	39.00	39.00	39.00	155.00	155.00	154.93	150.80	68.95	68.95	68.95	350.00	400.00	400.00
11	2.40	2.40	2.40	2.40	2.40	4.00	4.00	4.00	4.00	55.25	55.25	55.25	53.67	64.50	64.05	57.19	155.00	155.00	155.00	155.00	68.95	68.95	68.95	350.00	400.00	400.00
12	2.40	2.40	2.40	2.40	2.40	4.00	4.00	4.00	4.00	44.91	42.47	40.30	37.92	27.50	27.05	25.00	155.00	155.00	155.00	155.00	68.95	68.95	68.95	350.00	400.00	400.00
13	2.40	2.40	2.40	2.40	2.40	4.00	4.00	4.00	4.00	46.08	43.62	41.43	39.02	25.00	25.00	25.00	155.00	155.00	155.00	155.00	68.95	68.95	68.95	350.00	400.00	400.00
14	2.40	2.40	2.40	2.40	2.40	4.00	4.00	4.00	4.00	35.78	33.53	31.51	29.33	25.00	25.00	25.00	155.00	155.00	155.00	155.00	68.95	68.95	68.95	350.00	400.00	400.00
15	2.40	2.40	2.40	2.40	2.40	4.00	4.00	4.00	4.00	53.81	51.18	48.87	46.28	25.00	25.00	25.00	155.00	155.00	155.00	155.00	68.95	68.95	68.95	350.00	400.00	400.00
16	2.40	2.40	2.40	2.40	2.40	4.00	4.00	4.00	4.00	71.85	68.84	66.23	63.23	25.00	25.00	25.00	155.00	155.00	155.00	155.00	68.95	68.95	68.95	350.00	400.00	400.00
17	2.40	2.40	2.40	2.40	2.40	4.00	4.00	4.00	4.00	35.78	33.53	31.51	29.33	25.00	25.00	25.00	155.00	155.00	155.00	155.00	68.95	68.95	68.95	350.00	400.00	400.00
18	2.40	2.40	2.40	2.40	2.40	4.00	4.00	4.00	0.00	36.81	34.54	32.50	30.30	25.00	25.00	25.00	155.00	155.00	155.00	155.00	68.95	68.95	68.95	350.00	400.00	400.00
19	2.40	2.40	2.40	2.40	2.40	4.00	4.00	0.00	0.00	40.41	38.07	35.98	33.69	25.00	25.00	25.00	155.00	155.00	155.00	155.00	68.95	68.95	68.95	350.00	400.00	400.00
20	2.40	2.40	2.40	2.40	2.40	4.00	4.00	4.00	4.00	35.78	33.53	31.51	29.33	25.00	25.00	25.00	155.00	155.00	155.00	155.00	68.95	68.95	68.95	350.00	400.00	400.00
21	12.00	12.00	12.00	12.00	12.00	19.25	19.25	19.25	19.25	55.03	52.78	50.76	48.58	50.50	50.50	50.50	155.00	155.00	155.00	155.00	96.45	96.45	96.45	350.00	400.00	400.00
22	2.40	2.40	2.40	2.40	2.40	0.00	0.00	0.00	0.00	74.28	72.03	70.01	67.83	75.79	68.98	62.23	155.00	155.00	155.00	155.00	68.95	68.95	68.95	350.00	400.00	400.00
23	0.00	0.00	0.00	0.00	0.00	0.00	0.00	0.00	0.00	35.00	32.77	30.77	28.60	38.79	31.98	25.23	155.00	155.00	155.00	155.00	68.95	68.95	68.95	350.00	400.00	400.00
24	0.00	0.00	0.00	0.00	0.00	0.00	0.00	0.00	0.00	15.20	15.20	15.20	15.20	25.00	25.00	25.00	145.81	140.46	135.91	132.02	0.00	0.00	0.00	350.00	400.00	400.00

Table 3.7: ED, when solar share is selected at point d

t (h)	ED from each thermal unit after solar penetration at d point																								
	U1	**U2**	**U3**	**U4**	**U5**	**U6**	**U7**	**U8**	**U9**	**U10**	**U11**	**U12**	**U13**	**U14**	**U15**	**U16**	**U17**	**U18**	**U19**	**U20**	**U21**	**U22**	**U23**	**U24**	**U25**	**U26**
1	0.00	0.00	0.00	0.00	0.00	0.00	0.00	0.00	0.00	15.20	15.20	15.20	15.20	25.00	25.00	25.00	100.37	95.98	92.17	88.82	68.95	68.95	0.00	248.96	400.00	400.00
2	0.00	0.00	0.00	0.00	0.00	0.00	0.00	0.00	0.00	15.20	15.20	15.20	15.20	25.00	25.00	25.00	104.70	100.23	96.35	92.94	68.95	68.95	0.00	262.08	400.00	400.00
3	0.00	0.00	0.00	0.00	0.00	0.00	0.00	0.00	0.00	15.20	15.20	15.20	15.20	25.00	25.00	25.00	98.92	94.57	90.78	87.45	68.95	68.95	0.00	244.58	400.00	400.00
4	0.00	0.00	0.00	0.00	0.00	0.00	0.00	0.00	0.00	15.20	15.20	15.20	15.20	25.00	25.00	25.00	100.37	95.98	92.17	88.82	68.95	68.95	0.00	248.96	400.00	400.00
5	0.00	0.00	0.00	0.00	0.00	0.00	0.00	0.00	0.00	15.20	15.20	15.20	15.20	25.00	25.00	25.00	107.59	103.06	99.13	95.69	68.95	68.95	0.00	270.83	400.00	400.00
6	0.00	0.00	0.00	0.00	0.00	0.00	0.00	0.00	0.00	34.45	34.45	34.45	34.45	49.09	41.81	0.00	135.09	130.56	126.63	123.19	0.00	0.00	0.00	305.83	400.00	400.00
7	2.40	2.40	2.40	2.40	2.40	0.00	0.00	0.00	0.00	42.79	40.39	38.26	35.92	25.00	25.00	25.00	155.00	155.00	154.13	150.69	0.00	0.00	0.00	340.83	400.00	400.00
8	12.00	12.00	12.00	12.00	12.00	0.00	0.00	0.00	0.00	62.04	59.64	57.51	55.17	50.50	50.50	50.50	155.00	155.00	155.00	155.00	27.50	27.50	27.50	350.00	400.00	400.00
9	6.11	3.42	2.40	2.40	2.40	4.00	4.00	4.00	4.00	76.00	76.00	76.00	74.42	76.00	76.00	76.00	155.00	155.00	155.00	155.00	68.95	68.95	68.95	350.00	400.00	400.00
10	2.40	2.40	2.40	2.40	2.40	4.00	4.00	4.00	4.00	76.00	76.00	76.00	76.00	70.61	63.71	56.84	155.00	155.00	155.00	155.00	68.95	68.95	68.95	350.00	400.00	400.00
11	2.40	2.40	2.40	2.40	2.40	4.00	4.00	4.00	4.00	76.00	76.00	76.00	76.00	96.11	89.21	82.34	155.00	155.00	155.00	155.00	96.45	96.45	87.45	350.00	400.00	400.00
12	2.40	2.40	2.40	2.40	2.40	4.00	4.00	4.00	4.00	76.00	76.00	76.00	76.00	67.34	60.38	53.43	155.00	155.00	155.00	155.00	68.95	68.95	68.95	350.00	400.00	400.00
13	2.40	2.40	2.40	2.40	2.40	4.00	4.00	4.00	4.00	76.00	76.00	76.00	76.00	67.34	60.38	53.43	155.00	155.00	155.00	155.00	68.95	68.95	68.95	350.00	400.00	400.00
14	2.40	2.40	2.40	2.40	2.40	4.00	4.00	4.00	4.00	76.00	76.00	76.00	76.00	54.27	47.07	39.81	155.00	155.00	155.00	155.00	68.95	68.95	68.95	350.00	400.00	400.00
15	2.40	2.40	2.40	2.40	2.40	4.00	4.00	4.00	4.00	76.00	76.00	76.00	76.00	77.14	70.36	63.65	155.00	155.00	155.00	155.00	68.95	68.95	68.95	350.00	400.00	400.00
16	2.40	2.40	2.40	2.40	2.40	4.00	4.00	4.00	4.00	76.00	76.00	76.00	76.00	100.00	95.86	89.15	155.00	155.00	155.00	155.00	96.45	77.59	68.95	350.00	400.00	400.00
17	2.40	2.40	2.40	2.40	2.40	4.00	4.00	4.00	4.00	72.10	69.09	66.48	63.47	63.00	58.86	52.15	155.00	155.00	155.00	155.00	68.95	68.95	68.95	350.00	400.00	400.00
18	2.40	2.40	2.40	2.40	2.40	4.00	4.00	4.00	0.00	76.00	76.00	76.00	76.00	55.57	48.40	41.17	155.00	155.00	155.00	155.00	68.95	68.95	68.95	350.00	400.00	400.00
19	2.40	2.40	2.40	2.40	2.40	4.00	4.00	0.00	0.00	76.00	76.00	76.00	76.00	73.22	66.37	59.56	155.00	155.00	155.00	155.00	68.95	68.95	68.95	350.00	400.00	400.00
20	2.40	2.40	2.40	2.40	2.40	4.00	4.00	4.00	4.00	76.00	76.00	76.00	76.00	86.95	80.34	73.86	155.00	155.00	155.00	155.00	68.95	68.95	68.95	350.00	400.00	400.00
21	2.40	2.40	2.40	2.40	2.40	4.00	4.00	4.00	4.00	76.00	76.00	76.00	76.00	100.00	98.60	92.55	155.00	155.00	155.00	155.00	68.95	68.95	68.95	350.00	400.00	400.00
22	2.40	2.40	2.40	2.40	2.40	0.00	0.00	0.00	0.00	76.00	76.00	76.00	76.00	69.26	62.34	55.55	155.00	155.00	155.00	155.00	68.95	68.95	68.95	350.00	400.00	400.00
23	0.00	0.00	0.00	0.00	0.00	0.00	0.00	0.00	0.00	38.65	36.35	36.00	36.00	32.26	25.34	18.55	155.00	155.00	155.00	155.00	68.95	68.95	68.95	350.00	400.00	400.00
24	0.00	0.00	0.00	0.00	0.00	0.00	0.00	0.00	0.00	15.20	15.20	15.20	15.20	25.00	25.00	25.00	145.81	140.46	135.91	132.02	0.00	0.00	0.00	350.00	400.00	400.00

Table 3.8: SSR^t with solar share at point $'d'$

Time of the Day	**1**	**2**	**3**	**4**	**5**	**6**	**7**	**8**	**9**	**10**	**11**	**12**
	13	**14**	**15**	**16**	**17**	**18**	**19**	**20**	**21**	**22**	**23**	**24**
SSR^t for solar share at point d	353.50	353.50	353.50	353.50	353.50	262.35	215.85	227.06	260.35	268.00	223.85	268.00
	268.00	268.00	265.36	206.49	300.86	252.75	237.50	249.71	200.35	207.00	236.00	219.30

Table 3.9: SSR^t with solar share at point $'s'$

Time of the Day	**1**	**2**	**3**	**4**	**5**	**6**	**7**	**8**	**9**	**10**	**11**	**12**
	13	**14**	**15**	**16**	**17**	**18**	**19**	**20**	**21**	**22**	**23**	**24**
SSR^t for solar share at point $'s'$	353.50	353.50	353.50	353.50	353.50	262.35	215.85	227.06	260.35	345.00	349.27	345.00
	345.00	345.00	345.00	301.85	345.00	329.75	314.50	345.00	239.00	225.56	236.00	219.30

3.6 Conclusions

In this study, a comprehensive model was developed for the economic operation of HPS, which is more robust against the loss of load in case of thermal contingencies as well as solar power outages. To facilitate the solution, a composite optimization was decomposed into two sub-problems. An ORC model for UC was proposed, and it adopted a new approach to allocate robust SSR as well as to determine the maximum limit of the solar share within the range of a robust SSR. The proposed model involved the computation of the limits of the robust SSR for the solar share, the maximum bound on the solar share within the limits of the robust SSR, and the ultimate SSR. Based on such evaluations, the optimization was solved for the committed thermal units to minimize fuel costs, maximize the solar share, maximize the number of participating solar plants, and minimize the solar cost. The following points have been concluded:

(i) Committed thermal units could provide a limited robust SSR to facilitate a given solar share. Thus, the amount of penetrated solar share at any time was limited by the available robust reserve at that time. For instance, robust SSR^{10} came out to be 345 MW and 108 MW for solar shares of 340 MW and 100 MW, respectively, depending on the condition whether $SSR^t_{opt(1,2)}$ was allowed to be dispatched or restricted for a solar power outage event. Beyond these allocations, the robust SSR starts to become smaller than the

solar share; therefore, loss of load would be experienced by the power system for a complete outage of the solar share.

(ii) Aset of committed units in a time slot could provide a certain amount of the ultimate SSR, which is 540 MW in the case of the 10-th hour.

(iii) Only a few such solutions were obtainable within the feasible binary search space when Pareto-optimal solutions were obtained for the contradictory objectives of solar cost minimization and the maximization of the number of solar plants. The highest number of such solutions were obtained with the value of parameter K empirically set to 10^4. Although this work investigated many critical issues of HPS, some aspects, such as network constraints, storage systems, and RE sources other than solar power, have not been covered.

Furthermore, the inclusion of an ESS will enhance the range of the robust SSR, and thus, the maximum limit of RE share under a robust SSR will be increased. The thermal units fuel cost will also decrease under the effect of ESS, However, the addition of ESS feature will result in a more challenging optimization.

Chapter 4

Optimization of Solar PV and ESS Integrated Hybrid Power System

4.1 Introduction

Today's power systems are increasingly becoming hybrid in nature, with large scale integration of renewable energy (RE) sources and energy storage technologies. This hybridization is driven by the need for cleaner, more sustainable energy solutions, cost effectiveness, and increase in power demand worldwide. These RE sources and ESS's are playing a critical role in prolonging the life of depleting conventional energy resources and their usefulness. Also, supplementing conventional power generation with RE and ESS provide a way for the transition toward a more sustainable and economically vibrant energy future by reducing dependence on conventional energy sources, decreasing the power system's net present value (NPV), reducing the annual energy purchased from the grid, and lower the carbon emissions [91]. Research and development in energy storage technologies, suh as batteries and pump storages, are the key to addressing the challenges posed by intermittent nature of RE sources and allow for the capture and use of excess amount of energy from RE sources. The Intermittent nature of solar PV and wind turbines refers to the variability of power generation by these source due to diverse weather conditions.

The integration of RE with thermal power generation requires scheduling of sufficient SSR from thermal units to avoid loss of load due to its intermittent nature. The allocation of required SSR, forces the dispatched power of scheduled units to be deviated from their optimal points of dispatching powers. Also some additional units may need to be committed, which lead to a higher cost of operation. It is possible to decrease the cost on provision of sufficient SSR from thermal units by integrating an ESS. Thus, the transition to RE and ESS integrated power systems add new complexities and optimal operation of the system becomes a more challenging issue. It may not be viable for the system operator to penetrate all the available RE due to system constraints. In a HPS, storage systems must be applied in such a way to obtain maximum advantages in terms of thermal fuel cost, reserve cost, and solar share penetrat

When a storage system is added to a HPS, then UC will be performed without reserve constraint. Questions *i-iv*, presented in section 2.1 will be addressed in this

chapter in presence of ESS. This work aims to develop a robust reserve scheduling framework that ensures adequate reserve allocation while supporting higher solar integration without unnecessary commitment of conventional units. The proposed strategy partitions the ESS into three components, two of which are specifically dedicated to providing reserves, one for thermal contingencies and the other for complete solar generation outages. These ESS components are then combined with thermal reserves to formulate a contingency-based system reserve (CBSR), which enables the reserve requirement to be satisfied without explicit enforcement in the UC optimization, thereby allowing additional conventional units to remain offline and reducing operational costs. Accordingly, the main contribution of this study is the development of a CBSR framework that integrates thermal reserves with strategically partitioned ESS components, offering a distinctive mechanism that facilitates higher solar penetration with comparatively lower reserve requirements, reduces reliance on unnecessary unit commitments, and ensures reliable as well as operationally efficient system performance under simultaneous solar and thermal contingencies. To the best of the authors' knowledge, no recent study has rigorously addressed all of these issues. The proposed model tackles the aforementioned challenges by addressing the following research questions.

(i) To what extent can the solar share be maximized within robust system reserve?

(ii) How does the integration of ESS increase solar power penetration, and to what extent can this additional solar share be achieved?

(iii) What operational scheme can be developed for ESS to achieve the maximum benefits from RE sources?

The contributions of this chapter are summarized as follows:

(i) The range of robust system reserve within which solar share can be maximized is determined. The boundaries of this range, along with the corresponding solar shares, are evaluated to ensure no power deficit occurs.

(ii) The operational costs are minimized, while the number of solar plants in operation is maximized to enhance system reliability.

(iii) UC is implemented using LR, and ED is carried out through a Lambda iteration along with the binary search method. Additionally, a set of Pareto-optimal solutions is obtained for selecting the solar plants.

(iv) A new formulation of CBSR integrates ESS in a way that allows the UC to be executed without explicit reserve constraints, thereby relieving thermal units from the burden of providing reserve power during thermal contingencies.

(v) Solar share is further increased due to the aforementioned scheme for operating the ESS.

(vi) The proposed model is implemented and simulated on an IEEE-RTS 26-unit system.

The rest of this chapter is organized as follows. The system model and problem formulation are presented in Section 4.2. Section 4.3 describes the proposed solution, the simulations results and discussions are provided in Section 4.4, and conclusion is presented in Section 4.5.

4.2 System model and problem formulation

4.2.1 System model

We consider an HPS consisting of n thermal units and m solar plants supplying power to satisfy the load demand P_d as shown in Figure 4.1. Let P_i^t denote the power share of i-th thermal generating unit at any time t, the corresponding fuel cost is given by

$$F_i(P_i^t) = a_i(P_i^t)^2 + b_i P_i^t + c_i, \tag{4.1}$$

where a_i, b_i, and c_i are the fuel cost coefficients of i-th thermal unit. Depending on system requirements, the i-th thermal generation unit may be in the ON or OFF state at any given time t. This ON or OFF status of the i-th generation unit is represented by a binary variable U_i^t. The status of the i-th unit is given by

$$U_i^t = \begin{cases} 1, & \text{if } i\text{-th generation unit is ON,} \\ 0, & \text{otherwise.} \end{cases} \tag{4.2}$$

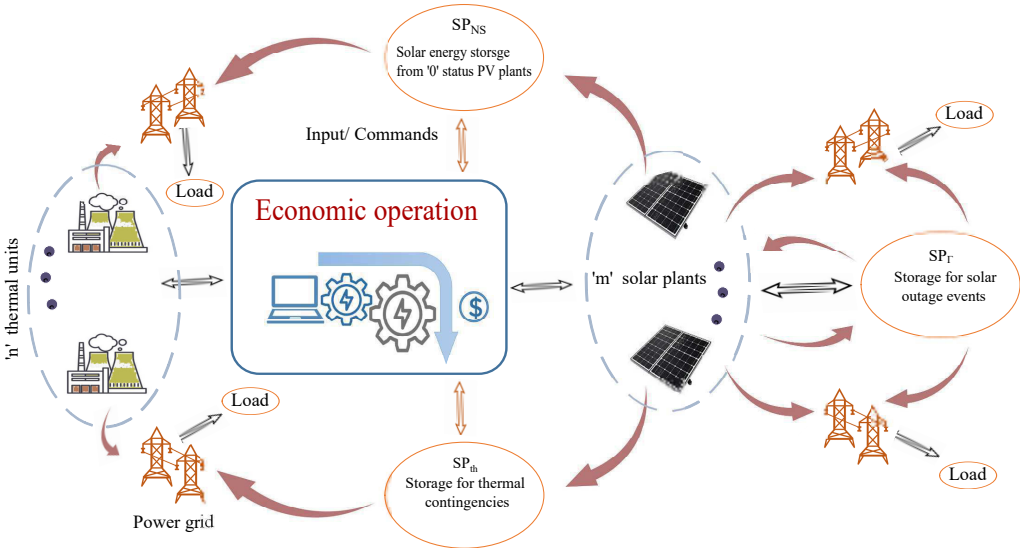

Figure 4.1: System model.

Furthermore, P_i^t must not surpass its prescribed upper and lower bounds, i.e.,

$$P_{i,\min} U_i^t \leq P_i^t \leq P_{i,\max} U_i^t \quad \forall i = 1, 2, ..., n, \tag{4.3}$$

where $P_{i,\min}$ and $P_{i,\max}$ correspond to the minimum and maximum power limits of the i-th thermal generation unit, respectively. The power P_i^t cannot respond immediately to sudden load fluctuations. Instead, it can only be adjusted within defined ramp-up and ramp-down limits. Thus, the available up reserve and down reserve at any given time are constrained by

$$R_{i,\text{up}}^t = \min(P_{i,\max} U_i^t - P_i^t U_i^t, \tau R_i^{\uparrow} U_i^t), \tag{4.4}$$

$$R_{i,\text{down}}^t = \min(P_i^t U_i^t - P_{i,\min} U_i^t, \tau R_i^{\downarrow} U_i^t), \tag{4.5}$$

where $R_i^{\uparrow}$, $R_i^{\downarrow}$, and τ are the ramp up rate, ramp down rate, and time allowed for ramping, respectively. The reserves of each on-bar thermal unit aggregate to form the SSR, i.e.,

$$SSR^t = \sum_{i=1}^{n} U_i^t R_{i,up}^t. \tag{4.6}$$

In thermal generation units, transition from one operating state to another cannot take place until the minimum time for that state has elapsed. For instance, once a generation unit is turned ON, it cannot be switched OFF until the minimum ON time has passed. Similarly, transition from OFF state to ON state cannot

occur until the minimum OFF time has elapsed. Thus, the following transition constraints must be satisfied for i-th generation unit

$$(T_{i,\text{on}}^{t-1} - T_{i,\text{up}})(U_i^t - U_i^{t-1}) \leq 0, \tag{4.7}$$

$$(T_{i,\text{off}}^{t-1} - T_{i,\text{down}})(U_i^{t-1} - U_i^t) \leq 0, \tag{4.8}$$

where $T_{i,\text{on}}$ is the cumulative ON time, $T_{i,\text{off}}$ is the cumulative OFF time, $T_{i,\text{up}}$ is the minimum up time, and $T_{i,\text{down}}$ is the minimum down time for the i-th generation unit. During any two successive time slots, the power output of the i-th generation unit must remain within specified ramping limits, provided that the unit stays ON during those intervals. Any increase in power should not exceed the ramp-up rate, and any decrease should not surpass the ramp-down rate, i.e.,

$$P_i^t - P_i^{t-1} \leq \tau R_i^{\uparrow}, \quad \text{if } U_i^t = 1, U_i^{t-1} = 1, \tag{4.9}$$

$$P_i^{t-1} - P_i^t \leq \tau R_i^{\downarrow}, \quad \text{if } U_i^t = 1, U_i^{t-1} = 1, \tag{4.10}$$

where τ is the maximum time allowed to complete the ramping process. At any time t, let Pgs_j^t represent the power of the j-th solar plant. The system operator is required to pay the following cost to the plant owner

$$G_j^t(Pgs_j^t) = \Upsilon_j Pgs_j^t, \tag{4.11}$$

where Υ_j is the per unit cost of j-th solar plant. where ρ_j is the rated power of j-th solar plant, α_j is the temperature coefficient, T_a^t is the ambient temperature, T_r^t is the reference cell temperature, and S_j^t is the solar radiation at any given time t. The ESS serves the purpose of storing electrical energy and supplying it during outages or power shortages. The expressions for the energy charged to and discharged from the ESS at any given time t are given by

$$SP_{ch}^t = SP_{ch0} + \frac{1}{E_{cap}} \int_0^t \eta_{ch} \cdot P_{ch}^{\tau'} d\tau', \tag{4.12}$$

$$SP_{dis}^t = SP_{dis0} - \frac{1}{E_{cap}} \int_0^t \frac{P_{dis}^{\tau'}}{\eta_{dis}} d\tau', \tag{4.13}$$

where SP_{ch0} and SP_{dis0} represent the initial charging and discharging states, E_{cap} is the energy storage capacity, P_{ch} and P_{dis} denote the charging and discharging powers, η_{ch} and η_{dis} are the corresponding charging and discharging efficiencies, and τ' is the time interval over which charging or discharging takes place.

4.2.2 Problem formulation

This study addresses the economic operation of an ESS-integrated HPS with the objectives of minimizing fuel costs, minimizing solar power costs, maximizing solar share, and increasing the number of operational solar plants, while ensuring CBSR. At any operating instant, the allocation of a robust CBSR guarantees uninterrupted system operation in the event of simultaneous solar and thermal contingencies, thereby enhancing system reliability and preventing loss of load. The CBSR denotes the portion of the total system reserve that is available based on prevailing operating conditions and is represented by $\mathcal{R}^t$. Furthermore, the proposed model charges the ESS using surplus solar power to maximize RE benefits. For discharging, the ESS is partitioned into three components, of which one component, SP_{NS}, is discharged during normal operation. The remaining components are reserved exclusively for contingencies and will be described later in this section. The problem is formulated as

$$\min_{P_i^t, Ps^t, U_i^t, Us_j^t, \Gamma^t} \sum_{t=1}^{T} \left[\sum_{i=1}^{n} F_i\left(P_i^t\right) U_i^t - \alpha \chi^t Ps^t - \beta \chi^t \sum_{j=1}^{m} Us_j^t + \chi^t \sum_{j=1}^{m} G_j^t\left(Pgs_j^t\right) Us_j^t \right] \tag{4.14}$$

$$\text{s.t.,} \quad Ps^t + \sum_{i=1}^{n} P_i^t U_i^t + SP_{ns}^t (1-\chi)^t \zeta_{dis}^t - P_d^t = 0, \tag{4.15}$$

$$\chi^t \cdot \zeta_{ch}^t + \zeta_{dis}^t \leq 1, \tag{4.16}$$

$$0 \leq Ps^t \leq \chi^t \cdot \min\left(\Gamma^t, \sum_{j=1}^{m} Pgs_j\right), \tag{4.17}$$

$$0 \leq \Gamma^t \leq \chi^t \cdot \Gamma_{\max}^t, \tag{4.18}$$

$$\chi^t \cdot \left(\sum_{j=1}^{m} Pgs_j Us_j^t - Ps^t\right) \geq 0, \tag{4.19}$$

$$\chi^t \cdot \left(\zeta_{ch}^t P_{ch}^t - \sum_{j=1}^{m} Pgs_j\left(1 - Us_j^t\right)\right) \leq 0, \tag{4.20}$$

$$(4.3), (4.4), (4.5), (4.6), (4.7), (4.8), (4.9), \text{ and } (4.10), \tag{4.21}$$

where α and β are weighting coefficients introduced to reconcile the differences in physical units among the objective function terms. Ps^t represents the maximum solar share that can be accommodated by the system, Γ^t is the reserve-based solar

share used to trace the reserve–share operating region, Us_j^t denotes the binary, either 1 or 0, state of operation of j-th solar plant, P_d^t is the load demand, SP_{ns}^t is the power discharged by ESS, Γ^t is the reserve-based solar share, Γ_{max}^t is the maximum limit of reserve-based solar share, ζ_{ch}^t is the binary indicator of charging, ζ_{dis}^t is the binary indicator of discharging, and χ^t is a binary time-activation indicator. $\chi^t \in \{0, 1\}$ is defined as

$$\chi^t = \begin{cases} 1, & \text{if } t' \leq t \leq t'', \\ 0, & \text{otherwise.} \end{cases}$$

Depending on operational requirements, the output of the j-th solar plant may either be dispatched to meet the load or remain unused as surplus power. A value of 1 for Us_j^t indicates that the j-th solar plant is contributing to system operation by serving the load, whereas a value of 0 signifies that its power is treated as surplus. The power balance constraint (4.15) asserts that sufficient power from the generation sources, including thermal units, solar plants, and ESS, must be available at all times to meet the load demand. Constraint (4.16) ensures that simultaneous charging and discharging of an ESS is not possible. Constraint (4.17) defines the solar share and states that it must remain within its specified upper and lower bounds. The upper bound is defined as the minimum of the solar share determined by the CBSR and the total available solar power. Constraint (4.18) defines the solar share based on the reserve and specifies that the solar power integrated into the system must not exceed the limits set by the CBSR. The CBSR is robust, if it satisfy the limit $0 \leq \mathcal{R}^t \leq \Gamma^t$, and this CBSR makes the system robust against solar power outage from the system. The maximum limits of the reserve-based solar share are given by

$$\Gamma_{\max}^t = \Gamma_x^t, \quad \text{if } 0 \leq \mathcal{R}^t \leq \Gamma^t, \tag{4.22}$$

where Γ_x^t is the maximum solar share with sufficient CBSR and $x \in \{d, d_1, s\}$, at which the power system does not experience a power deficit, depending on whether the solar power outage and thermal contingency event occur simultaneously or not. Depending on availability of ESS and conditions applied on dispatching of CBSR, Γ_x^t varies, therefore, Constraint (4.19) ensures that the solar plants are chosen in

a way that provides enough on-bar solar power to achieve the desired solar share. Finally, constraint (4.20) ensures that the ESS is charged only by surplus solar generation by restricting its charging power to the surplus available at time t. The factor χ^t restricts charging to solar hours, while the term $\sum_{j=1}^{m} Pgs_j^t(1-Us_j^t)$ guarantees that the process relies on the surplus output from solar plants.

As the CBSR is designed to address potential contingencies, its formulation is critical to ensure that adequate reserves are available during extreme events. Unlike traditional reserve structures, the CBSR proposed in this study integrates the SSR of thermal units with a strategically managed ESS reserve. Accordingly, the ESS is partitioned into three components, as illustrated in Figure 4.2. In this figure, SP_{th} and SP_{Γ} are reserved for thermal and solar contingencies, respectively, while all components are charged using surplus solar power. Since thermal contingencies may occur at any time, SP_{th} remains active across all time slots, ready for discharge when needed. In contrast, SP_{Γ} is active only during time slots when solar power is available, and SP_{NS} operates during non-solar periods. Upon a thermal outage, the thermal contingency detector triggers the coordinated discharge of SP_{th} along with the thermal SSR to address the contingency. Similarly, the solar contingency detector activates SP_{Γ} in the event of a solar contingency, while SP_{NS} continues to discharge regularly, analogous to pre-contingency operation.

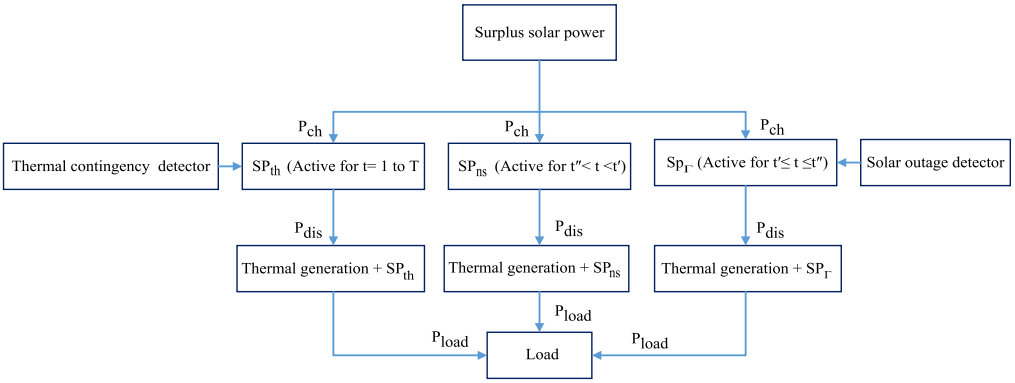

Figure 4.2: operational strategy of ESS for contingency and normal operation.

To formally define the CBSR, the total power capacity of the ESS is first considered. Let SP represent the total power capacity of the ESS, it can be expressed as

$$SP = SP_{th} + SP_{\Gamma} + SP_{NS}, \tag{4.23}$$

where SP_{th}, SP_{Γ}, and SP_{NS} are storage components reserved for thermal contingencies, solar power outages, and normal operation usage, respectively.

i) SP_{th}: This component of the ESS is designated for power dispatch during thermal contingency events. Let $\mathcal{R}_{req}$ represent the required reserve power by the system to cope with the power deficit in the event of a thermal contingency. This $\mathcal{R}_{req}$ has been allocated by $N-1$ deterministic criterion and SP_{th} is then given by

$$SP_{th} \geq \mathcal{R}_{req}. \tag{4.24}$$

ii) SP_{Γ}: SP_{Γ} is applied for the time zone t' to t'', to deal with solar power outage. t' and t'' represent the first and last hours, respectively, during which solar power is intended to penetrate. This storage has been provided for each time slot which is given by

$$SP_{\Gamma}^{t} = \frac{SP_{\Gamma}}{t'' - t'}. \tag{4.25}$$

iii) SP_{NS}: This part of the ESS has been utilized to dispatch stored energy consistently during each time interval of normal system operation except the time zone from t' to t''. The power dispatched in each time segment is given by

$$SP_{ns}^{t} = \frac{SP_{NS}}{NS}, \tag{4.26}$$

where NS is the total number of hours in which solar power is not penetrated. The following expression defines the power discharged from the ESS.

$$SP_{dis}^{t} = SP_{\Gamma}^{t} \cdot \Omega_1 \chi^{t} + SP_{ns}^{t} \cdot (1 - \chi^{t}) + SP_{th}^{t} \cdot \Omega_2, \tag{4.27}$$

where Ω_1 is the binary variable representing solar outage, Ω_2 represents binary variable for thermal contingency. $\Omega_1 = 1$ if a solar outage occurs, and $\Omega_1 = 0$ otherwise. Similarly, $\Omega_2 = 1$ if a thermal contingency takes place, and $\Omega_2 = 0$ otherwise. Prior to any outage or discharging of ESS, the total system reserve is given below

$$\mathcal{R}_{tot}^{t} = SSR^{t} + SP_{\Gamma}^{t} + SP_{ns}^{t} + SP_{th}^{t}. \tag{4.28}$$

To deal with the power outages, this research defines a CBSR as the reserve ready to be dispatched in case of solar or thermal contingency events. The CBSR is given by

$$\mathcal{R}^{t} = \left[(SSR^{t} + SP_{th}^{t}) \cdot \Omega_2\right](1 - \chi^{t}) + \left[SSR^{t} \cdot \Omega_1 + SP_{dis}^{t}\right]\chi^{t}. \tag{4.29}$$

4.3 Proposed solution

The optimization problem formulated in Eq. (4.14) involves continuous as well as binary decision variables, classifying it as a mixed-integer programming problem. The presence of variables with different characteristics contributes to the overall complexity of the model. Solving this optimization in its entirety is a challenging task, thus a decomposition approach is proposed to simplify the solution process. Therefore, the problem is decomposed into two independent sub-problems. The following subsections describe the nature and solution of these sub-problems.

4.3.1 Sub-problem I

Sub-problem I focuses on the interaction between fuel cost minimization and solar share maximization. In the composite formulation, weighting factors (e.g., α) were introduced to reconcile terms with different physical units. However, this sub-problem is reformulated as a bi-level optimization problem, where the two objectives are handled hierarchically rather than combined.

At the upper level, the objective is to maximize the solar share Ps^t by incrementally increasing its contribution to system generation. For each incremental level of solar share, the lower level solves the UC and ED problem with the objective of minimizing the total fuel cost of thermal units while satisfying system demand and reserve constraints. The process continues until the system reserve becomes insufficient to support the specified solar share, which defines the maximum feasible solar integration under the given operating conditions.

This approach eliminates the need for artificial weighting factors since the bi-level structure inherently represents the interaction between both objectives.

The bi-level structure of Sub-problem I can be expressed as

$$\begin{aligned}
&\textbf{Upper level:} \quad \underset{Ps^t,\Gamma^t}{max} \sum_{t=1}^{T} \chi^t \cdot Ps^t \\
&\qquad\qquad \text{s.t.,} \quad (4.17), (4.18), \\
&\textbf{Lower level:} \quad \underset{P_i^t,U_i^t}{min} \sum_{t=1}^{T} \sum_{i=1}^{n} F_i^t(P_i^t)U_i^t \\
&\qquad\qquad \text{s.t.,} \quad (4.15), (4.16), \text{ and } (4.21).
\end{aligned} \tag{4.30}$$

The methodology adopted to solve this sub-problem is depicted in Figure **??**. As a first step, prerequisite data, parameters, and initial conditions are determined to initialize the optimization process in the next step, by setting $t = 1$. For instance, the initial state of charge for each ESS component is evaluated by examining the results of the previous dispatch. Next, the algorithm solves the problem for all the non solar time slots $t < t'$. In this case, all the variables and constraints associated with solar dispatch are excluded from the problem, effectively reducing it to a conventional thermal dispatch optimization. The detailed solution approach for thermal dispatch is beyond the scope of this work, as it is extensively covered in the literature. Subsequently, if the current time slot falls within the designated solar dispatch window, i.e., from t' to t'', the optimization is carried out using CBSR analysis, the detailed procedure of which is presented below.

(i) Set $\Gamma^t = 0$ and $Ps^t = 0$, carry out UC via LR to minimize the scheduling cost.The Lagrangian function is formulated as

$$\mathcal{L}(U, P, \phi) = \sum_{i=1}^{n}\sum_{t=1}^{T} F_i(P_i^t)U_i^t + \sum_{t=1}^{T}\phi^t\left(P_d^t - \sum_{i=1}^{n} P_i^t U_i^t + SP_{dis}^t\right), \tag{4.31}$$

where ϕ is assigned as non-negative Lagrangian multiplier to coupling constraint (4.15). Power loss is ignored for simplicity in the power balance constraint. The LR method temporarily relaxes the coupling constraints, and then via dual optimization, the Lagrangian function $\mathcal{L}$ is maximized as a function of Lagrangian multiplier ϕ^t while minimizing as a function of control variables P_i^t and U_i^t; that is,

$$q(\phi^*) = \underset{\phi^t}{max}\, q(\phi), \tag{4.32}$$

where

$$q(\phi) = \min_{U,P} \mathcal{L}(U, P, \phi). \tag{4.33}$$

The alternative form of the Lagrangian in Eq. (4.31) is given by

$$\begin{aligned}&\mathcal{L}(U, P, \phi) = \\ &\sum_{t=1}^{T}\sum_{i=1}^{n} F_i(P_i^t)U_i^t - \sum_{t=1}^{T}\sum_{i=1}^{n}\phi^t(P_i^t)U_i^t + \sum_{t=1}^{T}\phi^t SP_{dis}^t + \sum_{t=1}^{T}\phi^t P_d^t.\end{aligned} \tag{4.34}$$

The last two terms in preceding equation are constants and can be dropped, so, the final expression of the Lagrangian function is presented below

$$\mathcal{L}(U, P, \phi) = \sum_{i=1}^{n} \sum_{t=1}^{T} \left[F_i(P_i^t) - \phi^t P_i^t \right] U_i^t. \tag{4.35}$$

The above expression can be minimized separately for each individual thermal generation unit, thus, the simplified problem is given as follows

$$\begin{aligned} &min\, \mathcal{L}(U, P, \phi) = \\ &\sum_{i=1}^{n} min \sum_{t=1}^{T} \left[F_i(P_i^t) - \phi^t P_i^t \right] U_i^t. \end{aligned} \tag{4.36}$$

Execute ED optimization to evaluate the values of optimal power for the generation units committed in the previous step, applying the binary search lambda iteration algorithm. The cumulative power of all committed thermal units should meet the power demand in a certain hour. The optimal power output of each unit is calculated as

If $P_i^t < P_{i,min}$, then $P_i^t = P_{i,min}$, and
if $P_i^t > P_{i,max}$, then $P_i^t = P_{i,max}$.
Binary search proceeds as follows:

$$P_i^t = (\lambda^t - b_i)/2c_i, \tag{4.37}$$

$$\Delta\lambda = (\lambda_{max} - \lambda_{min})/2, \tag{4.38}$$

$$\lambda_i = \lambda_{min} + \Delta\lambda. \tag{4.39}$$

The conditions listed below are checked, and λ is updated accordingly. If $\sum_{i=1}^{n} P_i^t > P_d^t$, then
$\Delta\lambda = \Delta\lambda/2$ and $\lambda_{i+1} = \lambda_i - \Delta\lambda$.
If $\sum_{i=1}^{n} P_i^t < P_d^t$, then
$\Delta\lambda = \Delta\lambda/2$ and $\lambda_{i+1} = \lambda_i + \Delta\lambda$, and
If $\sum_{i=1}^{n} P_i^t - P_d^t \leq$ tolerance, the algorithm is terminated.

(ii) Increment Γ^t as well as Ps^t, each by a step of δ. Calculate the range of reserve values $\mathcal{R}^t$ and their corresponding solar share levels Γ^t while maximizing the solar share Ps^t. In this framework, Γ^t serves as the stepwise solar share used to trace the feasible reserve–share region, while Ps^t reflects the actual solar

share integrated into the system. By construction, Ps^t follows Γ^t until it reaches the limit imposed by the available solar power or other operating conditions. Beyond this point, Γ^t may continue to increase mathematically, yet it no longer corresponds to additional solar integration. To calculate the range $\mathcal{R}^t$, both UC and ED are executed. For convenience, the CBSR i.e., $\mathcal{R}^t$ in a certain time duration from t' to t'' is expressed as $\mathcal{R}^t_\Gamma$. Let $\mathcal{R}'^t_{d_1}$ denote the robust range of $\mathcal{R}^t_\Gamma$ within which the solar share can be maximized. The solar share Γ^t is initialized with a value equal to zero and increased iteratively with step size δ. This range is a multiset and is obtained iteratively by executing UC and ED, i.e.,

$$\mathcal{R}'^t_{d_1} = \{\mathcal{R}'^t_{d_1 1}, \mathcal{R}'^t_{d_1 2}, ..., \mathcal{R}'^t_{d_1 i}, ..., \mathcal{R}'^t_{d_1 D}\} \quad \forall i \in D \leq Y, \tag{4.40}$$

where D and Y correspond to the maximum number of iterations for robust range and the total number of iterations, respectively. As Γ^t is increased, at some point d_1 , the Γ^t becomes equal or nearly equal to $\mathcal{R}^t_\Gamma$. At this stage, the CBSR is represented by $\mathcal{R}^t_{d_1}$ and solar share is expressed as $\Gamma^t_{d_1}$. At any iteration, $\mathcal{R}^t_\Gamma$ is allocated to the robust range based on following criterion.

$$\text{If } \Gamma^t \leq \mathcal{R}^t_\Gamma, \Rightarrow \mathcal{R}^t_\Gamma \in \mathcal{R}'^t_{d1} \tag{4.41}$$

$$\mathcal{R}^t_\Gamma = \mathcal{R}'^t_{d1i}, \quad \forall i \in D \leq Y \tag{4.42}$$

The algorithm keeps on increasing Γ^t and allocating $\mathcal{R}^t_\Gamma$ to the robust range until the criterion (4.41) is satisfied.

(iii) Evaluate the point of operation by calculating the maximum limit of robust CBSR and corresponding solar share as

$$\mathcal{R}^t_{d_1} = max(\mathcal{R}'^t_{d_1}), \tag{4.43}$$

$$\Gamma^t_{d_1} = \Gamma^t(ind_{d_1}), \tag{4.44}$$

where ind_{d_1} is the index of the maximum value in $\mathcal{R}'^t_{d_1}$, i.e.,

$$ind_{d_1} = \arg\max_x (\mathcal{R}'^t_{d_1}). \tag{4.45}$$

In the absence of ESS, the SSR is adequately allocated based on the following constraint, to maintain continuous power system operation during thermal contingency events

$$SSR^t \geq SSR^t_{\text{opt}(1,2)}, \tag{4.46}$$

where $SSR^t_{\text{opt}(1,2)}$ represents the predefined optimal SSR for the first-order and second-order contingencies and must be computed as in [63]. The sub-problem I is solved with an additional constraint (4.46). RCUC is executed using Eq. (4.36) to commit a set of thermal units. Once an optimal set of thermal units is committed, ED is executed for same set of committed units iteratively for each increment of δ and $\mathcal{R}^t_\Gamma$ is calculated.

(iv) Repeat the steps (i) to (iii) for all time slots.

Lastly, the problem is solved for time slots $t > t''$, using the same approach as for $t < t'$.

4.3.2 Sub-problem II

The second sub-problem aims to minimize solar cost while maximizing the number of solar plants in ON condition to enhance the reliability of the solar-integrated HPS. This problem is expressed as

$$\underset{Us^t_j}{min} \sum_{t}^{T} \chi^t \cdot \left[w_1 \sum_{j=1}^{m} \Upsilon^t_j Pgs^t_j Us^t_j - \beta w_2 \sum_{j=1}^{m} Us^t_j \right] \tag{4.47}$$

$$\text{s.t.,} \quad (4.19),$$

where w_1 and w_2 are the weights attributed to the solar cost and the number of committed solar plants, respectively. β is the weighting coefficient that scales the term involving the number of solar plants in the objective function, specifically balancing it with the first objective. Its purpose is to ensure compatibility between the two objectives in the problem. It adjusts the influence of the number of committed plants relative to the solar cost, helping maintain a balanced approach to both objectives.

For simplicity, the objectives in Eq. (4.47) are represented by $\mathscr{F}_1$ and $\mathscr{F}_2$ as given below:

$$\mathscr{F}^t_1 = w_1 \sum_{j=1}^{m} \Upsilon^t_j Pgs^t_j Us^t_j \tag{4.48}$$

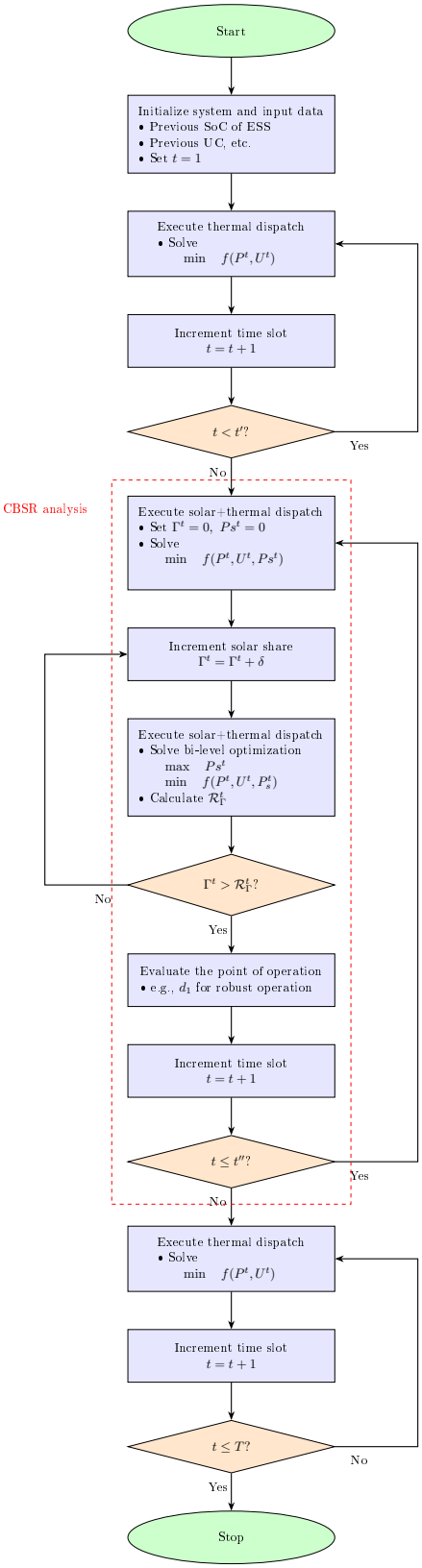

Figure 4.3: Flowchart of the proposed solution to sub-problem I.

$$\mathscr{F}_2^t = \beta w_2 \sum_{j=1}^{m} U s_j^t \tag{4.49}$$

4.4 Test system and simulation results

The test system involves 26 thermal units, 40 solar plants and an ESS. The data for thermal units and load profile are obtained from [90]. The Per unit cost from each solar plant is provided in Table 4.1 and ESS has been divided into three parts which are SP_{th}, SP_{NS}, and SP_{Γ} with power capacities of 400 MW, 280 MW, and 240 MW, respectively. The capacity SP_{th} has been selected according to $'N-1'$ criterion which is the capacity of largest thermal unit and rest of the capacities have been selected arbitrarily. With the allocation of aforementioned storage capacities, SP_{Γ}^t and SP_{NS}^t came out to be 24 MW and 20 MW, respectively. The solar power is supposed to be available during 10:00 hours to 18:00 hours of a fair day, therefore, $t' = 10$ and $t'' = 18$. The simulation results have been presented for the time slots in which solar power is integrated. In this study, the step size has been taken as $\delta = 20$. Following subsections present the results under various practical conditions.

4.4.1 System operation with ESS fully charged

This scenario considers the case where all components of the ESS are fully charged. Such a situation may occur when no contingencies have arisen in the recent past and sufficient surplus solar power has been available for a long enough duration to completely charge the ESS. The following subsections discuss the pre-contingency and post-contingency results for this scenario.

4.4.1.1 Pre-contingency dispatch

When the ESS is fully charged, it offsets the need for thermal units to maintain the required reserve margin. Therefore, the reserve constraint (4.46) is excluded from the optimization process. To compute the results for this scenario, the optimization was carried out by executing UC along with ED for every incremental increase in the solar share, and the CBSR was subsequently analyzed. The corresponding UC schedule is presented in Table 4.2. In the table, a value of zero denotes that

Table 4.1: Power ratings and per unit costs of solar plants.

Number of Plants	$\mathbf{P_{rated}}$ (MW)	Unit Rate ($/KWh)
3	10	0.19,2x0.18
5	12	5x0.19
1	15	0.2
3	18	3x0.2
2	20	2x0.23
4	24	4x0.23
4	25	4x0.23
2	30	2x0.24
5	35	0.25,0.26,0.23,2x0.24
7	40	2x0.27,2x0.275,3x0.28
2	50	2x0.18
1	60	0.21
1	80	0.22

a thermal generating unit is OFF, whereas a value of one indicates that it is ON. From this schedule, it is evident that all operational constraints are duly satisfied. For instance, Unit 21 has minimum up-time and down-time requirements of 5 and 4 time slots, respectively. This unit was decommitted in time slot 18 and remained OFF until after its minimum down-time expired, only returning to service in time slot 22. Likewise, following its commitment in time slot 8, the unit remained in operation for 10 consecutive time slots, thereby satisfying its specified minimum up-time requirement.

Table 4.2: UC schedule for system operation with ESS fully charged.

t (hr)	unit (1-26)																										
	U_1	U_2	U_3	U_4	U_5	U_6	U_7	U_8	U_9	U_{10}	U_{11}	U_{12}	U_{13}	U_{14}	U_{15}	U_{16}	U_{17}	U_{18}	U_{19}	U_{20}	U_{21}	U_{22}	U_{23}	U_{24}	U_{25}	U_{26}
1	0	0	0	0	0	0	0	0	0	0	0	0	0	0	0	0	1	1	1	1	0	0	0	1	1	1
2	0	0	0	0	0	0	0	0	0	0	0	0	0	0	0	0	1	1	1	1	0	0	0	1	1	1
3	0	0	0	0	0	0	0	0	0	0	0	0	0	0	0	0	1	1	1	1	0	0	0	1	1	1
4	0	0	0	0	0	0	0	0	0	0	0	0	0	0	0	0	1	1	1	1	0	0	0	1	1	1
5	0	0	0	0	0	0	0	0	0	0	0	0	0	0	0	0	1	1	1	1	0	0	0	1	1	1
6	0	0	0	0	0	0	0	0	0	1	1	1	1	0	0	0	1	1	1	1	0	0	0	1	1	1
7	0	0	0	0	0	0	0	0	0	1	1	1	1	0	0	0	1	1	1	1	0	0	0	1	1	1
8	1	1	1	1	1	0	0	0	0	1	1	1	1	1	1	1	1	1	1	1	1	1	1	1	1	1
9	1	1	1	1	1	0	0	0	0	1	1	1	1	1	1	1	1	1	1	1	1	1	1	1	1	1
10	1	1	1	1	1	0	0	0	0	1	1	1	1	1	1	1	1	1	1	1	1	1	1	1	1	1
11	1	1	1	1	1	0	0	0	0	1	1	1	1	1	1	1	1	1	1	1	1	1	1	1	1	1
12	0	0	0	0	0	0	0	0	0	1	1	1	1	1	1	1	1	1	1	1	1	1	1	1	1	1
13	0	0	0	0	0	0	0	0	0	1	1	1	1	1	1	1	1	1	1	1	1	1	1	1	1	1
14	0	0	0	0	0	0	0	0	0	1	1	1	1	1	1	1	1	1	1	1	1	1	1	1	1	1
15	1	1	1	1	1	0	0	0	0	1	1	1	1	1	1	1	1	1	1	1	1	1	1	1	1	1
16	1	1	1	1	1	0	0	0	0	1	1	1	1	1	1	1	1	1	1	1	1	1	1	1	1	1
17	0	0	0	0	0	0	0	0	0	1	1	1	1	1	1	1	1	1	1	1	1	1	1	1	1	1
18	0	0	0	0	0	0	0	0	0	1	1	1	1	1	1	1	1	1	1	1	0	0	0	1	1	1
19	1	1	1	1	1	0	0	0	0	1	1	1	1	1	1	1	1	1	1	1	0	0	0	1	1	1
20	1	1	1	1	1	0	0	0	0	1	1	1	1	1	1	1	1	1	1	1	0	0	0	1	1	1
21	1	1	1	1	1	0	0	0	0	1	1	1	1	1	1	1	1	1	1	1	0	0	0	1	1	1
22	1	1	1	1	1	0	0	0	0	1	1	1	1	1	1	1	1	1	1	1	1	1	1	1	1	1
23	0	0	0	0	0	0	0	0	0	1	1	1	1	0	0	0	1	1	1	1	1	1	1	1	1	1
24	0	0	0	0	0	0	0	0	0	0	0	0	0	0	0	0	1	1	1	1	1	1	1	1	1	1

The variations in $\mathcal{R}_{\Gamma}^{10}$ with increasing solar share are depicted in Figure 4.4 and these results are further elaborated in Table 4.3. It can be seen from the

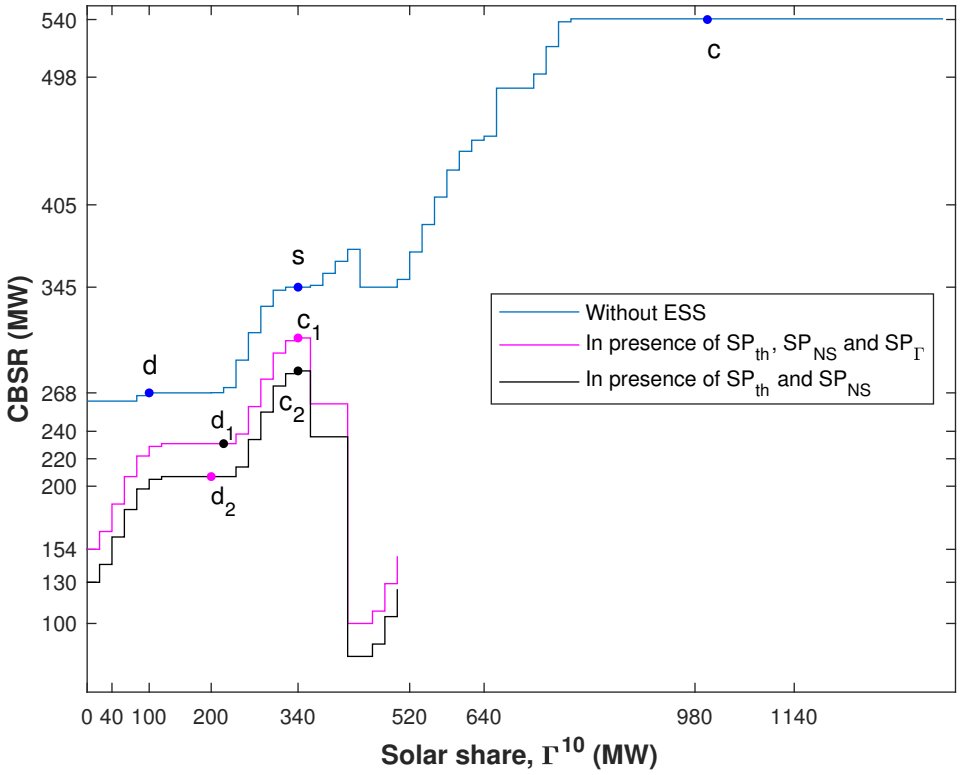

Figure 4.4: CBSR variations at w.r.t solar share at $t = 10:00$ hours.

table that the evaluations of $\mathcal{R}_{\Gamma}^{10}$ come out to be greater than or equal to the solar share Γ^{10} till a certain value of solar share and beyond this value the evaluations of $\mathcal{R}_{\Gamma}^{10}$ become smaller than the solar share. The point d_1 is identified to such value of solar share beyond which the evaluation of $\mathcal{R}_{\Gamma}^{10}$ becomes smaller than the solar share and at this point d_1, the CBSR is indicated by $\mathcal{R}_{d_1}^{10}$. For instance, till Γ^{10} reaches 220 MW, the $\mathcal{R}_{\Gamma}^{10}$ comes out to be greater than 220 MW. As the Γ^{10} increases to 240 MW, the $\mathcal{R}_{\Gamma}^{10}$ comes out to be 238 MW which is less than its corresponding solar share of 240 MW. Therefore, the point d_1 is assigned to the solar share of 220 MW with corresponding $\mathcal{R}_{\Gamma}^{10}$ of 231 MW, i.e., $d_1(220, 231)$ and CBSR analysis was terminated once the point d_1 was located. The point d_1 represents the upper bound of the robust CBSR range and corresponds to the maximum achievable solar share while maintaining robustness. At this operating point, the HPS can withstand both individual and simultaneous solar and thermal

Table 4.3: Allocation of robust CBSR at point d_1 and solar share maximization via CBSR analysis.

	time (10-18 hrs)								
Γ^t	10	11	12	13	14	15	16	17	18
0	188	154	157	157	197	204	178	199	218
20	208	154	177	177	215	204	178	203	238
40	225	154	197	197	226	204	196	219	239
60	225	154	215	215	231	204	216	228	239
80	227	159	226	224	231	218	226	231	239
100	229	177	231	231	231	237	226	231	239
120	231	197	231	231	231	251	226	231	239
140	231	215	231	231	183	251	226	231	239
160	231	231	231	231	183	251	226	231	239
180	231	231	231	231	231	251	229	231	248
200	231	231	231	231	248	231	231	239	268
220	$\mathcal{R}^{10}_{d_1}\rightarrow$ 231	231	231	231	268	224	231	259	288
240	238	231	248	248	288	121	231	280	303
260			268	268	303			286	308
280			288	288	308			286	260
300			270	292	298			260	

contingencies. Therefore, to ensure robustness and maximize solar contribution, the system should be operated at d_1.

Any further increase in Γ^{10} beyond d_1 resulted in non-robust range of CBSR. The point c_1 was located to evaluate the maximum limit of this range. This point determines the maximum $\mathcal{R}^{10}_{\Gamma}$ that can be delivered by the system. Interestingly, as the solar share was further increased beyond the point c_1, a steep dip in $\mathcal{R}^{10}_{\Gamma}$ was observed at solar share of 420 MW. This dip determines the limit beyond which the algorithm fails due to power mismatch. This is because the penetration of too high solar share results in too low thermal share for a specified load demand. Therefore, the algorithm cannot select appropriate thermal units to satisfy such low demands due to various system constraints. Beyond this dip, the $\mathcal{R}^{10}_{\Gamma}$ may increase again, however, the power mismatch persists.

4.4.1.2 Post-contingency dispatch

Consider the HPS operating at point d_1, which corresponds to a robust solar share

of 220 MW and CBSR of 231MW. The pre-contingency operating points and upward reserves of the thermal units are presented in Figure 4.5(a). As shown, Unit 21 provides the highest up-reserve of 27.5 MW while generating 69 MW. Suppose this unit experiences an outage simultaneously with the solar source, creating a worst-case contingency that results in a total loss of 289 MW. Once the contingency occurs, both the power output and reserve of Unit 21 become unavailable. To manage this contingency, the remaining online units ramp up and

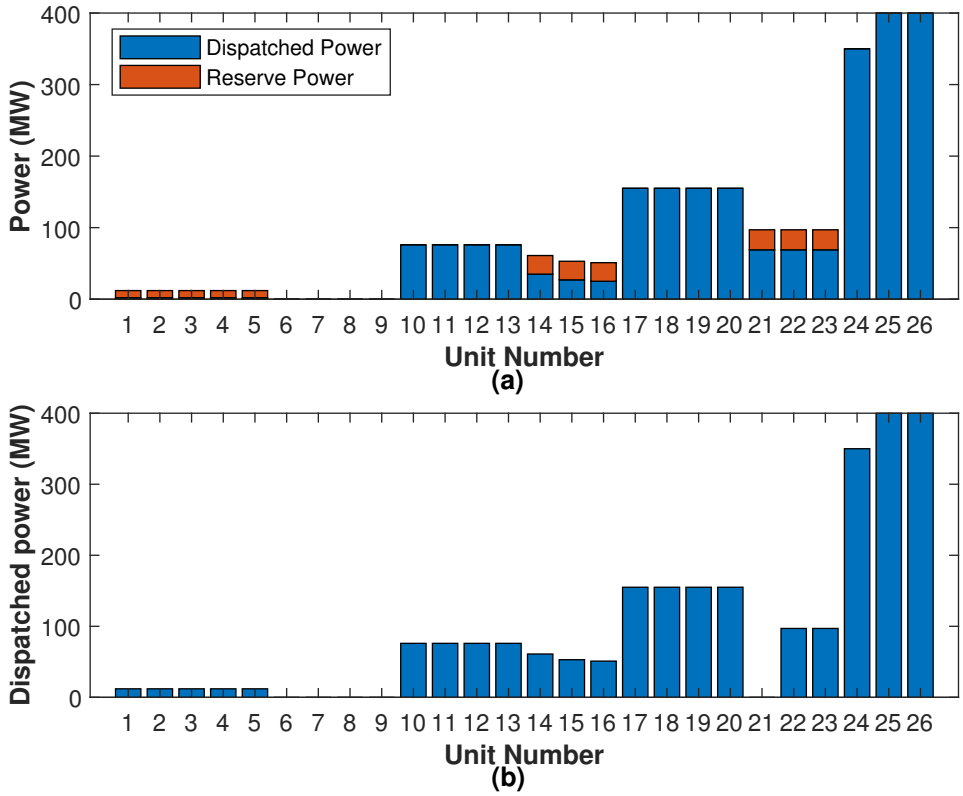

Figure 4.5: Power outputs and up-reserves of thermal units for operating point d_1
(a) Pre-contingency scenario
(b) Post-contingency scenario

settle at new operating points, as depicted in Figure 4.5(b). It can be observed that the units ramp within their prescribed limits and fully dispatch their available reserves. However, the remaining resulting CBSR is 203.5 MW. Now 69MW of thermal power outage will be coped with SP_{th} and 220MW lost power of solar share will be tackle by CBSR. This shortfall of 220-203.5= 16.5MW arises which can be handeled by increasing the storage size of SP_{T}. So, the practical values of

istalled SP_{Γ} will be 24MW+16MW, after CBSR analysis. This study addresses worst-case deficits through the dynamic allocation of SP_{Γ}^{t}. In this instance, the outage was successfully compensated by allocating an additional 85.5 MW of SP_{Γ}^{t}.

4.4.2 System operation with ESS fully discharged

This scenario considers the case where all components of the ESS are fully discharged. Such a situation may occur when potential contingencies have arisen in the previous dispatch and sufficient surplus solar power has not been available to recharge the ESS. The following subsections discuss the pre-contingency and post-contingency results for this scenario.

4.4.2.1 Pre-contingency dispatch

When the ESS is completely discharged, the thermal units must maintain adequate reserve margins to handle potential thermal outages. To guarantee this reserve provision, the RCUC was executed by integrating the reserve constraint (4.46) into the optimization model, which will cause to commit more thermal units i order to maintai the reserve as compared to UC results in Table 4.2. The resulting optimal schedule of the thermal units is shown in Table 4.4. It is evident from the table that the system operates within the given limits. All the units switch from one state of operation to another only if the respective minimum time has elapsed. For instance, the minimum down time for Unit 14 is -2. It can be seen from that table that Unit 14 was turned OFF in slot 6 and remained in OFF condition for consecutive two slots. Furthermore, ramp rate limits of the thermal units are satisfied as well. As an evidence, the power settlements and ramps of Unit 14 are depicted in Figure 4.6. The ramp-up and the ramp-down limits of this unit are 51 and 74 MW/h, respectively. The unit is turned OFF at time slot 6 and turned ON again at time slot 8. In the figure, a ramp-up of 25.5 MW can be observed at transition from OFF condition at slot 7 to ON condition at slot 8, which is less than the up-rate limit. Similarly, the ramp-ups at other time slots are well within the up-rate limit. In this figure, the maximum up-rate of 25.5 MW occurs at slot transitions 7-8, 8-9, 12-13, 14-15, and 18-19. Likewise, the maximum down-rate of -34.5 MW is experienced at transition from from slot 11 to slot 12. For further

Table 4.4: RCUC schedule for system operation with ESS fully discharged.

t (hr)	unit (1-26)																									
	U_1	U_2	U_3	U_4	U_5	U_6	U_7	U_8	U_9	U_{10}	U_{11}	U_{12}	U_{13}	U_{14}	U_{15}	U_{16}	U_{17}	U_{18}	U_{19}	U_{20}	U_{21}	U_{22}	U_{23}	U_{24}	U_{25}	U_{26}
1	0	0	0	0	0	0	0	0	0	1	1	1	1	1	1	1	1	1	1	1	0	0	0	1	1	1
2	0	0	0	0	0	0	0	0	0	1	1	1	1	1	1	1	1	1	1	1	0	0	0	1	1	1
3	0	0	0	0	0	0	0	0	0	1	1	1	1	1	1	1	1	1	1	1	0	0	0	1	1	1
4	0	0	0	0	0	0	0	0	0	1	1	1	1	1	1	1	1	1	1	1	0	0	0	1	1	1
5	0	0	0	0	0	0	0	0	0	1	1	1	1	1	1	1	1	1	1	1	0	0	0	1	1	1
6	0	0	0	0	0	0	0	0	0	1	1	1	1	0	0	0	1	1	1	1	0	0	0	1	1	1
7	1	1	1	1	1	0	0	0	0	1	1	1	1	0	0	0	1	1	1	1	0	0	0	1	1	1
8	1	1	1	1	1	0	0	0	0	1	1	1	1	1	1	1	1	1	1	1	1	1	0	1	1	1
9	1	1	1	1	1	1	1	1	1	1	1	1	1	1	1	1	1	1	1	1	1	1	1	1	1	1
10	1	1	1	1	1	1	1	1	1	1	1	1	1	1	1	1	1	1	1	1	1	1	1	1	1	1
11	1	1	1	1	1	1	1	1	1	1	1	1	1	1	1	1	1	1	1	1	1	1	1	1	1	1
12	1	1	1	1	1	1	1	1	1	1	1	1	1	1	1	1	1	1	1	1	1	1	1	1	1	1
13	1	1	1	1	1	0	0	0	0	1	1	1	1	1	1	1	1	1	1	1	1	1	1	1	1	1
14	1	1	1	1	1	0	0	0	0	1	1	1	1	1	1	1	1	1	1	1	1	1	1	1	1	1
15	1	1	1	1	1	1	1	1	1	1	1	1	1	1	1	1	1	1	1	1	1	1	1	1	1	1
16	1	1	1	1	1	1	1	1	1	1	1	1	1	1	1	1	1	1	1	1	1	1	1	1	1	1
17	1	1	1	1	1	1	1	1	1	1	1	1	1	1	1	1	1	1	1	1	1	1	1	1	1	1
18	1	1	1	1	1	0	0	0	0	1	1	1	1	1	1	1	1	1	1	1	1	1	1	1	1	1
19	1	1	1	1	1	0	0	0	0	1	1	1	1	1	1	1	1	1	1	1	1	1	1	1	1	1
20	1	1	1	1	1	1	0	0	0	1	1	1	1	1	1	1	1	1	1	1	1	1	1	1	1	1
21	1	1	1	1	1	1	1	1	1	1	1	1	1	1	1	1	1	1	1	1	1	1	1	1	1	1
22	1	1	1	1	1	0	0	0	0	1	1	1	1	1	1	1	1	1	1	1	1	1	1	1	1	1
23	0	0	0	0	0	0	0	0	0	1	1	1	1	1	1	1	1	1	1	1	1	1	1	1	1	1
24	0	0	0	0	0	0	0	0	0	1	1	1	1	1	1	1	1	1	1	1	0	0	0	1	1	1

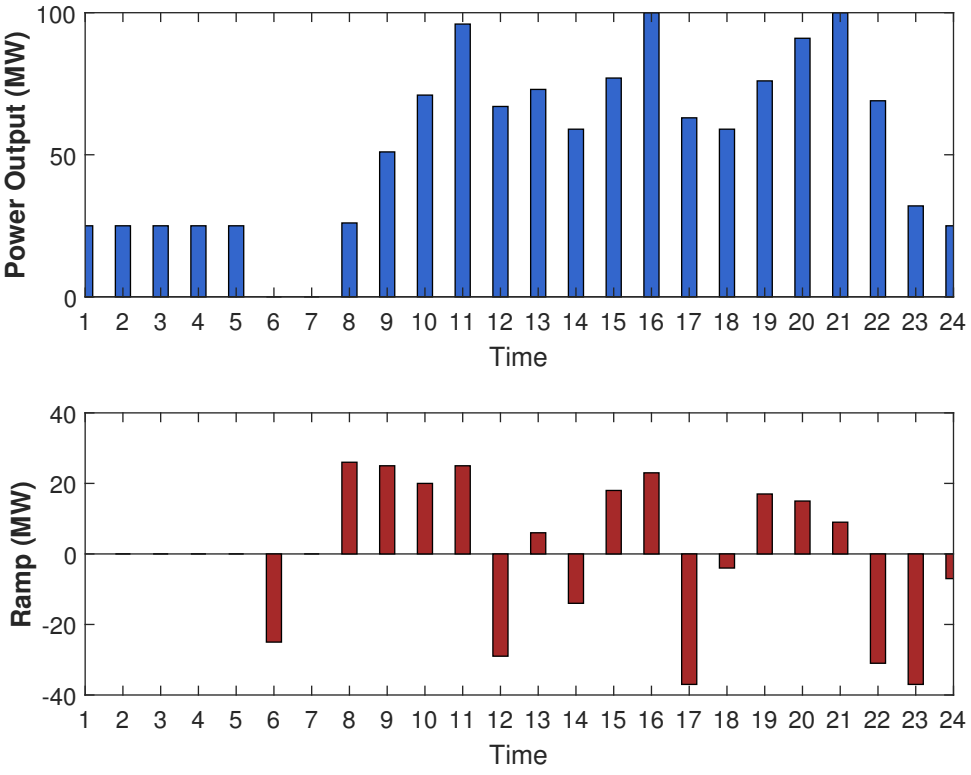

Figure 4.6: Power output and ramping profile of Unit 14 across different hours.

clarifications, the ramps of all thermal units are given in Table 4.5. The SSR allocated by RCUC is shown in Figure 4.7. In this figure, it can be seen that allocated SSR is higher than $SSR^t_{opt(1,2)}$ across all time slots. This is attributed to the binary selection of the thermal generation units and corresponding minimum power limits of the committed units. Furthermore, it can be noticed that allocated SSR follows $SSR^t_{opt(1,2)}$ during time slots 6, 7, 8, 9, and 24, which represents the ideal case. However, the variations in allocated SSR are independent of $SSR^t_{opt(1,2)}$ for the rest of the time slots, which is attributed to the significant variations in load demand as well as the UC schedule. Furthermore, the maximum solar share Γ^t has been evaluated for points d, s, and c using SSR analysis [92] as shown in Figure 4.4. The solar shares at points d and s i.e., Γ^t_d and Γ^t_s correspond to solar share penetration within the robust range of SSR. With penetration of Γ^t_d, the HPS is robust against contingency events of simultaneous solar and thermal power outages. In contrast, the operating point s corresponds to robustness of the HPS against either a solar or a thermal power outage due to higher penetration of solar share. Finally, if the system is operated at point c, the system will become non-robust and loss of load will be experienced in case of any potential outage.

It can be observed from the figure that point d corresponds to a 100 MW solar share which is significantly smaller than the share at point d_1. This is due to the fact that without ESS, a significant part of SSR i.e., $SSR^{10}_{opt(1,2)}$ was dedicated to address thermal contingency events. Furthermore, the $\mathcal{R}^{10}_{\Gamma}$ in this case always comes out to be greater than that of with ESS fully charged. This is because the UC is carried out only initially and subsequent computations of power dispatch use the same RCUC schedule.

Table 4.5: Ramps experienced by the thermal units during dispatch.

t (hr)	unit (1-26)																									
	U_1	U_2	U_3	U_4	U_5	U_6	U_7	U_8	U_9	U_{10}	U_{11}	U_{12}	U_{13}	U_{14}	U_{15}	U_{16}	U_{17}	U_{18}	U_{19}	U_{20}	U_{21}	U_{22}	U_{23}	U_{24}	U_{25}	U_{26}
1	0	0	0	0	0	0	0	0	0	0	0	0	0	0	0	0	0	0	0	0	0	0	0	0		
2	0	0	0	0	0	0	0	0	0	0	0	0	0	0	0	0	4.34	4.25	4.17	4.12	0	0	0	13.13	0	0
3	0	0	0	0	0	0	0	0	0	0	0	0	0	0	0	0	-5.79	-5.66	-5.56	-5.49	0	0	0	-17.5	0	0
4	0	0	0	0	0	0	0	0	0	0	0	0	0	0	0	0	1.45	1.41	1.39	1.37	0	0	0	4.37	0	0
5	0	0	0	0	0	0	0	0	0	0	0	0	0	0	0	0	7.23	7.08	6.96	6.87	0	0	0	21.88	0	0
6	0	0	0	0	0	0	0	0	0	14.61	12.49	10.56	8.52	-25	-25	-25	27.47	27.5	27.5	27.5	0	0	0	18.85	0	0
7	12	12	9.72	7.3	5.01	0	0	0	0	19.25	19.25	19.25	19.25	0	0	0	0	4.93	9.18	12.86	0	0	0	0	0	0
8	0	0	2.28	4.7	6.99	0	0	0	0	19.25	19.25	19.25	19.25	25.5	25.5	25.5	0	0	0	0	27.5	27.5	0	0	0	0
9	0	0	0	0	0	15.25	15.25	15.25	15.25	7.69	9.81	11.74	13.78	25.5	25.5	25.5	0	0	0	0	41.45	41.45	27.5	0	0	0
10	-9.6	-9.6	-9.6	-9.6	-9.6	-11.25	-11.25	-11.25	-11.25	0	0	0	0	19.61	12.71	5.84	0	0	0	0	0	0	41.45	0	0	0
11	0	0	0	0	0	0	0	0	0	0	0	0	0	25.5	25.5	25.5	0	0	0	0	27.5	27.5	18.5	0	0	0
12	0	0	0	0	0	0	0	0	0	0	0	0	0	-28.77	-28.83	-28.91	0	0	0	0	-27.5	-27.5	-18.5	0	0	0
13	0	0	0	0	0	-4	-4	-4	-4	0	0	0	0	5.23	5.32	5.45	0	0	0	0	0	0	0	0	0	0
14	0	0	0	0	0	0	0	0	0	0	0	0	0	-13.07	-13.31	-13.62	0	0	0	0	0	0	0	0	0	0
15	0	0	0	0	0	4	4	4	4	0	0	0	0	17.64	17.97	18.39	0	0	0	0	0	0	0	0	0	0
16	0	0	0	0	0	0	0	0	0	0	0	0	0	22.86	25.5	25.5	0	0	0	0	27.5	9.64	0	0	0	0
17	0	0	0	0	0	0	0	0	0	-3.9	-6.91	-9.52	-12.53	-37	-37	-37	0	0	0	0	-27.5	-8.64	0	0	0	0
18	0	0	0	0	0	-4	-4	-4	-4	3.9	6.91	9.52	12.53	-3.5	-6.47	-6.89	0	0	0	0	0	0	0	0	0	0
19	0	0	0	0	0	0	0	0	0	0	0	0	0	16.34	16.64	16.02	0	0	0	0	0	0	0	0	0	0
20	0	0	0	0	0	4	0	0	0	0	0	0	0	15.03	15.3	15.67	0	0	0	0	0	0	0	0	0	0
21	0	0	0	0	0	0	4	4	4	0	0	0	0	9.13	14.27	14.6	0	0	0	0	0	0	0	0	0	0
20	-2.4	0	0	0	0	-4	-4	-4	-4	0	0	0	0	-30.74	-36.26	-37	0	0	0	0	0	0	0	0	0	0
23	0	-2.4	-2.4	-2.4	-2.4	0	0	0	0	-40	-40	-40	-40	-37	-37	-30.55	0	0	0	-3.45	0	0	0	0	0	0
24	0	0	0	0	0	0	0	0	0	-20.8	-20.8	-20.8	-20.8	-7.26	-0.34	0	-9.19	-14.54	-19.09	-19.53	-68.95	-68.95	-68.95	0	0	0

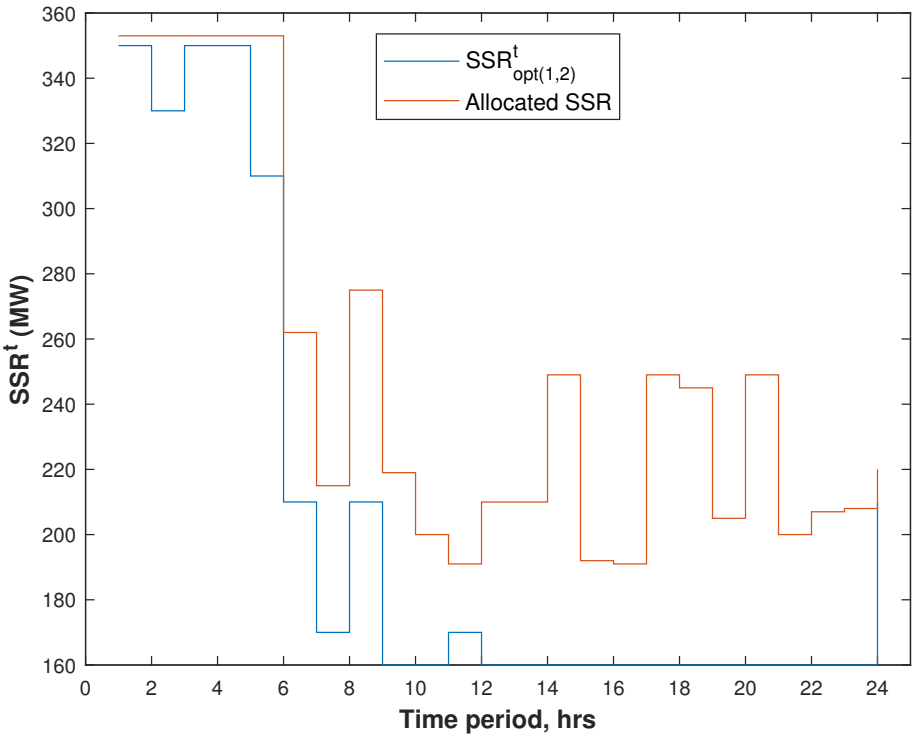

Figure 4.7: Allocated SSR vs. optimal SSR with value of lost load = 1000 $/MWh.

4.4.2.2 Post-contingency dispatch

The system is assumed to be operating at point $d(100, 268)$, with the corresponding pre-contingency operating points and up-reserves of the thermal units illustrated in Figure 4.8(a). A simultaneous outage of solar generation and Unit 21 is considered, resulting in a combined contingency of 169 MW. To manage this contingency, the online units ramp up to dispatch their respective reserve powers, as depicted in Figure 4.8(b). In this case, the dispatched SSR is 169 MW, indicating that the simultaneous contingency has been successfully mitigated. Consider another scenario in which the system is operating at point $s(340, 345)$ prior to the contingency. Here, the solar share is 340 MW and the corresponding SSR is 345 MW. Under this operating condition, the system can handle any contingency of up to 345 MW. However, since the solar contribution alone accounts for 340 MW, a solar outage would consume almost the entire SSR, leaving insufficient reserve to accommodate an additional unit outage. Thus, at operating point s, the system

lacks the capability to handle a simultaneous solar and thermal contingency.

Finally, operating the system at point $c(780, 540)$ results in a power deficit of 240 MW in the event of a solar outage.

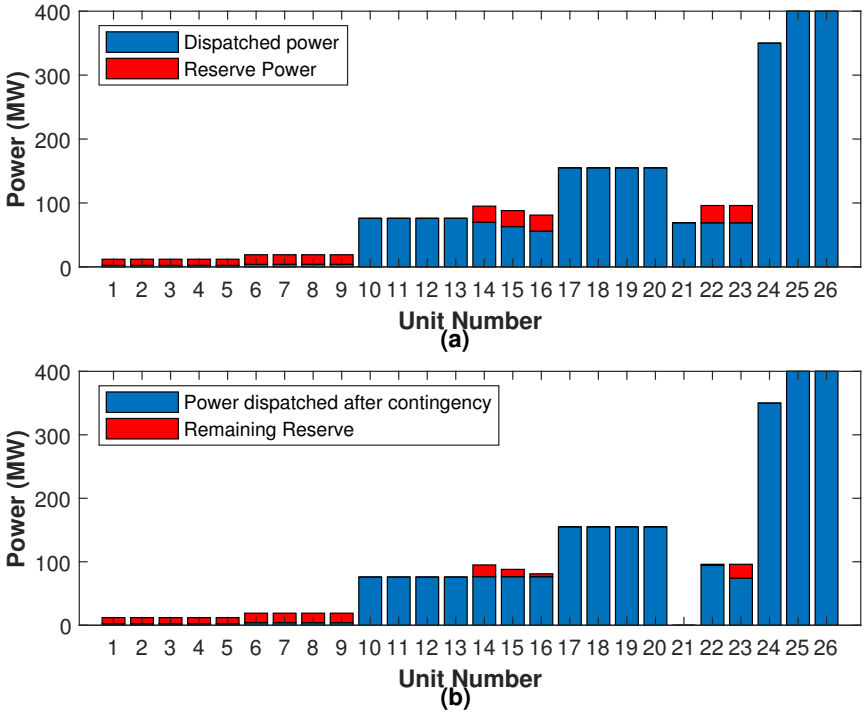

Figure 4.8: Power outputs and up-reserves of thermal units for operating point d
(a) Pre-contingency scenario
(b) Post-contingency scenario

4.4.3 System operation with SP_{Γ} discharged

In this scenario, it is assumed that SP_{Γ} is not available to address the solar outages. Such situation may arise due to various reasons. For instance, the SP_{Γ} has been fully discharged while addressing the solar outage and the outage occurs the next day again with SP_{Γ} uncharged. This scenario is considered to investigate the impact of SP_{Γ}^{10} on solar power penetration within the robust range of $\mathcal{R}_{\Gamma}^{10}$. In Figure 4.4, black coloured graph depicts this scenario. In this graph, the point d_2 is located to determine the maximum value of robust range of $\mathcal{R}_{\Gamma}^{10}$ i.e., $\mathcal{R}_{d_2}^{10}$. The results are depicted in Table 4.6 using the same CBSR analysis as already discussed in the previous subsections. It can be analyzed from the table that

$\mathcal{R}_{d_2}^{10}$ comes out to be 207 MW with corresponding solar share of 200 MW. It can be further analyzed from the table and the figure that the solar share and the corresponding $\mathcal{R}_{\Gamma}^{10}$ comes out to be less than the respective values obtained in presence of SP_{Γ}. Thus, without SP_{Γ}, the system may be operated with reduced solar share. Similarly, the post-contingency dispatch exhibits the same behavior as discussed in Section 4.4.1.2, with only the resulting values being reduced.

The overall results for the above mentioned scenarios of solar share and ESS are summarized in Table 4.8.

Table 4.6: Allocation of robust CBSR at point d_2 and solar share maximization via CBSR analysis.

	time (10-18 hrs)								
Γ^t	10	11	12	13	14	15	16	17	18
0	164	130	133	133	173	180	154	175	194
20	184	130	153	153	191	180	154	179	214
40	201	130	173	173	202	180	172	195	215
60	201	130	191	191	207	180	192	204	215
80	203	135	202	200	207	194	202	207	215
100	205	153	207	207	207	213	202	207	215
120	207	173	207	207	207	227	202	207	215
140	207	191	207	207	159	227	202	207	215
160	207	207	207	207	159	227	202	207	215
180	207	207	207	207	207	227	205	207	224
200 $\mathcal{R}_{d_2}^{10}\rightarrow$	207	207	207	207	224	227	207	215	244
220	207	207	207	207	244	200	207	235	264
240					264			255	279
260					279			262	284
280					284			262	236
300					274				

4.4.4 Optimization of solar cost and plant selection

After evaluating the maximum value of Ps^t within the robust range of CBSR, the optimization for minimizing solar costs and selecting the appropriate plants is solved. The system involves 40 solar plants with diverse power ratings, strategically distributed across the power network and integrated into its operational framework.

The weight w_1 is initially set to 1 and is progressively reduced with each iteration, while the weight w_2 is increased in such a way that $w_1 + w_2 = 1$. It can be observed that fewer solar plants are selected in the initial iterations, and the number of selected plants increases as the iterations proceed as shown in Figure 4.9. Likewise, the solar cost increases in the same manner as the iterations progress. This rise in the number of solar plants and the cost of solar energy is attributed to the varying values of w_2 and w_1, respectively. For instance, fewer plants are selected during initial iterations because w_2 is initialized at a minimum value. Since our objective is to maximize the number of solar plants, higher values are gradually assigned to w_2 as the iterations progress, thereby increasing the significance of maximizing $\mathscr{F}_2$. Therefore, more solar plants are chosen with the increase in the number of iterations. In contrast, the solar cost increases with the rise in the number of iterations due to the successive decrease in its corresponding weight, w_1. As w_1 decreases, the significance of minimizing solar cost is reduced, resulting in an increase in solar cost as more iterations elapse. As the sub-problem II is essentially a binary optimization, both the objectives $\mathscr{F}_1$ and $\mathscr{F}_2$ are discrete functions of their associated weights. For instance, in Figure 4.9, 13 solar plants are chosen up to the 14th iteration, and changing the value of w_2 from 0.0100 to 0.1400 does not affect the maximization of solar plants. A further increase in w_2 by 0.0100 at the 15th iteration causes the number of selected plants to increase to 15, which remains the same until the 60th iteration. Therefore, this optimization yields only a few Pareto optimal solutions. Thus, appropriate settings of parameters such as step sizes of w_i, number of iterations, and β are critical in this optimization.

During the process of finding the Pareto optimal solutions, it was observed that the value of β has a significant impact on both the number of solutions and the number of iterations. Therefore, the value of β is adjusted empirically such that the maximum number of Pareto optimal solutions are obtained in minimum number of iterations. With the initial setting of $\beta = 10^3$, in Figure 4.9, four Pareto optimal solutions are achieved, and the algorithm takes 67 iterations to converge. A further increase in the value of β to 10^4 results in four solutions being reached within 16 iterations, which is depicted in Figure B.1. The procedure is

continued by progressively increasing the value of β and the resulting number of solutions and corresponding iterations are evaluated in Table 4.7. It is evident from the table that the optimal setting of β is 4×10^4 for which four Pareto optimal solutions are achieved in six iterations. Although a further increase in the value of β corresponds to fewer iterations, it leads to a reduced number of solutions. For instance, setting $\beta = 10^5$ results in three solutions.

Among the aforementioned Pareto-optimal solutions, the system operator may select the most appropriate solution depending on its defined priorities. These priorities can vary among system operators, influenced by factors such as the local energy market dynamics and regional energy policies. In some cases, system operators may prioritize operational costs, while for others, ensuring the reliability of the system may be of higher significance.

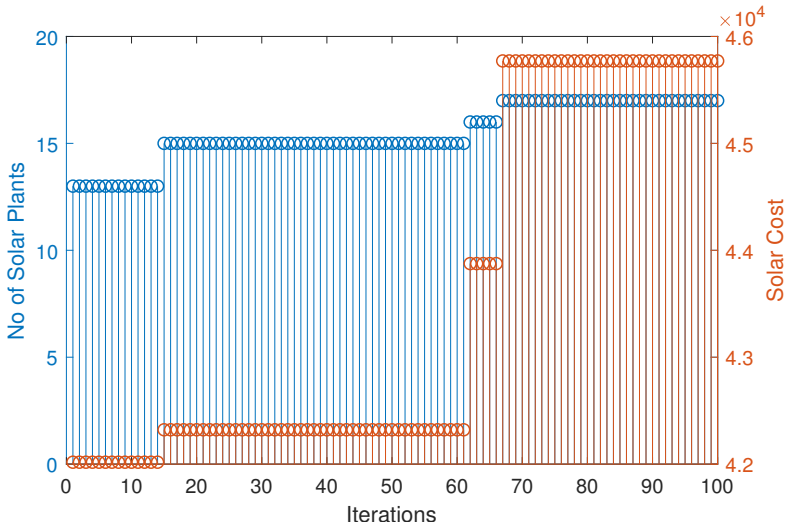

Figure 4.9: Results of sub-problem II: number of selected solar plants vs. solar cost over 100 iterations, with solar share at d_1 for $\beta = 10^3$.

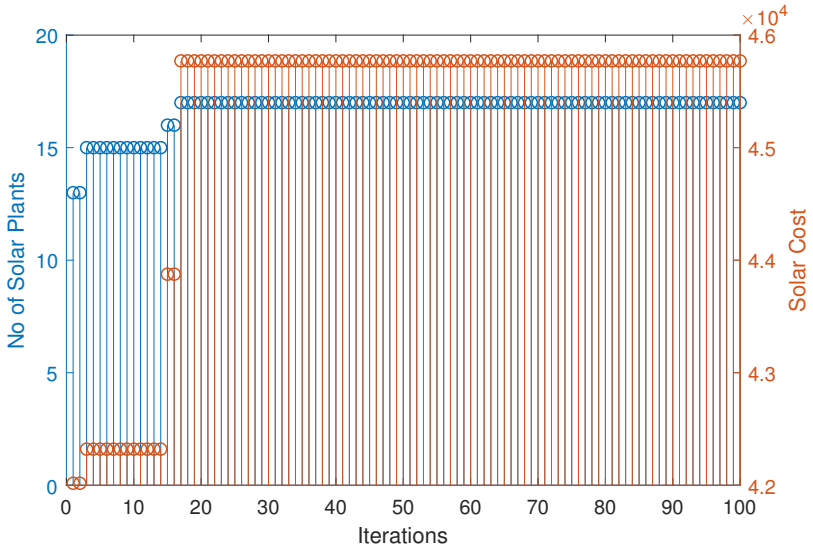

Figure 4.10: Results of sub-problem II: number of selected solar plants vs. solar cost over 100 iterations, with solar share at point d_1 for $\beta = 10^4$.

Table 4.7: Effect of β on number of solutions and number of iterations.

Value of β	Number of solutions	Number of iterations
10^3	4	67
10^4	4	16
2×10^4	4	10
3×10^4	4	7
4×10^4	4	6
4×10^5	3	5
10^5	3	3

Table 4.8: Overall performance metrics of proposed model vs. baseline (without ESS).

Time of the day	**10:00**	**11:00**	**12:00**	**13:00**	**14:00**	**15:00**	**16:00**	**17:00**	**18:00**
(RCUC is applied without ESS)									
$\mathcal{R}^t$ *for solar share at point* d=$\mathcal{R}^t_d$	108	21	118	118	110	106	31	110	92
Solar share at point $d = \Gamma^t_d$ *(MW)*	100	20	100	100	100	100	20	100	80
Thermal generation (MW) for Γ^t_d	2500	2650	2490	2490	2450	2520	2630	2450	2450
Thermal fuel cost ($/MWh) with Γ^t_d	34981	37908	35016	34792	34042	35359	37473	34337	33776
$\mathcal{R}^t$ for solar share at point s	344	268	345	345	345	345	301	345	330
Solar share at point $s = \Gamma^t_s$ (MW)	340	260	340	340	340	340	300	340	320
(UC is executed without reserve constraint in presence of ESS)									
$\mathcal{R}^t$ *for solar share at point* d_1=$\mathcal{R}^t_{d_1}$	231	231	288	288	308	224	231	286	308
Solar share at point $d_1 = \Gamma^t_{d_1}(MW)$	220	220	280	280	280	220	220	280	260
Thermal generation (MW) *for* $\Gamma^t_{d_1}$	2600-220	2670-220	2590-280	2590-280	2550-280	2620-220	2650-220	2550-280	2530-260
Thermal fuel cost ($/MWh) with $\Gamma^t_{d_1}$	31962	33264	30893	30893	30317	32046	32694	30101	30317
(UC is applied without reserve constraint, SP^t_Γ *is unavailable)*									
$\mathcal{R}^t$ *for solar share at point* d_2 =$\mathcal{R}^t_{d_2}$	207	207	207	207	284	227	207	262	284
Solar share at point $d_2 = \Gamma^t_{d_2}$ (MW)	200	200	200	200	280	200	200	260	260
Thermal generation (MW)	2600-200	2670-200	2590-200	2590-200	2550-280	2620-200	2650-200	2550-260	2530-260
Thermal fuel cost ($/MWh)	32332	33639	32146	32146	30056	32744	33264	30344	30159
$P^t_d(MW)$	2600	2670	2590	2590	2550	2620	2650	2550	2530

4.5 Conclusions

Simulation results verified that the ESS plays a critical role in sharing the reserve requirement with thermal units, thereby reducing the number of units committed for reserve provision and lowering the overall operating cost. Furthermore, the allocation of robust CBSR was found to directly influence the achievable level of solar integration. In particular, a solar share of 220 MW was successfully integrated at operating point d_1, where the post-contingency evaluation confirmed that simultaneous outages of solar and thermal generation could be handled effectively. However, it was also observed that a fixed allocation of SP^t_Γ may lead to a power deficit if a thermal unit with a large up-reserve trips; this limitation could be mitigated through dynamic allocation of SP^t_Γ. In contrast, non-robust operation at point c_1 resulted in a loss of load of 10.4% under similar contingencies. When the ESS was discharged, the system could integrate only 100 MW of solar generation under conventional SSR allocation at operating point d. An additional operating point, s, was identified in this scenario that could withstand either a solar or a thermal contingency of 345 MW. Nevertheless, non-robust operation at point c in this case led to a substantially higher loss of load of 44.4% under contingency conditions.These results confirmed that, through appropriate allocation of robust reserve and coordination with the ESS, substantial improvements in economic efficiency, renewable utilization, and reliability can be achieved.

This work addressed several critical aspects of the economic operation of the HPS. However, certain factors such as network constraints, emissions, load management, and the integration of additional renewable energy sources were not considered. Future research could extend the proposed model to incorporate these elements. Including these features would enhance the practicality and completeness of the model, although it would result in a more computationally intensive optimization.

Chapter 5

Conclusions and future recommendations

5.1 Conclusions and future recommendations

The Conclusion and Future Recommendations is the final chapter in this thesis in which the key findings, descriptive overview, and the contributions of this research are summarized, and directions for further work are suggested.

5.2 Conclusion

In this research, a comprehensive model was developed for economic operation of HPS, which is more robust against the loss of load in case of thermal contingencies as well as solar power outages. In literature, the optimization of solar power penetration for worst case scenario has not been yet considered. We have optimized HPS and found the robust limit of solar power penetration under consideration of worst case scenario. The presented model of HPS is studied in presence and absence of ESS. To facilitate the solution, a composite optimization was decomposed into the sub-problems. Solution of presented model contains computation of the limits of the robust SSR for the solar share, the maximum bound on the solar share within the limits of the robust SSR, the ultimate SSR and novel application scheme of ESS. In the presence and absence of ESS, the optimization was solved for the committed thermal units to minimize fuel costs, maximize the solar share by SSR analysis, maximize the number of participating solar plants, and minimize the solar cost. Pareto optimal solution were obtained to provide flexible choices for system operators. The following points have been concluded:

(i) Committed thermal units could provide a limited robust SSR to facilitate a given solar share. Thus, the amount of penetrated solar share at any time was limited by the available robust reserve at that time. For instance, SSR^{10} within the range of robust SSR always equal to or less then the SSR, depending on the condition whether $SSR^{t}_{opt(1,2)}$ was allowed to be dispatched or restricted for a solar power outage event.

Beyond these allocations, the robust SSR starts to become smaller than the solar share, therefore, loss of load would be experienced by the power system for a complete outage of the solar share.

(ii) A set of committed units in a time slot could provide a certain amount of the ultimate SSR.

(iii) When a power storage system was applied to a HPS, the burden of providing SSR was removed from committed thermal units. This provided decrease in thermal fuel cost by excluding reserve constraint from UC. It was found that the range of robust reserve could be enhanced by provision of power storage system to HPS which results in increase in injected solar power.

(iv) Only a few such solutions were obtainable within the feasible binary search space when Pareto-optimal solutions were obtained for the contradictory objectives of solar cost minimization and the maximization of the number of solar plants. The highest number of such solutions were obtained with the value of parameter K empirically set to 10^4. Although this work investigated many critical issues of HPS, some aspects, such as network constraints, storage systems, and RE sources other than solar power, have not been covered.

5.3 Future recomendations

Future directions to this work may involve the addition of dispatch-able loads, emissions, network constraints, and other RE sources to our proposed model. The sustainability of hybrid power systems integrated with various renewable energy sources can be evaluated using the proposed SS/CBSR analysis. The inclusion of all these features will make our model more practical and more complete. However, the addition of all these features will result in a more challenging optimization.

Appendix

Appendix A

Supplementary Data

Table A.1: ED at Γ^t=0

t (h)	ED without any solar share																									
	U1	**U2**	**U3**	**U4**	**U5**	**U6**	**U7**	**U8**	**U9**	**U10**	**U11**	**U12**	**U13**	**U14**	**U15**	**U16**	**U17**	**U18**	**U19**	**U20**	**U21**	**U22**	**U23**	**U24**	**U25**	**U26**
1	0.00	0.00	0.00	0.00	0.00	0.00	0.00	0.00	0.00	15.20	15.20	15.20	15.20	25.00	25.00	25.00	100.37	95.98	92.17	88.82	68.95	68.95	0.00	248.96	400.00	400.00
2	0.00	0.00	0.00	0.00	0.00	0.00	0.00	0.00	0.00	15.20	15.20	15.20	15.20	25.00	25.00	25.00	104.70	100.23	96.35	92.94	68.95	68.95	0.00	262.08	400.00	400.00
3	0.00	0.00	0.00	0.00	0.00	0.00	0.00	0.00	0.00	15.20	15.20	15.20	15.20	25.00	25.00	25.00	98.92	94.57	90.78	87.45	68.95	68.95	0.00	244.58	400.00	400.00
4	0.00	0.00	0.00	0.00	0.00	0.00	0.00	0.00	0.00	15.20	15.20	15.20	15.20	25.00	25.00	25.00	100.37	95.98	92.17	88.82	68.95	68.95	0.00	248.96	400.00	400.00
5	0.00	0.00	0.00	0.00	0.00	0.00	0.00	0.00	0.00	15.20	15.20	15.20	15.20	25.00	25.00	25.00	107.59	103.06	99.13	95.69	68.95	68.95	0.00	270.83	400.00	400.00
6	0.00	0.00	0.00	0.00	0.00	0.00	0.00	0.00	0.00	34.45	34.45	34.45	34.45	49.09	41.81	0.00	135.09	130.56	126.63	123.19	0.00	0.00	0.00	305.83	400.00	400.00
7	2.40	2.40	2.40	2.40	2.40	0.00	0.00	0.00	0.00	42.79	40.39	38.26	35.92	25.00	25.00	25.00	155.00	155.00	154.13	150.69	0.00	0.00	0.00	340.83	400.00	400.00
8	12.00	12.00	12.00	12.00	12.00	0.00	0.00	0.00	0.00	62.04	59.64	57.51	55.17	50.50	50.50	50.50	155.00	155.00	155.00	155.00	27.50	27.50	27.50	350.00	400.00	400.00
9	12.00	12.00	12.00	12.00	10.58	4.00	4.00	4.00	4.00	76.00	76.00	76.00	74.42	76.00	76.00	76.00	155.00	155.00	155.00	155.00	55.00	55.00	55.00	350.00	400.00	400.00
10	2.40	2.40	2.40	2.40	2.40	4.00	4.00	4.00	4.00	76.00	76.00	76.00	76.00	100.00	98.60	92.55	155.00	155.00	155.00	155.00	68.95	68.95	68.95	350.00	400.00	400.00
11	2.40	2.40	2.40	2.40	2.40	4.00	4.00	4.00	4.00	76.00	76.00	76.00	76.00	100.00	100.00	100.00	155.00	155.00	155.00	155.00	96.45	95.83	75.72	350.00	400.00	400.00
12	2.40	2.40	2.40	2.40	2.40	4.00	4.00	4.00	4.00	76.00	76.00	76.00	76.00	100.00	93.66	87.49	155.00	155.00	155.00	155.00	68.95	68.95	68.95	350.00	400.00	400.00
13	2.40	2.40	2.40	2.40	2.40	4.00	4.00	4.00	4.00	76.00	76.00	76.00	76.00	100.00	93.66	87.49	155.00	155.00	155.00	155.00	68.95	68.95	68.95	350.00	400.00	400.00
14	2.40	2.40	2.40	2.40	2.40	4.00	4.00	4.00	4.00	76.00	76.00	76.00	76.00	86.95	80.34	73.86	155.00	155.00	155.00	155.00	68.95	68.95	68.95	350.00	400.00	400.00
15	2.40	2.40	2.40	2.40	2.40	4.00	4.00	4.00	4.00	76.00	76.00	76.00	76.00	100.00	100.00	99.36	155.00	155.00	155.00	155.00	80.74	68.95	68.95	350.00	400.00	400.00
16	2.40	2.40	2.40	2.40	2.40	4.00	4.00	4.00	4.00	76.00	76.00	76.00	76.00	100.00	100.00	100.00	155.00	155.00	155.00	155.00	99.33	79.72	68.95	350.00	400.00	400.00
17	2.40	2.40	2.40	2.40	2.40	4.00	4.00	4.00	4.00	76.00	76.00	76.00	76.00	86.95	80.34	73.86	155.00	155.00	155.00	155.00	68.95	68.95	68.95	350.00	400.00	400.00
18	2.40	2.40	2.40	2.40	2.40	4.00	4.00	4.00	0.00	76.00	76.00	76.00	76.00	81.72	75.02	68.41	155.00	155.00	155.00	155.00	68.95	68.95	68.95	350.00	400.00	400.00
19	2.40	2.40	2.40	2.40	2.40	4.00	4.00	0.00	0.00	76.00	76.00	76.00	76.00	73.22	66.37	59.56	155.00	155.00	155.00	155.00	68.95	68.95	68.95	350.00	400.00	400.00
20	2.40	2.40	2.40	2.40	2.40	4.00	4.00	4.00	4.00	76.00	76.00	76.00	76.00	86.95	80.34	73.86	155.00	155.00	155.00	155.00	68.95	68.95	68.95	350.00	400.00	400.00
21	2.40	2.40	2.40	2.40	2.40	4.00	4.00	4.00	4.00	76.00	76.00	76.00	76.00	100.00	98.60	92.55	155.00	155.00	155.00	155.00	68.95	68.95	68.95	350.00	400.00	400.00
22	2.40	2.40	2.40	2.40	2.40	0.00	0.00	0.00	0.00	76.00	76.00	76.00	76.00	69.26	62.34	55.55	155.00	155.00	155.00	155.00	68.95	68.95	68.95	350.00	400.00	400.00
23	0.00	0.00	0.00	0.00	0.00	0.00	0.00	0.00	0.00	36.00	36.00	36.00	36.00	32.26	25.34	25.00	155.00	155.00	155.00	151.55	68.95	68.95	68.95	350.00	400.00	400.00
24	0.00	0.00	0.00	0.00	0.00	0.00	0.00	0.00	0.00	15.20	15.20	15.20	15.20	25.00	25.00	25.00	145.81	140.46	135.91	132.02	0.00	0.00	0.00	350.00	400.00	400.00

Table A.2: Reserve of individual thermal unit after solar share penetration at s point for $t = 10$

t (h)	Available up-reserve from each thermal unit after solar penetration at s point																									
	U1	**U2**	**U3**	**U4**	**U5**	**U6**	**U7**	**U8**	**U9**	**U10**	**U11**	**U12**	**U13**	**U14**	**U15**	**U16**	**U17**	**U18**	**U19**	**U20**	**U21**	**U22**	**U23**	**U24**	**U25**	**U26**
1	0.00	0.00	0.00	0.00	0.00	0.00	0.00	0.00	0.00	19.25	19.25	19.25	19.25	25.50	25.50	25.50	27.50	27.50	27.50	27.50	27.50	27.50	0.00	35.00	0.00	0.00
2	0.00	0.00	0.00	0.00	0.00	0.00	0.00	0.00	0.00	19.25	19.25	19.25	19.25	25.50	25.50	25.50	27.50	27.50	27.50	27.50	27.50	27.50	0.00	35.00	0.00	0.00
3	0.00	0.00	0.00	0.00	0.00	0.00	0.00	0.00	0.00	19.25	19.25	19.25	19.25	25.50	25.50	25.50	27.50	27.50	27.50	27.50	27.50	27.50	0.00	35.00	0.00	0.00
4	0.00	0.00	0.00	0.00	0.00	0.00	0.00	0.00	0.00	19.25	19.25	19.25	19.25	25.50	25.50	25.50	27.50	27.50	27.50	27.50	27.50	27.50	0.00	35.00	0.00	0.00
5	0.00	0.00	0.00	0.00	0.00	0.00	0.00	0.00	0.00	19.25	19.25	19.25	19.25	25.50	25.50	25.50	27.50	27.50	27.50	27.50	27.50	27.50	0.00	35.00	0.00	0.00
6	0.00	0.00	0.00	0.00	0.00	0.00	0.00	0.00	0.00	19.25	19.25	19.25	19.25	25.50	25.50	0.00	19.91	24.44	27.50	27.50	0.00	0.00	0.00	35.00	0.00	0.00
7	9.60	9.60	9.60	9.60	9.60	0.00	0.00	0.00	0.00	19.25	19.25	19.25	19.25	25.50	25.50	25.50	0.00	0.00	0.87	4.31	0.00	0.00	0.00	9.17	0.00	0.00
8	0.00	0.00	0.00	0.00	0.00	0.00	0.00	0.00	0.00	13.96	16.36	18.49	19.25	25.50	25.50	25.50	0.00	0.00	0.00	0.00	27.50	27.50	27.50	0.00	0.00	0.00
9	5.89	8.58	9.60	9.60	9.60	15.25	15.25	15.25	15.25	0.00	0.00	0.00	1.58	24.00	24.00	24.00	0.00	0.00	0.00	0.00	27.50	27.50	27.50	0.00	0.00	0.00
10	9.60	9.60	9.60	9.60	9.60	15.25	15.25	15.25	15.25	19.25	19.25	19.25	19.25	25.50	25.50	25.50	0.00	0.00	0.00	0.00	27.50	27.50	27.50	0.00	0.00	0.00
11	9.60	9.60	9.60	9.60	9.60	15.25	15.25	15.25	15.25	19.25	19.25	19.25	19.25	25.50	25.50	25.50	0.00	0.00	0.07	4.20	27.50	27.50	27.50	0.00	0.00	0.00
12	9.60	9.60	9.60	9.60	9.60	15.25	15.25	15.25	15.25	19.25	19.25	19.25	19.25	25.50	25.50	25.50	0.00	0.00	0.00	0.00	27.50	27.50	27.50	0.00	0.00	0.00
13	9.60	9.60	9.60	9.60	9.60	15.25	15.25	15.25	15.25	19.25	19.25	19.25	19.25	25.50	25.50	25.50	0.00	0.00	0.00	0.00	27.50	27.50	27.50	0.00	0.00	0.00
14	9.60	9.60	9.60	9.60	9.60	15.25	15.25	15.25	15.25	19.25	19.25	19.25	19.25	25.50	25.50	25.50	0.00	0.00	0.00	0.00	27.50	27.50	27.50	0.00	0.00	0.00
15	9.60	9.60	9.60	9.60	9.60	15.25	15.25	15.25	15.25	19.25	19.25	19.25	19.25	25.50	25.50	25.50	0.00	0.00	0.00	0.00	27.50	27.50	27.50	0.00	0.00	0.00
16	9.60	9.60	9.60	9.60	9.60	15.25	15.25	15.25	15.25	4.15	7.16	9.77	12.77	25.50	25.50	25.50	0.00	0.00	0.00	0.00	27.50	27.50	27.50	0.00	0.00	0.00
17	9.60	9.60	9.60	9.60	9.60	15.25	15.25	15.25	15.25	19.25	19.25	19.25	19.25	25.50	25.50	25.50	0.00	0.00	0.00	0.00	27.50	27.50	27.50	0.00	0.00	0.00
18	9.60	9.60	9.60	9.60	9.60	15.25	15.25	15.25	0.00	19.25	19.25	19.25	19.25	25.50	25.50	25.50	0.00	0.00	0.00	0.00	27.50	27.50	27.50	0.00	0.00	0.00
9	9.60	9.60	9.60	9.60	9.60	15.25	15.25	0.00	0.00	19.25	19.25	19.25	19.25	25.50	25.50	25.50	0.00	0.00	0.00	0.00	27.50	27.50	27.50	0.00	0.00	0.00
29	9.60	9.60	9.60	9.60	9.60	15.25	15.25	15.25	15.25	19.25	19.25	19.25	19.25	25.50	25.50	25.50	0.00	0.00	0.00	0.00	27.50	27.50	27.50	0.00	0.00	0.00
21	0.00	0.00	0.00	0.00	0.00	0.75	0.75	0.75	0.75	19.25	19.25	19.25	19.25	25.50	25.50	25.50	0.00	0.00	0.00	0.00	27.50	27.50	27.50	0.00	0.00	0.00
22	9.60	9.60	9.60	9.60	9.60	0.00	0.00	0.00	0.00	1.72	3.97	5.99	8.17	24.21	25.50	25.50	0.00	0.00	0.00	0.00	27.50	27.50	27.50	0.00	0.00	0.00
23	0.00	0.00	0.00	0.00	0.00	0.00	0.00	0.00	0.00	19.25	19.25	19.25	19.25	25.50	25.50	25.50	0.00	0.00	0.00	0.00	27.50	27.50	27.50	0.00	0.00	0.00
24	0.00	0.00	0.00	0.00	0.00	0.00	0.00	0.00	0.00	19.25	19.25	19.25	19.25	25.50	25.50	25.50	9.19	14.54	19.09	22.98	0.00	0.00	0.00	0.00	0.00	0.00

Table A.3: Up-reserve of each thermal unit, when solar share is selected at point d

t (h)	Available up-reserve from each thermal unit after solar penetration at d point																									
	U1	**U2**	**U3**	**U4**	**U5**	**U6**	**U7**	**U8**	**U9**	**U10**	**U11**	**U12**	**U13**	**U14**	**U15**	**U16**	**U17**	**U18**	**U19**	**U20**	**U21**	**U22**	**U23**	**U24**	**U25**	**U26**
1	0.00	0.00	0.00	0.00	0.00	0.00	0.00	0.00	0.00	19.25	19.25	19.25	19.25	25.50	25.50	25.50	27.50	27.50	27.50	27.50	27.50	27.50	0.00	35.00	0.00	0.00
2	0.00	0.00	0.00	0.00	0.00	0.00	0.00	0.00	0.00	19.25	19.25	19.25	19.25	25.50	25.50	25.50	27.50	27.50	27.50	27.50	27.50	27.50	0.00	35.00	0.00	0.00
3	0.00	0.00	0.00	0.00	0.00	0.00	0.00	0.00	0.00	19.25	19.25	19.25	19.25	25.50	25.50	25.50	27.50	27.50	27.50	27.50	27.50	27.50	0.00	35.00	0.00	0.00
4	0.00	0.00	0.00	0.00	0.00	0.00	0.00	0.00	0.00	19.25	19.25	19.25	19.25	25.50	25.50	25.50	27.50	27.50	27.50	27.50	27.50	27.50	0.00	35.00	0.00	0.00
5	0.00	0.00	0.00	0.00	0.00	0.00	0.00	0.00	0.00	19.25	19.25	19.25	19.25	25.50	25.50	25.50	27.50	27.50	27.50	27.50	27.50	27.50	0.00	35.00	0.00	0.00
6	0.00	0.00	0.00	0.00	0.00	0.00	0.00	0.00	0.00	19.25	19.25	19.25	19.25	25.50	25.50	0.00	19.91	24.44	27.50	27.50	0.00	0.00	0.00	35.00	0.00	0.00
7	9.60	9.60	9.60	9.60	9.60	0.00	0.00	0.00	0.00	19.25	19.25	19.25	19.25	25.50	25.50	25.50	0.00	0.00	0.87	4.31	0.00	0.00	0.00	9.17	0.00	0.00
8	0.00	0.00	0.00	0.00	0.00	0.00	0.00	0.00	0.00	13.96	16.36	18.49	19.25	25.50	25.50	25.50	0.00	0.00	0.00	0.00	27.50	27.50	27.50	0.00	0.00	0.00
9	5.89	8.58	9.60	9.60	9.60	15.25	15.25	15.25	15.25	0.00	0.00	0.00	1.58	24.00	24.00	24.00	0.00	0.00	0.00	0.00	27.50	27.50	27.50	0.00	0.00	0.00
10	9.60	9.60	9.60	9.60	9.60	15.25	15.25	15.25	15.25	0.00	0.00	0.00	0.00	25.50	25.50	25.50	0.00	0.00	0.00	0.00	27.50	27.50	27.50	0.00	0.00	0.00
11	9.60	9.60	9.60	9.60	9.60	15.25	15.25	15.25	15.25	0.00	0.00	0.00	0.00	3.89	10.79	17.66	0.00	0.00	0.00	0.00	27.50	27.50	27.50	0.00	0.00	0.00
12	9.60	9.60	9.60	9.60	9.60	15.25	15.25	15.25	15.25	0.00	0.00	0.00	0.00	25.50	25.50	25.50	0.00	0.00	0.00	0.00	27.50	27.50	27.50	0.00	0.00	0.00
13	9.60	9.60	9.60	9.60	9.60	15.25	15.25	15.25	15.25	0.00	0.00	0.00	0.00	25.50	25.50	25.50	0.00	0.00	0.00	0.00	27.50	27.50	27.50	0.00	0.00	0.00
14	9.60	9.60	9.60	9.60	9.60	15.25	15.25	15.25	15.25	0.00	0.00	0.00	0.00	25.50	25.50	25.50	0.00	0.00	0.00	0.00	27.50	27.50	27.50	0.00	0.00	0.00
15	9.60	9.60	9.60	9.60	9.60	15.25	15.25	15.25	15.25	0.00	0.00	0.00	0.00	22.86	25.50	25.50	0.00	0.00	0.00	0.00	27.50	27.50	27.50	0.00	0.00	0.00
16	9.60	9.60	9.60	9.60	9.60	15.25	15.25	15.25	15.25	0.00	0.00	0.00	0.00	0.00	4.14	10.85	0.00	0.00	0.00	0.00	27.50	27.50	27.50	0.00	0.00	0.00
17 9.60	9.60	9.60	9.60	9.60	15.25	15.25	15.25	15.25	3.90	6.91	9.52	12.53	25.50	25.50	25.50	0.00	0.00	0.00	0.00	27.50	27.50	27.50	0.00	0.00	0.00	
18	9.60	9.60	9.60	9.60	9.60	15.25	15.25	15.25	0.00	0.00	0.00	0.00	0.00	25.50	25.50	25.50	0.00	0.00	0.00	0.00	27.50	27.50	27.50	0.00	0.00	0.00
19	9.60	9.60	9.60	9.60	9.60	15.25	15.25	0.00	0.00	0.00	0.00	0.00	0.00	25.50	25.50	25.50	0.00	0.00	0.00	0.00	27.50	27.50	27.50	0.00	0.00	0.00
20	9.60	9.60	9.60	9.60	9.60	15.25	15.25	15.25	15.25	0.00	0.00	0.00	0.00	13.05	19.66	25.50	0.00	0.00	0.00	0.00	27.50	27.50	27.50	0.00	0.00	0.00
21	9.60	9.60	9.60	9.60	9.60	15.25	15.25	15.25	15.25	0.00	0.00	0.00	0.00	0.00	1.40	7.45	0.00	0.00	0.00	0.00	27.50	27.50	27.50	0.00	0.00	0.00
22	9.60	9.60	9.60	9.60	9.60	0.00	0.00	0.00	0.00	0.00	0.00	0.00	0.00	25.50	25.50	25.50	0.00	0.00	0.00	0.00	27.50	27.50	27.50	0.00	0.00	0.00
23	0.00	0.00	0.00	0.00	0.00	0.00	0.00	0.00	0.00	19.25	19.25	19.25	19.25	25.50	25.50	25.50	0.00	0.00	0.00	0.00	27.50	27.50	27.50	0.00	0.00	0.00
24	0.00	0.00	0.00	0.00	0.00	0.00	0.00	0.00	0.00	19.25	19.25	19.25	19.25	25.50	25.50	25.50	9.19	14.54	19.09	22.98	0.00	0.00	0.00	0.00	0.00	0.00

Appendix B

Additional Results

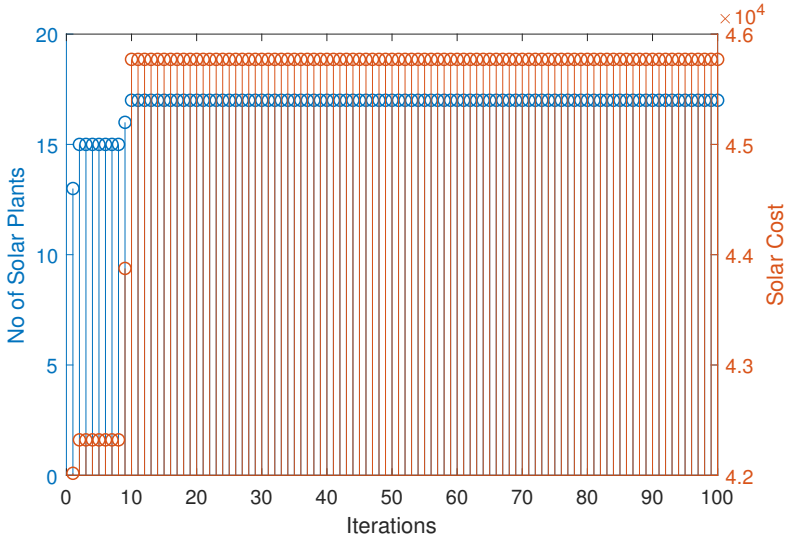

Figure B.1: Results of sub-problem II: number of selected solar plants vs. solar cost over 100 iterations, with solar share at point d_1 for $\beta = 2 \times 10^4$.

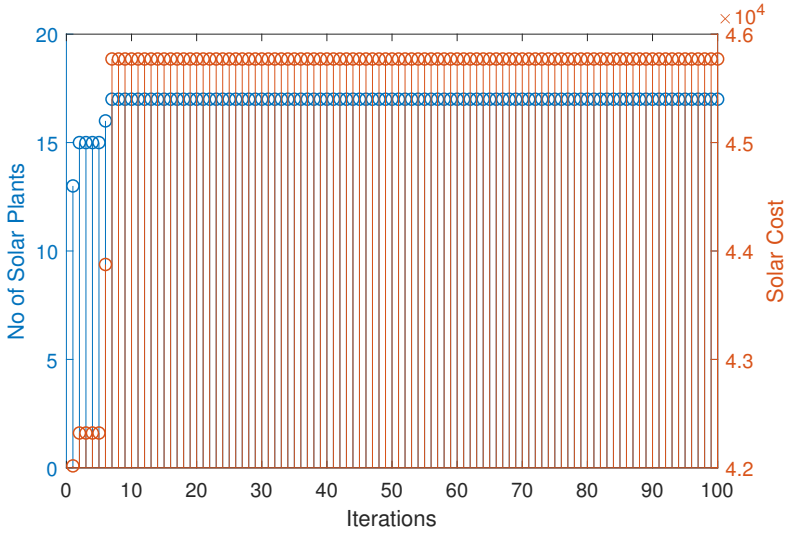

Figure B.2: Results of sub-problem II: number of selected solar plants vs. solar cost over 100 iterations, with solar share at point d_1 for $\beta = 3 \times 10^4$.

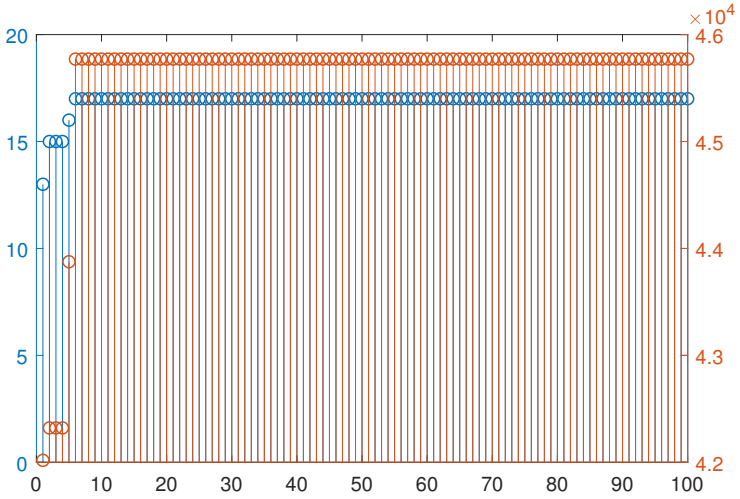

Figure B.3: Results of sub-problem II: number of selected solar plants vs. solar cost over 100 iterations, with solar share at point d_1 for $\beta = 4 \times 10^4$.

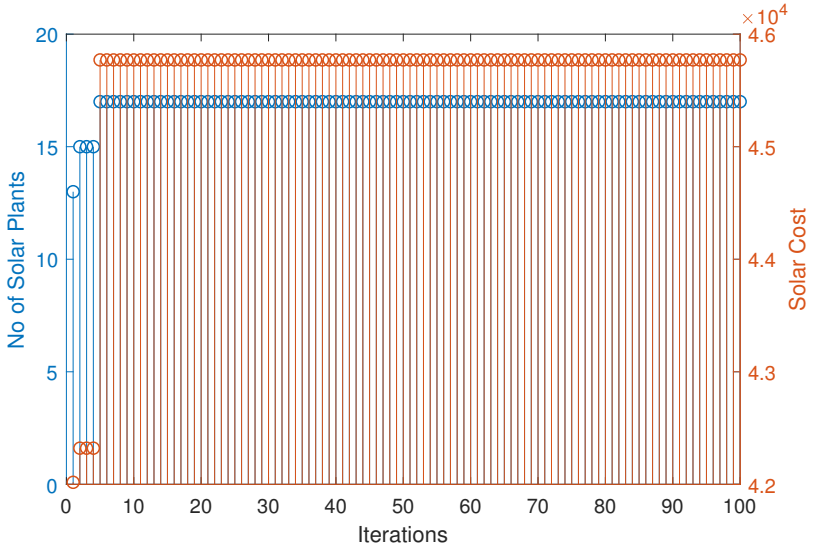

Figure B.4: Results of sub-problem II: number of selected solar plants vs. solar cost over 100 iterations, with solar share at point d_1 for $\beta = 5 \times 10^4$.

References

[1] F. Marzbani and A. Abdelfatah, "Economic dispatch optimization strategies and problem formulation: A comprehensive review," *Energies*, vol. 17, no. 3, p. 550, 2024.

[2] N. Bizon, H. Shayeghi, and N. M. Tabatabaei, *Analysis, control and optimal operations in hybrid power systems: Advanced techniques and applications for linear and nonlinear systems*. Springer, 2013.

[3] A. J. Wood, B. F. Wollenberg, and G. B. Sheblé, *Power generation, operation, and control*. John Wiley & Sons, 2013.

[4] J. Zhu, *Optimization of power system operation*. John Wiley & Sons, 2015.

[5] C. L. Chiang, "Genetic-based algorithm for power economic load dispatch," *IET Gener. Transm. Distrb.*, vol. 1, no. 2, pp. 261–269, 2007.

[6] D. Jeyakumar, T. Jayabarathi, and T. Raghunathan, "Particle swarm optimization for various types of economic dispatch problems," *Int. J. Electr. Power Energy Syst.*, vol. 28, no. 1, pp. 36–42, 2006.

[7] K. Y. Lee, A. Sode-Yome, and J. H. Park, "Adaptive hopfield neural networks for economic load dispatch," *IEEE Trans. Power Syst.*, vol. 13, no. 2, pp. 519–526, 1998.

[8] A. Mantawy, S. Soliman, and M. El-Hawary, "A new tabu search algorithm for the long-term hydro scheduling problem," in *Proc. LESCOPE'02. 2002 Large Eng. Syst. Conf. Power Eng. Conf.* IEEE, 2002, pp. 29–34.

[9] N. A. Khan, G. A. S. Sidhu, and F. Gao, "Optimizing combined emission economic dispatch for solar integrated power systems," *IEEE Access*, vol. 4, pp. 3340–3348, 2016.

[10] E. Zafiropoulos, C. Christodoulou, V. Vita, C. Dikaiakos, I. Gonos, E. Zubieta, G. Santamaria, N. Lai, N. Baltas, and P. Rodriguez, "Smart grid flexibility solutions for transmission networks with increased res penetration," *Proceedings of the CIGRE Paris Session*, p. 10711, 2022.

[11] I. Ahmed, M. Rehan, A. Basit, and K.-S. Hong, "Greenhouse gases emission reduction for electric power generation sector by efficient dispatching of thermal plants integrated with renewable systems," *Scientific Reports*, vol. 12, no. 1, p. 12380, 2022.

[12] Y. Wang, P. Dong, M. Xu, Y. Li, D. Zhou, and X. Liu, "Research on collaborative operation optimization of multi-energy stations in regional integrated energy system considering joint demand response," *International Journal of Electrical Power & Energy Systems*, vol. 155, p. 109507, 2024.

[13] M. Khalid, "Smart grids and renewable energy systems: Perspectives and grid integration challenges," *Energy Strategy Reviews*, vol. 51, p. 101299, 2024.

[14] O. B. Adewumi, G. Fotis, V. Vita, D. Nankoo, and L. Ekonomou, "The impact of distributed energy storage on distribution and transmission networks' power quality," *Applied Sciences*, vol. 12, no. 13, p. 6466, 2022.

[15] M. A. Raza, M. M. Aman, A. G. Abro, M. A. Tunio, K. L. Khatri, and M. Shahid, "Challenges and potentials of implementing a smart grid for pakistan's electric network," *Energy Strategy Reviews*, vol. 43, p. 100941, 2022.

[16] A. J. Wood and B. F. Wollenberg, *Power generation, operation, and control*. John Wiley & Sons, 2012.

[17] M. Wang, H. Gooi, and S. Chen, "Optimising probabilistic spinning reserve using an analytical expected-energy-not-supplied formulation," *IET generation, transmission & distribution*, vol. 5, no. 7, pp. 772–780, 2011.

[18] F. F. Ardakani, S. B. Mozafari, and S. Soleymani, "Scheduling energy and spinning reserve based on linear chance constrained optimization for a wind integrated power system," *Ain Shams Engineering Journal*, vol. 13, no. 3, p. 101582, 2022.

[19] A. Ahmadi-Khatir, M. Bozorg, and R. Cherkaoui, "Probabilistic spinning reserve provision model in multi-control zone power system," *IEEE Transactions on Power Systems*, vol. 28, no. 3, pp. 2819–2829, 2013.

[20] C. Lee, C. Liu, S. Mehrotra, and M. Shahidehpour, "Modeling transmission line constraints in two-stage robust unit commitment problem," *IEEE Transactions on Power Systems*, vol. 29, no. 3, pp. 1221–1231, 2013.

[21] Y. An and B. Zeng, "Exploring the modeling capacity of two-stage robust optimization: Variants of robust unit commitment model," *IEEE transactions on Power Systems*, vol. 30, no. 1, pp. 109–122, 2014.

[22] J. Bai, H. Gooi, L. Xia, G. Strbac, and B. Venkatesh, "A probabilistic reserve market incorporating interruptible load," *IEEE Transactions on Power Systems*, vol. 21, no. 3, pp. 1079–1087, 2006.

[23] A. Ahmadi-Khatir and R. Cherkaoui, "A probabilistic joint energy and spinning reserve market model," in *IEEE PES General Meeting*. IEEE, 2010, pp. 1–6.

[24] K. Afshar, M. Ehsan, M. Fotuhi-Firuzabad, and N. Amjady, "Cost-benefit analysis and milp for optimal reserve capacity determination in power system," *Applied Mathematics and Computation*, vol. 196, no. 2, pp. 752–761, 2008.

[25] M. Q. Wang and H. Gooi, "Spinning reserve estimation in microgrids," *IEEE Transactions on Power Systems*, vol. 26, no. 3, pp. 1164–1174, 2011.

[26] D. H. Barus and R. Dalimi, "Determining optimal operating reserves toward wind power penetration in indonesia based on hybrid artificial intelligence," *IEEE Access*, vol. 9, pp. 165 173–165 183, 2021.

[27] P. Nikolaidis and A. Poullikkas, "A novel cluster-based spinning reserve dynamic model for wind and pv power reinforcement," *Energy*, vol. 234, p. 121270, 2021.

[28] Y.-Y. Hong, G. F. D. Apolinario, T.-K. Lu, and C.-C. Chu, "Chance-constrained unit commitment with energy storage systems in electric power systems," *Energy Reports*, vol. 8, pp. 1067–1090, 2022.

[29] I. Farhat and M. El-Hawary, "Interior point methods application in optimum operational scheduling of electric power systems," *IET Gener. Transm. Distrb.*, vol. 3, no. 11, pp. 1020–1029, 2009.

[30] S. Kar, G. Hug, J. Mohammadi, and J. M. Moura, "Distributed state estimation and energy management in smart grids: A consensus innovations approach," *IEEE J. Sel. Topics Signal Process.*, vol. 8, no. 6, pp. 1022–1038, 2014.

[31] H. Happ, "Optimal power dispatch-a comprehensive survey," *IEEE Transactions on Power Apparatus and Systems*, vol. 96, no. 3, pp. 841–854, 1977.

[32] P. Nikolaidis and A. Poullikkas, "Enhanced lagrange relaxation for the optimal unit commitment of identical generating units," *IET Generation, Transmission & Distribution*, vol. 14, no. 18, pp. 3920–3928, 2020.

[33] X. Yu and H. Sun, "Unit commitment by enhanced adaptive lagrangian relaxation with an improved unit substitution heuristic," in *2016 IEEE Advanced Information Management, Communicates, Electronic and Automation Control Conference (IMCEC)*. IEEE, 2016, pp. 5–9.

[34] X. Yu and X. Zhang, "Unit commitment using lagrangian relaxation and particle swarm optimization," *International Journal of Electrical Power & Energy Systems*, vol. 61, pp. 510–522, 2014.

[35] X. Guan, Q. Zhai, and A. Papalexopoulos, "Optimization based methods for unit commitment: Lagrangian relaxation versus general mixed integer programming," in *2003 IEEE Power Engineering Society General Meeting (IEEE Cat. No. 03CH37491)*, vol. 2. IEEE, 2003, pp. 1095–1100.

[36] W. L. Peterson and S. R. Brammer, "A capacity based lagrangian relaxation unit commitment with ramp rate constraints," *IEEE Transactions on Power Systems*, vol. 10, no. 2, pp. 1077–1084, 1995.

[37] F. Zhuang and F. D. Galiana, "Towards a more rigorous and practical unit commitment by lagrangian relaxation," *IEEE Transactions on Power Systems*, vol. 3, no. 2, pp. 763–773, 1988.

[38] B. H. Chowdhury and S. Rahman, "A review of recent advances in economic dispatch," *IEEE Transactions on Power Systems*, vol. 5, no. 4, pp. 1248–1259, 1990.

[39] M. Huneault and F. Galiana, "A survey of the optimal power flow literature," *IEEE Trans. Power Syst.*, vol. 6, no. 2, pp. 762–770, 1991.

[40] S. Yang, S. Tan, and J.-X. Xu, "Consensus based approach for economic dispatch problem in a smart grid," *IEEE Trans. Power Syst.*, vol. 28, no. 4, pp. 4416–4426, 2013.

[41] A. S. Reddy and K. Vaisakh, "Shuffled differential evolution for large scale economic dispatch," *Electr. Power Syst. Res.*, vol. 96, pp. 237–245, 2013.

[42] W.-M. Lin, F.-S. Cheng, and M.-T. Tsay, "Nonconvex economic dispatch by integrated artificial intelligence," *IEEE Power Eng. Rev.*, vol. 21, no. 5, pp. 64–64, 2001.

[43] A. Mahor, V. Prasad, and S. Rangnekar, "Economic dispatch using particle swarm optimization: a review," *Renew. Sustain. Energy Rev.*, vol. 13, no. 8, pp. 2134–2141, 2009.

[44] S. Titus and A. E. Jeyakumar, "Hydrothermal scheduling using an improved particle swarm optimization technique considering prohibited operating zones," *Int. J. Soft Comput.*, vol. 2, no. 2, pp. 313–319, 2007.

[45] M. Garcia and R. Baldick, "Approximating economic dispatch by linearizing transmission losses," *IEEE Transactions on Power Systems*, vol. 35, no. 2, pp. 1009–1022, 2019.

[46] J. Park, Y. Kim, I. Eom, and K. Lee, "Economic load dispatch for piecewise quadratic cost function using hopfield neural network," *IEEE Trans. Power Syst.*, vol. 8, no. 3, pp. 1030–1038, 1993.

[47] D. C. Walters and G. B. Sheble, "Genetic algorithm solution of economic dispatch with valve point loading," *IEEE Trans. Power Syst.*, vol. 8, no. 3, pp. 1325–1332, 1993.

[48] C.-L. Chiang, "Improved genetic algorithm for power economic dispatch of units with valve-point effects and multiple fuels," *IEEE Trans. Power Syst.*, vol. 20, no. 4, pp. 1690–1699, 2005.

[49] H.-T. Yang, P.-C. Yang, and C.-L. Huang, "Evolutionary programming based economic dispatch for units with non-smooth fuel cost functions," *IEEE Trans. Power Syst.*, vol. 11, no. 1, pp. 112–118, 1996.

[50] Y. M. Park, J. R. Won, and J. B. Park, "A new approach to economic load dispatch based on improved evolutionary programming," *Eng. Intell. Syst. Elect. Eng. Commun.*, vol. 6, no. 2, pp. 103–110, 1998.

[51] Z.-L. Gaing, "Particle swarm optimization to solving the economic dispatch considering the generator constraints," *IEEE Trans. Power Syst.*, vol. 18, no. 3, pp. 1187–1195, 2003.

[52] J.-B. Park, Y.-W. Jeong, J.-R. Shin, and K. Y. Lee, "An improved particle swarm optimization for nonconvex economic dispatch problems," *IEEE Trans. Power Syst.*, vol. 25, no. 1, pp. 156–166, 2010.

[53] G. Abbas, J. Gu, U. Farooq, M. U. Asad, and M. El-Hawary, "Solution of an economic dispatch problem through particle swarm optimization: A detailed survey-part i," *IEEE Access*, vol. 5, pp. 15 105–15 141, 2017.

[54] B. N. Alhasnawi, B. H. Jasim, V. Bureš, B. E. Sedhom, A. N. Alhasnawi, R. Abbassi, M. R. M. Alsemawai, P. Siano, and J. M. Guerrero, "A novel economic dispatch in the stand-alone system using improved butterfly optimization algorithm," *Energy Strategy Reviews*, vol. 49, p. 101135, 2023.

[55] S. Brini, H. H. Abdallah, and A. Ouali, "Economic dispatch for power system included wind and solar thermal energy," *Leonardo J. Sci.*, vol. 14, pp. 204–220, 2009.

[56] N. A. Khan, G. A. S. Sidhu, A. B. Awan, Z. Ali, and A. Mahmood, "Modeling and operation optimization of re integrated microgrids considering economic, energy, and environmental aspects," *International Journal of Energy Research*, vol. 43, no. 13, pp. 6721–6739, 2019.

[57] N. A. Khan, A. B. Awan, A. Mahmood, I. Member, S. Razzaq, A. Zafar, and G. A. S. Sidhu, "Combined emission economic dispatch of power system including solar photo voltaic generation," *Energy Convers. Manag.*, vol. 92, pp. 82–91, 2015.

[58] P. Nikolaidis, S. Chatzis, and A. Poullikkas, "Renewable energy integration through optimal unit commitment and electricity storage in weak power networks," *International Journal of Sustainable Energy*, vol. 38, no. 4, pp. 398–414, 2019.

[59] A. Lorca and X. A. Sun, "Multistage robust unit commitment with dynamic uncertainty sets and energy storage," *IEEE Transactions on Power Systems*, vol. 32, no. 3, pp. 1678–1688, 2016.

[60] G. N. Psarros and S. A. Papathanassiou, "Comparative assessment of priority listing and mixed integer linear programming unit commitment methods for non-interconnected island systems," *Energies*, vol. 12, no. 4, p. 657, 2019.

[61] M. A. Ortega-Vazquez and D. S. Kirschen, "Estimating the spinning reserve requirements in systems with significant wind power generation penetration," *IEEE Transactions on power systems*, vol. 24, no. 1, pp. 114–124, 2008.

[62] X. Liu and A. J. Conejo, "Day-ahead reserve determination in power systems with high renewable penetration," *International Journal of Electrical Power & Energy Systems*, vol. 156, p. 109703, 2024.

[63] M. A. Ortega-Vazquez and D. S. Kirschen, "Optimizing the spinning reserve requirements using a cost/benefit analysis," *IEEE Transactions on Power Systems*, vol. 22, no. 1, pp. 24–33, 2007.

[64] M. Wang, M. Yang, Y. Liu, X. Han, and Q. Wu, "Optimizing probabilistic spinning reserve by an umbrella contingencies constrained unit commitment,"

International Journal of Electrical Power & Energy Systems, vol. 109, pp. 187–197, 2019.

[65] X. Wen, D. Abbes, and B. Francois, "Stochastic optimization for security-constrained day-ahead operational planning under pv production uncertainties: Reduction analysis of operating economic costs and carbon emissions," *IEEE Access*, vol. 9, pp. 97 039–97 052, 2021.

[66] P. Nikolaidis and A. Poullikkas, "Co-optimization of active power curtailment, load shedding and spinning reserve deficits through hybrid approach: Comparison of electrochemical storage technologies," *IET Renewable Power Generation*, vol. 16, no. 1, pp. 92–104, 2022.

[67] M. Håberg, "Fundamentals and recent developments in stochastic unit commitment," *International Journal of Electrical Power & Energy Systems*, vol. 109, pp. 38–48, 2019.

[68] A. Shukla and S. Singh, "Multi-objective unit commitment with renewable energy using gsa algorithm," *INAE Letters*, vol. 1, no. 1, pp. 21–27, 2016.

[69] B. Yuan, J. Zhou, G. Lu, D. Liu, P. Xia, and C. Wu, "Coordinated dispatch of power generation and spinning reserve in power systems with high renewable penetration," *Processes*, vol. 12, no. 12, p. 2779, 2024.

[70] A. Mahnitko, T. Lomane, and I. Zicmane, "Problematic aspects of energy systems with a high penetration of renewable energy sources," *Energies*, vol. 18, no. 16, p. 4282, 2025.

[71] O. Boqtob, H. El Moussaoui, H. El Markhi, and T. Lamhamdi, "Optimal robust unit commitment of microgrid using hybrid particle swarm optimization with sine cosine acceleration coefficients," *International Journal of Renewable Energy Research (IJRER)*, vol. 9, no. 3, pp. 1125–1134, 2019.

[72] P. Nikolaidis and S. Chatzis, "Gaussian process-based bayesian optimization for data-driven unit commitment," *International Journal of Electrical Power & Energy Systems*, vol. 130, p. 106930, 2021.

[73] B. Han, H. Li, and S. Wang, "Robust spinning reserve scheduling for power systems incorporating building energy flexibility by considering load rebound," *Journal of Energy Storage*, vol. 114, p. 115910, 2025.

[74] E. F. Alves, L. Polleux, G. Guerassimoff, M. Korpås, and E. Tedeschi, "Allocation of spinning reserves in autonomous grids considering frequency stability constraints and short-term solar power variations," *IEEE Access*, vol. 11, pp. 29 896–29 908, 2023.

[75] M. M. Rana, M. Uddin, M. R. Sarkar, S. T. Meraj, G. Shafiullah, S. Muyeen, M. A. Islam, and T. Jamal, "Applications of energy storage systems in power grids with and without renewable energy integration—a comprehensive review," *Journal of energy storage*, vol. 68, p. 107811, 2023.

[76] A. Saxena and R. Shankar, "Improved load frequency control considering dynamic demand regulated power system integrating renewable sources and hybrid energy storage system," *Sustainable Energy Technologies and Assessments*, vol. 52, p. 102245, 2022.

[77] D. T. George, R. E. Raj, A. Rajkumar, and M. C. Mabel, "Optimal sizing of solar-wind based hybrid energy system using modified dragonfly algorithm for an institution," *Energy Conversion and Management*, vol. 283, p. 116938, 2023.

[78] H. Chen, R. Zhang, G. Li, L. Bai, and F. Li, "Economic dispatch of wind integrated power systems with energy storage considering composite operating costs," *IET Generation, Transmission & Distribution*, vol. 10, no. 5, pp. 1294–1303, 2016.

[79] Y. Zhou, Y. Zhu, Q. Luo, Y. Wei, Y. Mei, and F.-J. Chang, "Optimizing pumped-storage power station operation for boosting power grid absorbability to renewable energy," *Energy Conversion and Management*, vol. 299, p. 117827, 2024.

[80] B. Alqahtani, J. Yang, and M. C. Paul, "Design and performance assessment of a pumped hydro power energy storage connected to a hybrid system of

photovoltaics and wind turbines," *Energy Conversion and Management*, vol. 293, p. 117444, 2023.

[81] A. M. Elsayed, A. M. Maklad, and S. M. Farrag, "A new priority list unit commitment method for large-scale power systems," in *2017 Nineteenth International Middle East Power Systems Conference (MEPCON)*. IEEE, 2017, pp. 359–367.

[82] B. Fu, C. Ouyang, C. Li, J. Wang, and E. Gul, "An improved mixed integer linear programming approach based on symmetry diminishing for unit commitment of hybrid power system," *Energies*, vol. 12, no. 5, p. 833, 2019.

[83] A. Shukla and S. N. Singh, "Multi-objective unit commitment with renewable energy using hybrid approach," *IET renewable power generation*, vol. 10, no. 3, pp. 327–338, 2016.

[84] S. Babaei, C. Zhao, and L. Fan, "A data-driven model of virtual power plants in day-ahead unit commitment," *IEEE Transactions on Power Systems*, vol. 34, no. 6, pp. 5125–5135, 2019.

[85] K. Hreinsson, A. Scaglione, and B. Analui, "Continuous time multi-stage stochastic unit commitment with storage," *IEEE Transactions on Power Systems*, vol. 34, no. 6, pp. 4476–4489, 2019.

[86] B. Zhou, X. Ai, J. Fang, W. Yao, W. Zuo, Z. Chen, and J. Wen, "Data-adaptive robust unit commitment in the hybrid ac/dc power system," *Applied Energy*, vol. 254, p. 113784, 2019.

[87] T. N. H. Nguyen, K. Yabe, M. Ito, V. T. Dao, H. Ishii, and Y. Hayashi, "Spinning reserve quantification considering confidence levels of forecast in systems with high wind and solar power penetration," *IEEJ Transactions on Electrical and Electronic Engineering*, vol. 14, no. 9, pp. 1304–1313, 2019.

[88] L. Idoko, O. Anaya-Lara, and A. McDonald, "Enhancing pv modules efficiency and power output using multi-concept cooling technique," *Energy Reports*, vol. 4, pp. 357–369, 2018.

[89] F. Bouffard and F. D. Galiana, "An electricity market with a probabilistic spinning reserve criterion," *IEEE Transactions on Power Systems*, vol. 19, no. 1, pp. 300–307, 2004.

[90] C. Wang and S. Shahidehpour, "Effects of ramp-rate limits on unit commitment and economic dispatch," *IEEE Transactions on Power Systems*, vol. 8, no. 3, pp. 1341–1350, 1993.

[91] T. Adefarati, R. Bansal, T. Shongwe, R. Naidoo, M. Bettayeb, and A. Onaolapo, "Optimal energy management, technical, economic, social, political and environmental benefit analysis of a grid-connected pv/wt/fc hybrid energy system," *Energy Conversion and Management*, vol. 292, p. 117390, 2023.

[92] R. M. M. Saeed, N. A. Khan, M. Shakir, G. A. S. Sidhu, A. B. Awan, and M. A. Baseer, "Maximizing solar share in robust system spinning reserve-constrained economic operation of hybrid power systems," *Energies*, vol. 17, no. 11, p. 2794, 2024.